NUMERICAL STUDIES OF INCOMPRESSIBLE VISCOUS FLOW IN A DRIVEN CAVITY

NATIONAL AERONAUTICS AND SPACE ADMINISTRATION

NUMERICAL STUDIES OF INCOMPRESSIBLE VISCOUS FLOW IN A DRIVEN CAVITY

By the Staff of Langley Research Center

Scientific and Technical Information Office 1975
NATIONAL AERONAUTICS AND SPACE ADMINISTRATION
Washington, D.C.

For sale by the National Technical Information Service
Springfield, Virginia 22161
Price – $5.75

PREFACE

This publication consists of a series of project papers prepared by graduate students in computational fluid dynamics. The work was performed during the 1973-74 academic year at Old Dominion University under the auspices of Professor Stanley G. Rubin, now with the Polytechnic Institute of New York. The class, taught at Langley Research Center, was comprised of Langley employees and contractors. Each paper briefly examines one of the numerical methods discussed during the lectures and applies the method to the Navier-Stokes equations governing incompressible flow in a driven cavity. Also, solutions obtained with a cubic spline procedure which was under investigation at the time are included.

It should be emphasized that most of these studies were completed in a period of approximately 6 weeks by different researchers with backgrounds varying from fluid mechanics to applied mathematics. (All had considerable experience with numerical computations.) Therefore, this publication should not be used as a definitive comparison of the various numerical methods discussed, since this would require a more extensive and unified study.

The results and discussion presented are instructive in that:

(1) They demonstrate a number of numerical procedures applied by experienced numerical analysts who, however, were not expert in the use of these methods and were required to complete their analyses within a specified time period.

(2) They include solutions for both primitive-variable and vorticity--stream-function systems of equations.

(3) They present solutions for the driven cavity obtained with popular numerical procedures (such as alternating direction implicit, successive overrelaxation, and Marker and Cell) as well as with several techniques that have not been applied extensively (e.g., direct Poisson solvers, spline methods, weighted differencing, artificial compressibility, and hopscotch).

(4) They include some solutions for Reynolds numbers larger than those for which solutions have previously been reported in the literature. This publication is considered suitable for providing graduate students and practitioners of computational fluid dynamics with reference material covering a relatively broad spectrum of numerical procedures for solving the Navier-Stokes equations.

Page Intentionally Left Blank

CONTENTS

1. INCOMPRESSIBLE VISCOUS FLOW IN A DRIVEN CAVITY

Stanley G. Rubin* and Julius E. Harris
Langley Research Center

SUMMARY

In this paper the driven cavity problem is introduced, and the governing equations are given in terms of primitive and vorticity—stream-function variables. The results of the papers in this publication are discussed briefly.

INTRODUCTION

The flow of an incompressible viscous fluid in a cavity driven by a uniformly moving boundary exhibits a number of complex fluid dynamic characteristics of interest including vortex development and boundary-layer development on the walls of the cavity (for high Reynolds numbers). Primarily because of the simple geometry, the incompressible driven cavity problem has received detailed attention in the literature as a test problem for evaluating numerical procedures for solving the Navier-Stokes equations. (See refs. 1 to 10.) Numerical results have been published for Reynolds numbers as large as 1000; however, these results indicate that most currently available numerical procedures deteriorate in accuracy and/or stability for Reynolds numbers much less than 1000. In most of these studies, numerical results were obtained for a Reynolds number of 100; therefore, the results for this Reynolds number should be used as a basis for the evaluation of the various numerical procedures presented in this publication.

SYMBOLS

h	depth of cavity
l	width of cavity
p	pressure
R	Reynolds number, Ul/ν
U	velocity of moving upper surface

*Visiting professor at Old Dominion University, Norfolk, Va. Now professor of aerospace engineering, Polytechnic Institute of New York, Farmingdale, N.Y.

u,v	velocity component in x- and y-direction, respectively
x,y	rectangular coordinates defined in figure 1
ζ	vorticity
ν	kinematic viscosity
ρ	density
ψ	stream function

Subscripts:

t	differentiation with respect to time
x,y	differentiation with respect to x or y

STATEMENT OF PROBLEM

In the present publication, incompressible viscous flow in a cavity driven by a uniformly moving upper surface (see fig. 1) is predicted by several numerical techniques. Solutions are obtained for the Navier-Stokes and continuity equations written in either primitive or vorticity—stream-function variables. These equations are as follows:

Primitive variables

Continuity

$$u_x + v_y = 0 \tag{1a}$$

x-momentum

$$u_t + uu_x + vu_y = -p_x + R^{-1}(u_{xx} + u_{yy}) \tag{1b}$$

y-momentum

$$v_t + uv_x + vv_y = -p_y + R^{-1}(v_{xx} + v_{yy}) \tag{1c}$$

Vorticity—stream-function variables

Vorticity

$$\zeta_t + u\zeta_x + v\zeta_y = R^{-1}(\zeta_{xx} + \zeta_{yy}) \tag{2a}$$

Stream function

$$\psi_{xx} + \psi_{yy} = \zeta \tag{2b}$$

All quantities are nondimensional. Velocities have been nondimensionalized with U, lengths with l, pressure with ρU^2, and time with l/U.

The boundary conditions are presented in figure 1. In several papers contained herein the authors consider a plate moving from right to left so that $u = \psi_y = -1$ at the upper boundary; in addition, ζ is defined as $v_x - u_y$. Direct comparisons with solutions for a plate moving with $u = 1$ are possible if u, v, and ψ are replaced with $-u$, $-v$, and $-\psi$, respectively.

DISCUSSION OF RESULTS

In each paper included in the present publication the square driven cavity has been studied for a standard test case of $R = 100$. This particular case has received the most detailed attention in the literature. In addition to the standard test case, numerical results are presented in some papers for values of R of 10, 1000, and 5000. Some solutions are also given for rectangular cavities having width-depth ratios of 2 and 4. Solutions for $R = 5000$ were obtained with a central-difference alternating-direction implicit procedure for the vorticity equation and a successive overrelaxation or a direct Poisson solver for the stream function. These results for the driven cavity represent, to the best of the authors' knowledge, solutions for the highest Reynolds number currently available in the literature. Other results were obtained with hopscotch, Marker-and-Cell, spline integration, Crocco, weighted-differencing, Chorin, and Spalding procedures.

The results presented in the papers indicate that convergence was more rapid with the vorticity—stream-function formulation. The accuracy of the primitive-variable solutions was extremely sensitive to the convergence tolerance assigned to the pressure solver. As this criterion was refined, computational times escalated.

Divergence form calculations were more accurate than nondivergence results, except for the nondivergence spline solutions. These were more accurate than any of the finite-difference results. This would reflect the higher order accuracy of the convection terms in the spline procedure.

It should be carefully noted that the computer codes developed for the procedures were not necessarily optimized; consequently, no comparisons among the papers are presented concerning computational efficiency (computer processing time and storage requirements). However, the numerical procedures are developed in sufficient detail so that they could be easily used by those interested in either making direct comparisons or applying the procedures to other problems. The intent of the authors is that the present publication should be an outline of the development of specific numerical procedures and their application to a standard test problem. From this viewpoint, the potential users of the various numerical techniques should be able to select the specific procedure which would best satisfy their particular computational requirements.

REFERENCES

1. Bozeman, James D.; and Dalton, Charles: Numerical Study of Viscous Flow in a Cavity. J. Comput. Phys., vol. 12, no. 3, July 1973, pp. 348-363.

2. Brailovskaya, I. Yu: A Difference Scheme for Numerical Solution of the Two-Dimensional Nonstationary Navier-Stokes Equations for a Compressible Gas. Sov. Phys. – Doklady, vol. 10, no. 2, Aug. 1965, pp. 107-110.

3. Burggraf, Odus R.: Analytical and Numerical Studies of the Structure of Steady Separated Flows. J. Fluid Mech., vol. 24, pt. 1, Jan. 1966, pp. 113-151.

4. Donovan, Leo F.: Numerical Solution of the Unsteady Navier-Stokes Equations and Application to Flow in a Rectangular Cavity With a Moving Wall. NASA TN D-6312, 1971.

5. Lambiotte, Jules J., Jr.; and Howser, Lona M.: Vectorization on the STAR Computer of Several Numerical Methods for a Fluid Flow Problem. NASA TN D-7545, 1974.

6. Mills, Ronald D.: Numerical Solutions of the Viscous Flow Equations for a Class of Closed Flows. J. Ray. Aeronaut. Soc., vol. 69, no. 658, Oct. 1965, pp. 714-718; Correction, vol. 69, no. 660, Dec. 1965, p. 880.

7. Nallasamy, M.; and Prasad, K. Krishna: Numerical Studies on Quasilinear and Linear Elliptic Equations. J. Comput. Phys., vol. 15, no. 4, Aug. 1974, pp. 429-448.

8. Pan, Frank; and Acrivos, Andreas: Steady Flows in Rectangular Cavities. J. Fluid Mech., vol. 28, pt. 4, June 22, 1967, pp. 643-655.

9. Roache, P. J.: Finite Difference Methods for the Steady-State Navier-Stokes Equations. Proceedings of the 3rd International Conference on Numerical Methods in Fluid Mechanics. Volume 1. Springer-Verlag, 1973, pp. 138-145.

10. Runchal, A. K.; Spalding, D. B.; and Wolfshtein, M.: The Numerical Solution of Elliptic Equations for Transport of Vorticity, Heat and Matter in Two-Dimensional Flows. Rep. No. SF/TN/2, Dep. Mech. Eng., Imperial College Sci. & Technol., Aug. 1967.

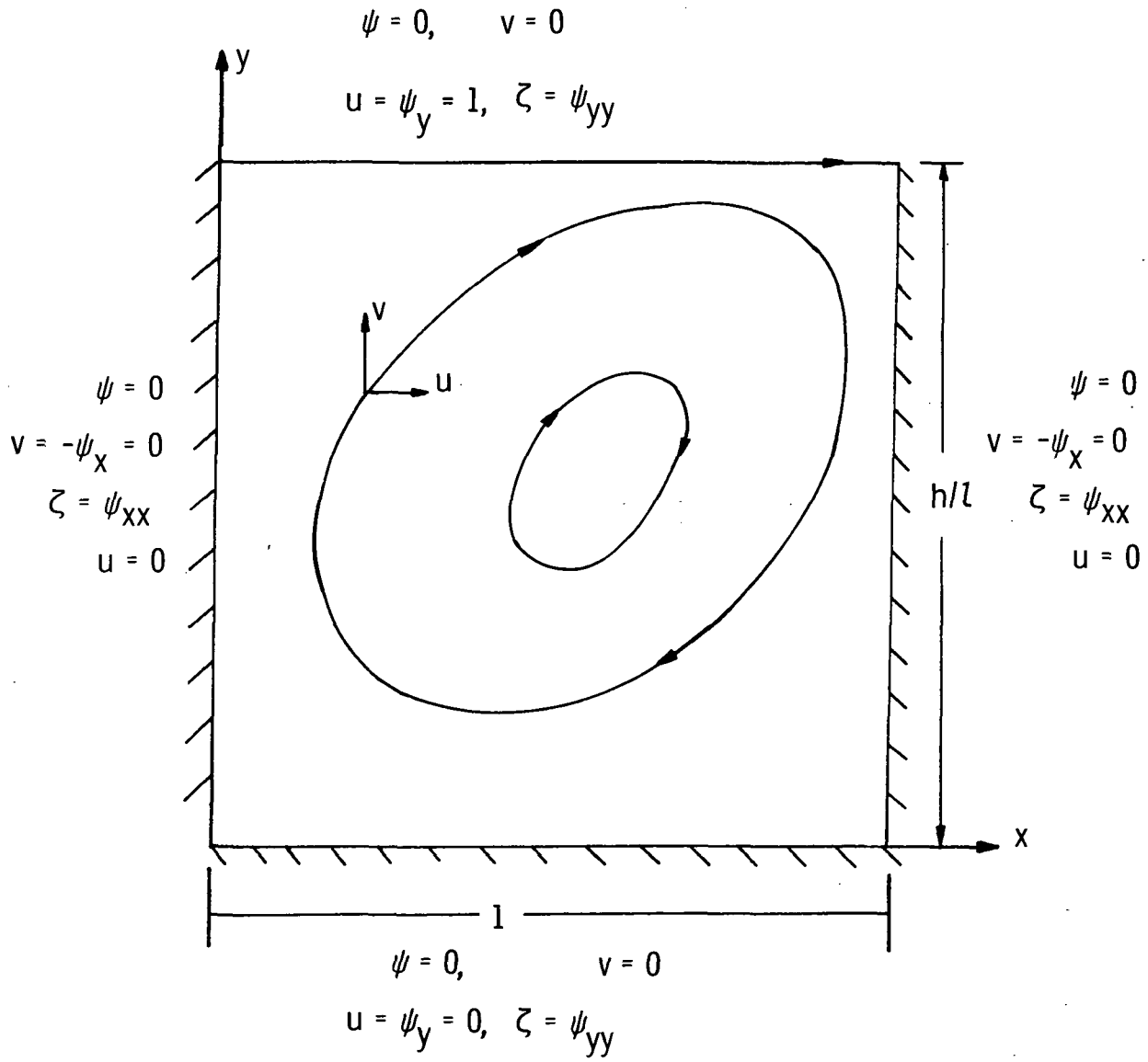

Figure 1.- Schematic of the driven cavity.

2. APPLICATION OF UPSTREAM WEIGHTED DIFFERENCING TO THE DRIVEN CAVITY PROBLEM

Lillian R. Boney
Langley Research Center

SUMMARY

The problem considered is steady plane flow of an incompressible viscous fluid in a two-dimensional square cavity in which the motion is driven by uniform translation of the upper wall which moves across the cavity from left to right at a constant speed of 1. Numerical solutions of the Navier-Stokes equations are obtained for a range of Reynolds number from 100 to 1000. Upstream weighted differencing is used when the local cell Reynolds number exceeds 2.

INTRODUCTION

It is well-known that the flow of viscous fluid can be treated successfully with the Navier-Stokes equations. Many authors have examined finite-difference solutions of the equations of steady-state motion and continuity in a two-dimensional domain. Some found that unless the mesh size was severely reduced, their computational procedures failed to converge when the Reynolds number became large.

This paper treats steady plane flow of an incompressible viscous fluid in a two-dimensional square cavity in which the motion is driven by uniform translation of the upper wall which moves across the cavity from left to right at a constant speed of 1. (See paper no. 1 by Rubin and Harris.) The two momentum equations and the continuity equation, written in normalized conservative form in terms of the primitive variables (velocity components u and v and the pressure p), are used rather than the stream-function and vorticity transport equations. The pressure term is treated by a Poisson equation. The primitive-variable system involves two parabolic momentum transport equations and one elliptic equation with all Neumann boundaries. Upstream weighted differencing (ref. 1) for the velocity gradients is chosen for its good stability properties and the transportive property which finite-difference formulation of a flow equation possesses if the effect of a perturbation in a transport property is advected only in the direction of the velocity.

SYMBOLS

K	constant in equation (5)
p	pressure
$\hat{p}$	error in initial estimate of p
p_o	initial estimate of p
R	Reynolds number
R_c	cell Reynolds number
S	$= \nabla^2 \hat{p}$
t	time
Δt	time step
u	axial velocity component
v	normal velocity component
W	weighting factor based on R_c (see eqs. (7))
w	factor in equation (22)
x	axial coordinate
y	normal coordinate
$\Delta x, \Delta y$	grid spacing in x- and y-directions
β	$= \Delta x / \Delta y$

Superscripts:

k	index of iteration
n	index of time step

Subscripts:

i,j	index of grid spacing in x- and y-direction, respectively
ref	reference

GOVERNING EQUATIONS

The governing equations are the two momentum equations and the continuity equation. These are written as follows in forms of the primitive variables, velocity components u and v and pressure p, in a normalized conservative form:

$$\frac{\partial u}{\partial t} + \frac{\partial (u^2)}{\partial x} + \frac{\partial (vu)}{\partial y} = -\frac{\partial p}{\partial x} + \frac{1}{R}\left(\frac{\partial^2 u}{\partial x^2} + \frac{\partial^2 u}{\partial y^2}\right) \tag{1}$$

$$\frac{\partial v}{\partial t} + \frac{\partial (uv)}{\partial x} + \frac{\partial (v^2)}{\partial y} = -\frac{\partial p}{\partial y} + \frac{1}{R}\left(\frac{\partial^2 v}{\partial x^2} + \frac{\partial^2 v}{\partial y^2}\right) \tag{2}$$

$$\frac{\partial u}{\partial x} + \frac{\partial v}{\partial y} = 0 \tag{3}$$

where R is the dimensionless Reynolds number. The Poisson equation for pressure is

$$\nabla^2 \hat{p} = S = -\frac{\partial u}{\partial x} - \frac{\partial v}{\partial y} \tag{4}$$

where

$$p = p_o - \hat{p}$$

and p_o is the initial estimate of p.

FINITE-DIFFERENCE REPRESENTATIONS

For numerical integration of the governing equations, the entire region of the cavity is divided into a finite number of grid points having coordinates $x = i\,\Delta x$ and $y = j\,\Delta y$. The grid spacings in the x- and y-directions are denoted by Δx and Δy. An approximate solution of the equations is obtained at these grid points at discrete times t^n. The symbol t^n denotes the time level after the nth time step. Practical stability imposes a restriction on the size of the time step Δt. Limited numerical experience suggests the following restriction:

$$\Delta t = \frac{K}{\frac{2}{R}\left[\frac{1}{(\Delta x)^2} + \frac{1}{(\Delta y)^2}\right] + \frac{|u_{i,j}|}{\Delta x} + \frac{|v_{i,j}|}{\Delta y}} \tag{5}$$

where K is generally taken to be 1.

An explicit procedure was used to calculate quantities at time $n + 1$ in terms of their values at time n. The velocity gradients are calculated by an upstream weighted differencing method. (See refs. 1.) This method involves one-sided rather than space-centered differencing. Backward differences are used when the velocities are positive and forward differences are used when the velocities are negative. Thus the one-sided difference is always on the upstream side of the point at which the gradients of the velocities are being evaluated. Upstream differencing is not stability limited by a cell Reynolds number

$$R_c = \frac{|u_{i,j}|\,\Delta x + |v_{i,j}|\,\Delta y}{1/R} \tag{6}$$

A weighting factor W based on R_c is introduced. For R_c less than or equal to 2, the weighting factor becomes zero, and the differencing method becomes space-centered differencing. As R_c approaches infinity, W approaches 1, and the differencing method becomes upstream differencing. That is,

$$\left.\begin{aligned} W &= 0 && (R_c \leq 2) \\ W &= 1 - \frac{2}{R_c} && (R_c > 2) \end{aligned}\right\} \tag{7}$$

Use of the weighting factor enables changes in flow direction to be accounted for, and adjustments are made with no discontinuity. For forward time differencing the equations are

$$\frac{\partial u}{\partial t} = \frac{u_{i,j}^{n+1} - u_{i,j}^{n}}{\Delta t} \tag{8}$$

$$\frac{\partial v}{\partial t} = \frac{v_{i,j}^{n+1} - v_{i,j}^{n}}{\Delta t} \tag{9}$$

The following terms are evaluated by central differencing:

$$\frac{\partial^2 v}{\partial x^2} = \frac{v_{i+1,j} + v_{i-1,j} - 2v_{i,j}}{(\Delta x)^2} \tag{10}$$

$$\frac{\partial^2 v}{\partial y^2} = \frac{v_{i,j+1} + v_{i,j-1} - 2v_{i,j}}{(\Delta y)^2} \tag{11}$$

$$\frac{\partial^2 u}{\partial x^2} = \frac{u_{i+1,j} + u_{i-1,j} - 2u_{i,j}}{(\Delta x)^2} \tag{12}$$

$$\frac{\partial^2 u}{\partial y^2} = \frac{u_{i,j+1} + u_{i,j-1} - 2u_{i,j}}{(\Delta y)^2} \tag{13}$$

$$\frac{\partial p}{\partial x} = \frac{p_{i+1,j} - p_{i-1,j}}{2\,\Delta x} \tag{14}$$

$$\frac{\partial p}{\partial y} = \frac{p_{i,j+1} - p_{i,j-1}}{2\,\Delta y} \tag{15}$$

The following terms are evaluated by upstream weighted differencing:

$$\frac{\partial u}{\partial x} = \frac{1}{\Delta x}\left[\frac{W}{2}\left(1 + \frac{u_{i,j}}{|u_{i,j}|}\right)(u_{i,j} - u_{i-1,j}) + \frac{W}{2}\left(1 - \frac{u_{i,j}}{|u_{i,j}|}\right)(u_{i+1,j} - u_{i,j}) + \frac{1 - W}{2}(u_{i+1,j} - u_{i-1,j})\right] \tag{16}$$

$$\frac{\partial u^2}{\partial x} = \frac{1}{\Delta x}\left[\frac{W}{2}\left(1 + \frac{u_{i,j}}{|u_{i,j}|}\right)\left(u_{i,j}^2 - u_{i-1,j}^2\right) + \frac{W}{2}\left(1 - \frac{u_{i,j}}{|u_{i,j}|}\right)\left(u_{i+1,j}^2 - u_{i,j}^2\right) + \frac{1 - W}{2}\left(u_{i+1,j}^2 - u_{i-1,j}^2\right)\right] \tag{17}$$

$$\frac{\partial v}{\partial y} = \frac{1}{\Delta y}\left[\frac{W}{2}\left(1 + \frac{v_{i,j}}{|v_{i,j}|}\right)\left(v_{i,j} - v_{i,j-1}\right) + \frac{W}{2}\left(1 - \frac{v_{i,j}}{|v_{i,j}|}\right)\left(v_{i,j+1} - v_{i,j}\right) + \frac{1 - W}{2}\left(v_{i,j+1} - v_{i,j-1}\right)\right] \tag{18}$$

$$\frac{\partial v^2}{\partial y} = \frac{1}{\Delta y}\left[\frac{W}{2}\left(1 + \frac{v_{i,j}}{|v_{i,j}|}\right)\left(v_{i,j}^2 - v_{i,j-1}^2\right) + \frac{W}{2}\left(1 - \frac{v_{i,j}}{|v_{i,j}|}\right)\left(v_{i,j+1}^2 - v_{i,j}^2\right) + \frac{1 - W}{2}\left(v_{i,j+1}^2 - v_{i,j-1}^2\right)\right] \tag{19}$$

$$\frac{\partial uv}{\partial x} = \frac{1}{\Delta x}\left[\frac{W}{2}\left(1 + \frac{u_{i,j}}{|u_{i,j}|}\right)\left(u_{i,j}v_{i,j} - u_{i-1,j}v_{i-1,j}\right) + \frac{W}{2}\left(1 - \frac{u_{i,j}}{|u_{i,j}|}\right)\left(u_{i+1,j}v_{i+1,j} - u_{i,j}v_{i,j}\right)\right.$$

$$\left. + \frac{1 - W}{2}\left(u_{i+1,j}v_{i+1,j} - u_{i-1,j}v_{i-1,j}\right)\right] \tag{20}$$

$$\frac{\partial vu}{\partial y} = \frac{1}{\Delta y}\left[\frac{W}{2}\left(1 + \frac{v_{i,j}}{|v_{i,j}|}\right)\left(v_{i,j}u_{i,j} - v_{i,j-1}u_{i,j-1}\right) + \frac{W}{2}\left(1 - \frac{v_{i,j}}{|v_{i,j}|}\right)\left(v_{i,j+1}u_{i,j+1} - v_{i,j}u_{i,j}\right)\right.$$

$$\left. + \frac{1 - W}{2}\left(v_{i,j+1}u_{i,j+1} - v_{i,j-1}u_{i,j-1}\right)\right] \tag{21}$$

SPALDING METHOD FOR PRESSURE CALCULATION

The Poisson equation for pressure (eq. (4)) with all Neumann boundaries on which values of the normal gradient $\partial\hat{p}/\partial n$ are zero is solved by an iterative Liebman method.

For the initial iteration, $\hat{p}_{i,j}$ is assumed to be zero at all grid points. For interior grid points,

$$\hat{p}_{i,j}^{k+1} = \hat{p}_{i,j}^{k} + \frac{w}{2(1+\beta^2)}\left[\hat{p}_{i+1,j}^{k} + \hat{p}_{i-1,j}^{k+1} + \beta^2\hat{p}_{i,j+1}^{k} + \beta^2\hat{p}_{i,j-1}^{k+1} - (\Delta x)^2 S_{i,j} - 2(1+\beta^2)\hat{p}_{i,j}^{k}\right] \tag{22}$$

where

$$\beta = \frac{\Delta x}{\Delta y} = 1 \qquad w = 1 \qquad S_{i,j} = -\frac{\partial u}{\partial x} - \frac{\partial v}{\partial y}$$

An arbitrary limit is set to the number of iterations for the interior grid points, and the Neumann conditions are applied at the boundaries by setting the boundary points equal to the adjacent interior points.

The pressure p_{ref} is held at zero at a reference location chosen to be the center of the wall opposite the "driving" boundary. After an arbitrary number of iterations the pressure is corrected at all grid points by $p = p_o - \hat{p}^{k+1} + \hat{p}_{ref}$. The values of $u_{i,j}^{n+1}$ and $v_{i,j}^{n+1}$ are corrected by setting

$$u_{i,j}^{n+1} = u_{i,j}^{n+1} + \left(\hat{p}_{i+1,j}^{k+1} - \hat{p}_{i-1,j}^{k+1}\right)\frac{\Delta t}{2\,\Delta x} \tag{23}$$

$$v_{i,j}^{n+1} = v_{i,j}^{n+1} + \left(\hat{p}_{i,j+1}^{k+1} - \hat{p}_{i,j-1}^{k+1}\right)\frac{\Delta t}{2\,\Delta y} \tag{24}$$

The velocities u^n and v^n are replaced by u^{n+1} and v^{n+1}, and the procedure is repeated for the next time step. Numerical calculations were carried forward in time until a steady state was approached. Calculations were discontinued when the maximum values of $|u^{n+1} - u^n|$ and $|v^{n+1} - v^n|$ were less than 0.0005. Values of $(u^{n+1} - u^n)/u^{n+1}$, $(u^{n+1} - u^n)/\Delta t$, and $\sum_{i,j}\left|u_{i,j}^{n+1} - u_{i,j}^{n}\right| + \left|v_{i,j}^{n+1} - v_{i,j}^{n}\right|$ were also computed for comparison.

Approximately 0.25 second was required on the CDC 6600 computer for one time step and a 15×15 grid.

RESULTS

Table I contains the number of time steps required to approach steady state at various conditions. Reynolds numbers of 100, 400, and 1000 were chosen. Grid sizes of 15×15, 29×29, and 57×57 and factors of 0.5, 1, 2, and 2.5 for the Δt restriction were used. Generally 10 iterations for $\hat{p}$ were calculated, and a check was made by using 5 and 20 iterations.

Table II contains the numerical values of p, u, and v after 187 time steps for $R = 100$, a 15×15 grid, $\Delta t = 0.0458$, and 10 iterations of $\hat{p}$. Figure 1 indicates the direction but not the magnitude of the velocity vectors and figure 2 is a contour plot of lines of constant pressure for the same case. Figures 3 and 4 show the velocity and the pressure profiles through the center of the vortex.

The velocity vectors and velocity profiles through the center of vortex for $R = 100$ compare well with those shown by Mills (ref. 2). The pressure distributions through the center of the vortex are similar but less smooth than those shown by Mills. The lines of constant pressure were compared with those shown by Kawaguti (ref. 3) for $R = 64$ and were less smooth.

CONCLUDING REMARKS

The method of upstream weighted differencing has been applied to the driven cavity problem. Results for the square cavity with a Reynolds number of 100 have indicated that the velocity information obtained is in good agreement with results obtained by other methods. The pressure information obtained does not agree as well and seems to be less reliable.

REFERENCES

1. Roache, Patrick J.: Computational Fluid Dynamics. Hermosa Publ., c.1972.

2. Mills, Ronald D.: Numerical Solutions of the Viscous Flow Equations for a Class of Closed Flows. J. Roy. Aeronaut. Soc., vol. 69, no. 658, Oct. 1965, pp. 714-718; Correction, vol. 69, no. 660, Dec. 1965, p. 880.

3. Kawaguti, Mitutosi: Numerical Solution of the Navier-Stokes Equations for the Flow in a Two-Dimensional Cavity. J. Phys. Soc. Jap., vol. 16, no. 11, Nov. 1961, pp. 2307-2315.

TABLE I.- TIME STEPS TO APPROACH STEADY STATE

R	Grid	K (eq. (5))	Δt	$\hat{p}$ iterations	Time steps	Convergence, $u^{n+1} - u^n$
100	15 × 15	1.0	0.0458	10	187	0.48×10^{-3}
		1.0	.0458	5	220	$.45 \times 10^{-3}$
		1.0	.0458	20	170	$.50 \times 10^{-3}$
100	15 × 15	.5	.0229	10	220	$.49 \times 10^{-3}$
		2.0	.0916	10	150	$.50 \times 10^{-3}$
		2.5	.1144	10	20	Nonconvergence
100	29 × 29	.5	.0084	10	500	$.33 \times 10^{-3}$
		1.0	.0168	10	360	$.50 \times 10^{-3}$
400	15 × 15	1.0	.0627	10	250	$.50 \times 10^{-3}$
1000	15 × 15	.5	.0338	10	1730	$.46 \times 10^{-2}$
		1.0	.0676	10	1170	$.87 \times 10^{-3}$
1000	29 × 29	.5	.0160	10	960	$.11 \times 10^{-2}$
		1.0	.0321	10	600	$.13 \times 10^{-2}$
1000	57 × 57	1.0	.0146	10	240	$.20 \times 10^{-2}$

TABLE II.- NUMERICAL VALUES OF PRIMATIVE VARIABLES AFTER 187 TIME STEPS

[Each value computed at a grid point (i,j); columns correspond to i = 1, 2, 3, . . ., 15 and lines to j = 15, 14, 13, . . ., 1]

Pressure, p														
-.152	-.152	-.025	-.049	-.011	-.022	-.020	-.024	-.027	-.021	-.000	.043	.101	.264	.264
-.152	-.152	-.025	-.049	-.011	-.022	-.020	-.024	-.027	-.021	-.000	.043	.101	.264	.264
-.064	-.064	-.036	-.044	-.031	-.036	-.035	-.037	-.040	-.034	-.026	.010	.037	.127	.127
-.057	-.057	-.033	-.039	-.027	-.031	-.031	-.034	-.036	-.031	-.024	.008	.033	.095	.095
-.027	-.027	-.025	-.028	-.026	-.029	-.030	-.033	-.034	-.030	-.026	-.003	.009	.041	.041
-.022	-.022	-.021	-.021	-.020	-.022	-.023	-.024	-.024	-.020	-.014	.002	.013	.028	.028
-.011	-.011	-.013	-.014	-.015	-.016	-.017	-.017	-.016	-.012	-.008	.003	.010	.014	.014
-.007	-.007	-.009	-.009	-.010	-.010	-.010	-.010	-.009	-.005	-.001	.005	.009	.008	.008
-.003	-.003	-.005	-.005	-.006	-.006	-.006	-.005	-.004	-.001	.002	.005	.007	.005	.005
-.001	-.001	-.004	-.003	-.004	-.003	-.003	-.002	-.001	.001	.003	.005	.006	.004	.004
-.000	-.000	-.002	-.002	-.002	-.002	-.002	-.001	.000	.002	.004	.004	.005	.003	.003
-.000	-.000	-.002	-.001	-.002	-.001	-.001	.000	.001	.002	.004	.004	.005	.003	.003
-.001	-.001	-.003	-.002	-.002	-.002	-.001	-.000	.001	.002	.003	.004	.004	.003	.003
-.001	-.001	-.003	-.003	-.003	-.002	-.001	0.000	.002	.003	.005	.005	.006	.005	.005
-.001	-.001	-.003	-.003	-.003	-.002	-.001	0.000	.002	.003	.005	.005	.006	.005	.005
Axial velocity, u														
1.000	1.000	1.000	1.000	1.000	1.000	1.000	1.000	1.000	1.000	1.000	1.000	1.000	1.000	1.000
0.000	.130	.193	.289	.340	.402	.446	.484	.512	.526	.517	.487	.382	.294	0.000
0.000	-.040	-.020	.023	.060	.112	.150	.190	.216	.234	.225	.204	.129	.084	0.000
0.000	-.056	-.065	-.053	-.041	-.012	.009	.032	.043	.047	.030	.011	-.029	-.021	0.000
0.000	-.030	-.048	-.061	-.068	-.065	-.063	-.060	-.062	-.067	-.081	-.086	-.091	-.059	0.000
0.000	-.023	-.044	-.065	-.081	-.092	-.103	-.111	-.122	-.131	-.140	-.133	-.112	-.065	0.000
0.000	-.016	-.037	-.061	-.083	-.102	-.120	-.135	-.148	-.155	-.155	-.139	-.104	-.054	0.000
0.000	-.013	-.034	-.058	-.081	-.103	-.122	-.138	-.149	-.153	-.146	-.124	-.084	-.040	0.000
0.000	-.010	-.029	-.052	-.074	-.096	-.114	-.128	-.136	-.136	-.125	-.101	-.063	-.027	0.000
0.000	-.008	-.025	-.046	-.066	-.085	-.101	-.112	-.117	-.114	-.100	-.078	-.046	-.018	0.000
0.000	-.006	-.020	-.038	-.055	-.072	-.085	-.094	-.097	-.092	-.078	-.059	-.033	-.013	0.000
0.000	-.004	-.015	-.030	-.044	-.058	-.069	-.075	-.076	-.071	-.060	-.044	-.025	-.009	0.000
0.000	-.002	-.010	-.021	-.032	-.042	-.050	-.055	-.056	-.052	-.043	-.031	-.017	-.007	0.000
0.000	.001	-.004	-.011	-.017	-.024	-.029	-.032	-.032	-.030	-.024	-.017	-.010	-.004	0.000
0.000	0.000	0.000	0.000	0.000	0.000	0.000	0.000	0.000	0.000	0.000	0.000	0.000	0.000	0.000
Normal velocity, v														
0.000	0.000	0.000	0.000	0.000	0.000	0.000	0.000	0.000	0.000	0.000	0.000	0.000	0.000	0.000
0.000	.173	.118	.112	.080	.062	.047	.035	.023	.009	-.017	-.051	-.108	-.172	0.000
0.000	.203	.164	.166	.125	.107	.086	.066	.043	.014	-.037	-.107	-.200	-.279	0.000
0.000	.150	.179	.187	.164	.145	.119	.092	.058	.011	-.054	-.143	-.230	-.274	0.000
0.000	.132	.167	.181	.166	.150	.125	.094	.053	-.003	-.076	-.167	-.236	-.249	0.000
0.000	.102	.146	.163	.157	.143	.120	.087	.044	-.014	-.082	-.159	-.202	-.189	0.000
0.000	.084	.124	.140	.136	.124	.102	.071	.029	-.024	-.083	-.142	-.166	-.138	0.000
0.000	.064	.099	.114	.113	.102	.083	.055	.018	-.027	-.073	-.115	-.125	-.093	0.000
0.000	.049	.077	.089	.089	.080	.063	.040	.010	-.025	-.059	-.086	-.088	-.059	0.000
0.000	.035	.057	.066	.067	.060	.047	.029	.006	-.020	-.043	-.059	-.058	-.036	0.000
0.000	.023	.039	.046	.047	.042	.033	.020	.004	-.013	-.028	-.037	-.034	-.019	0.000
0.000	.014	.024	.029	.030	.027	.022	.014	.004	-.007	-.015	-.019	-.017	-.008	0.000
0.000	.007	.013	.016	.016	.015	.013	.009	.004	-.001	-.005	-.006	-.005	-.001	0.000
0.000	.004	.006	.007	.007	.007	.006	.005	.004	.002	.001	.000	.001	.002	0.000
0.000	0.000	0.000	0.000	0.000	0.000	0.000	0.000	0.000	0.000	0.000	0.000	0.000	0.000	0.000

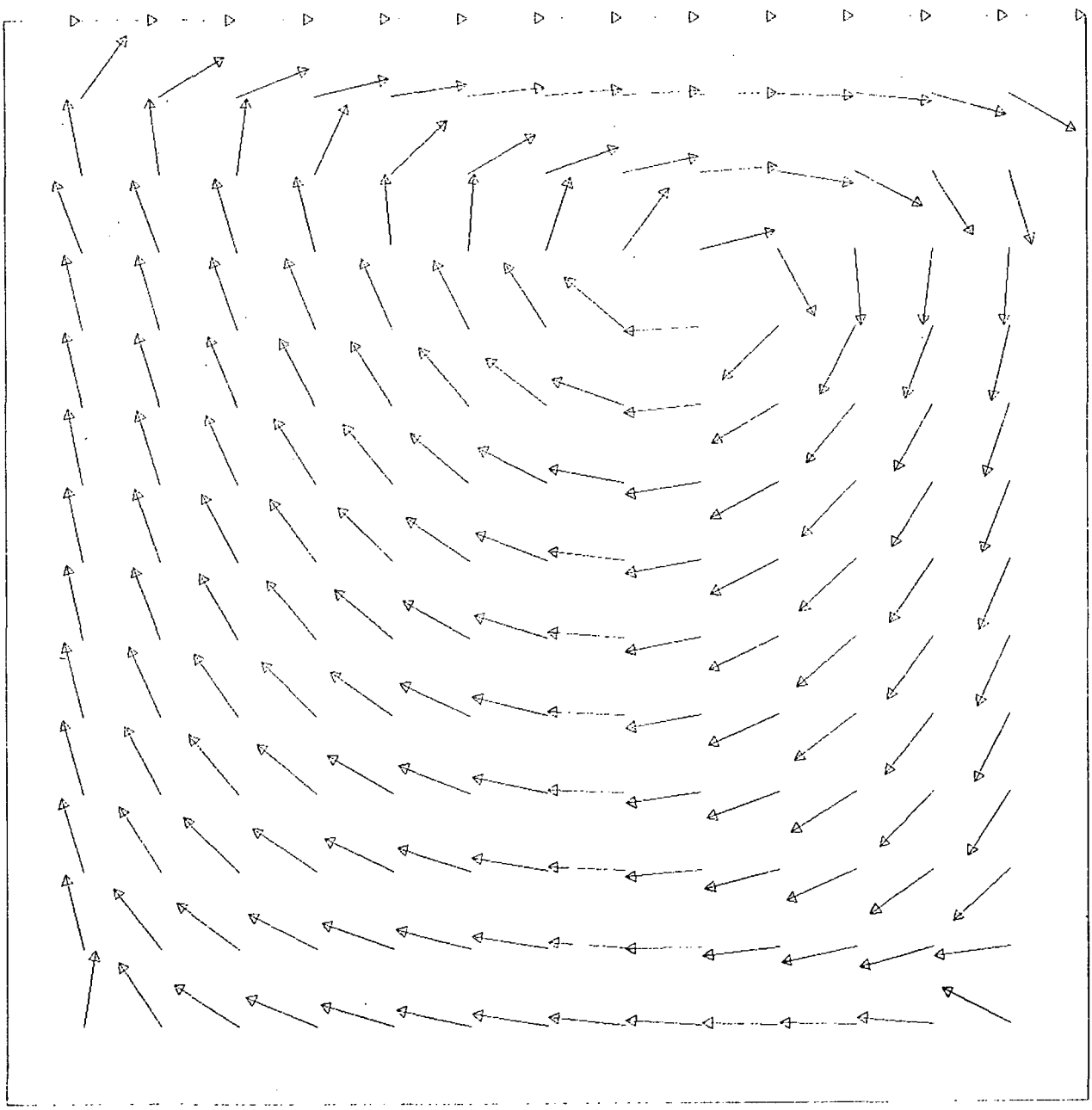

Figure 1.- Direction of velocity vectors. R = 100; 15 × 15 grid.

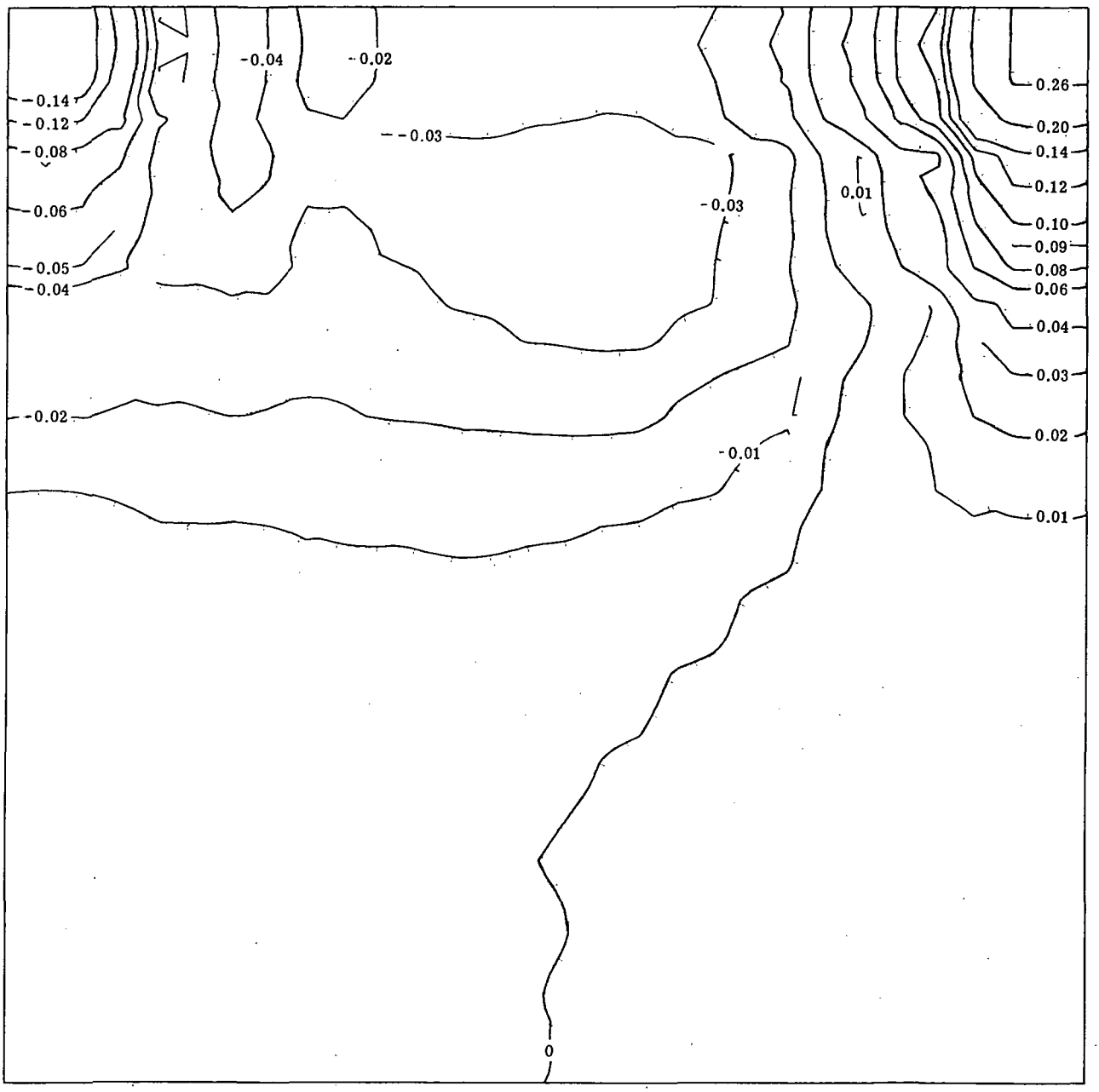

Figure 2.- Contour plot of lines of constant pressure. R = 100; 15 × 15 grid.

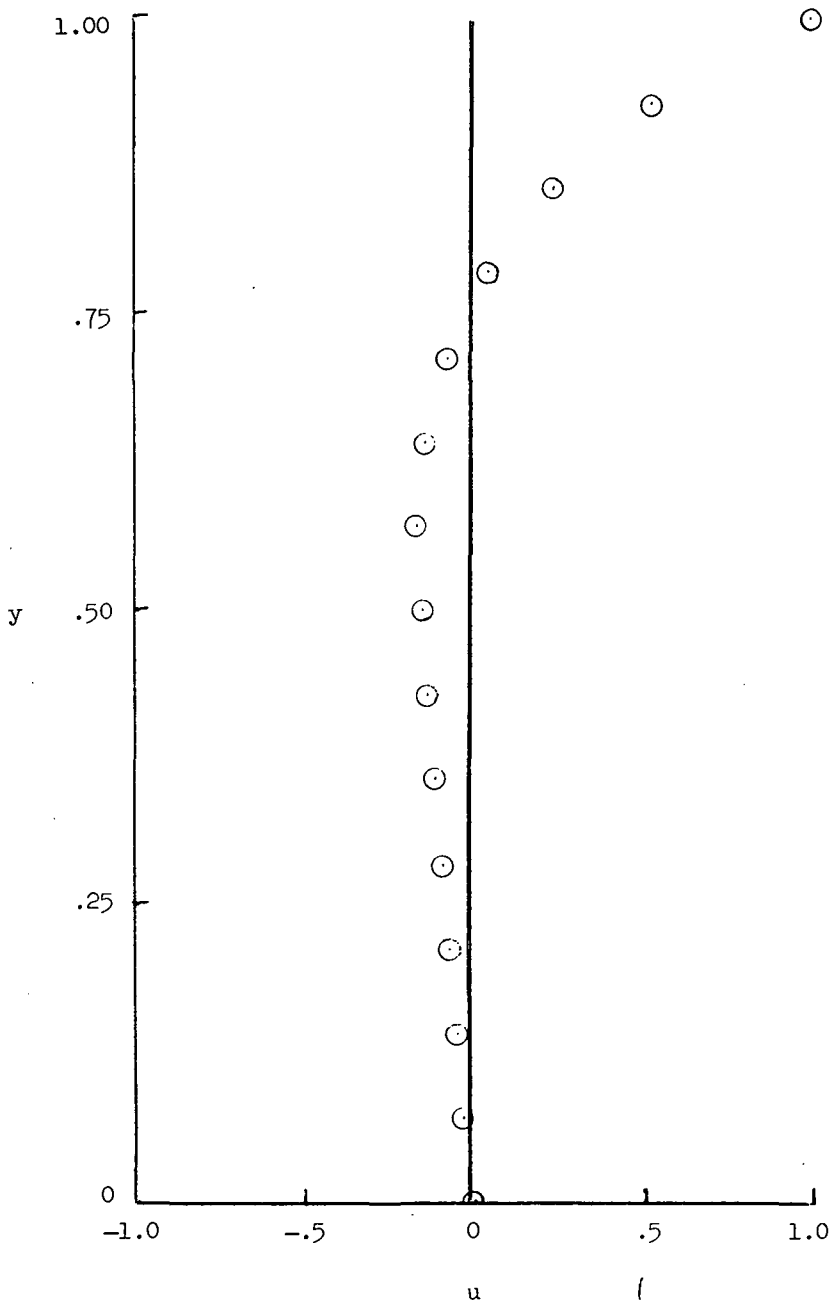

(a) u-profile.

Figure 3.- Velocity profiles through center of vortex.
R = 100; 15 × 15 grid.

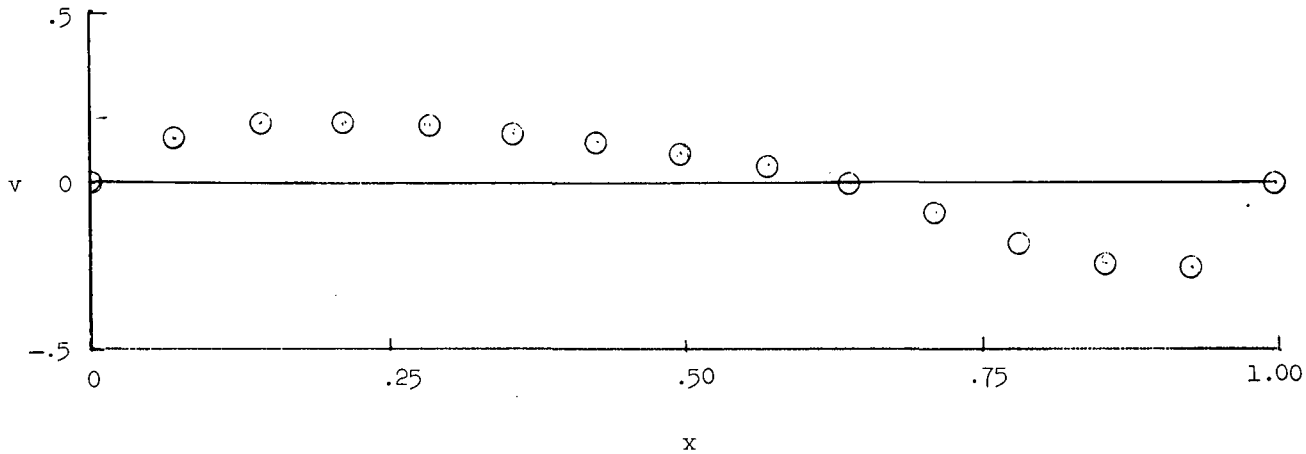

(b) v-profile.

Figure 3.- Concluded.

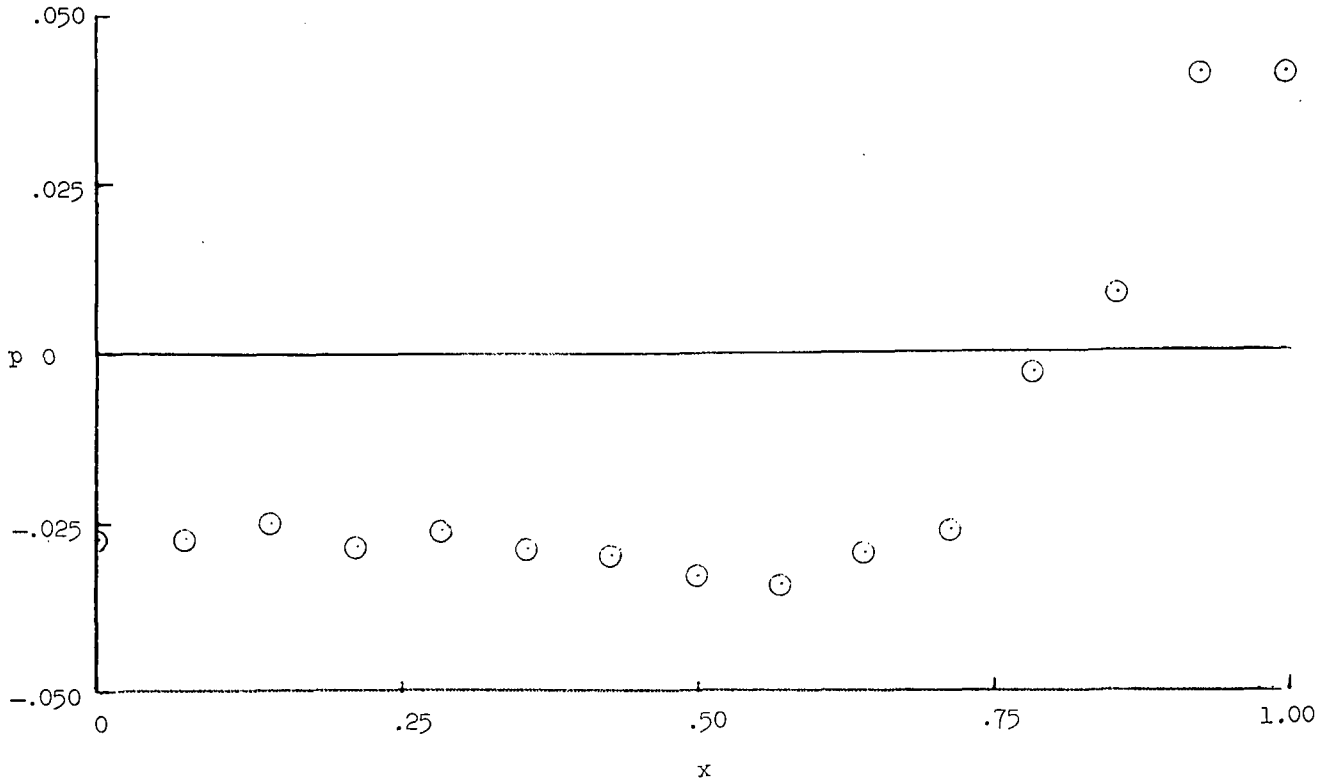

(a) Horizontal pressure profile.

Figure 4.- Pressure profiles through center of vortex. R = 100; 15 × 15 grid.

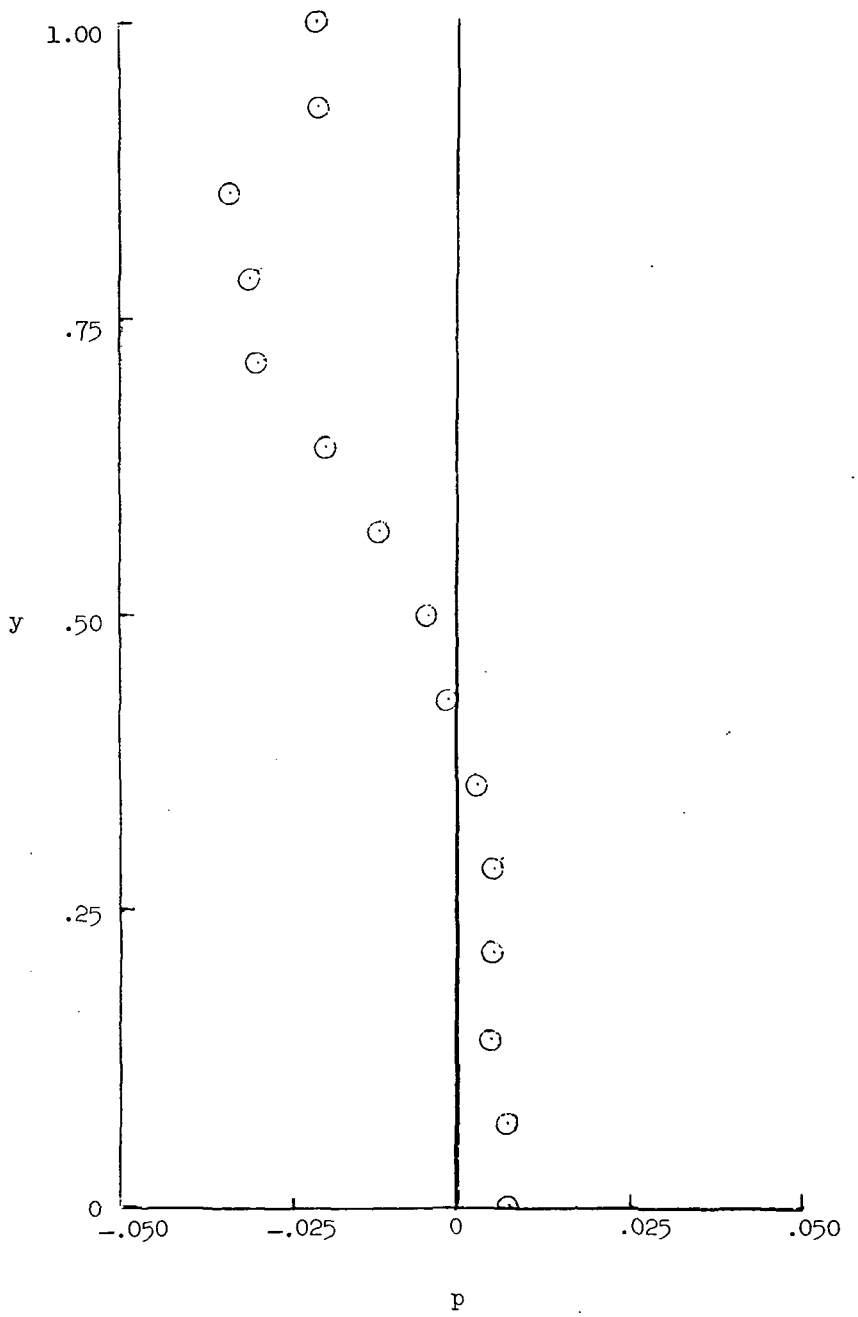

(b) Vertical pressure profile.

Figure 4.- Concluded.

3. SOLUTION OF THE INCOMPRESSIBLE DRIVEN CAVITY PROBLEM USING THE CROCCO METHOD

Jerry N. Hefner
Langley Research Center

SUMMARY

The Crocco method has been used to solve the steady Navier-Stokes equations for two-dimensional flow in a square driven cavity for a Reynolds number of 100. The The Spalding SIMPLE procedure was used to solve the pressure-linked equations. Results for velocity and pressure were found to be inaccurate, although the overall recirculation and vortex center were correctly predicted.

INTRODUCTION

During the past decade, the evolution of large high-speed computers has allowed the development of numerous explicit and implicit finite-difference schemes for solving the steady Navier-Stokes equations. In general, these numerical procedures have not been rigorously tested on a variety of problems. Consequently, the value of a given method for solving a multiplicity of fluid dynamics problems often has not been ascertained. In this paper, results of a numerical study to predict the velocity profiles and pressure distribution in the simple two-dimensional driven cavity with width-depth ratio of 1 (square cavity) and Reynolds number of 100 are presented. (See paper no. 1 by Rubin and Harris for details of driven cavity problem.) The method used is that attributed to Crocco (ref. 1) with the Spalding SIMPLE procedure (ref. 2) for solving the pressure-linked equations.

SYMBOLS

l	width of cavity
Δl	spatial increment in x and y
p	pressure
$\hat{p}$	error in pressure (eq. (9))
p_0	initial estimate of p

q	actual velocity vector
q*	calculated velocity vector (eq. (9))
R	Reynolds number, $\frac{\overline{U}\overline{l}}{\overline{\nu}}$
t	time
Δt	time step
$\overline{U}$	velocity in x-direction at edge of cavity
u	velocity in x-direction
v	velocity in y-direction
x,y	axial and normal coordinate of cavity, respectively
Γ	variable used in equations (5) to (8)
$\overline{\nu}$	viscosity
$\overline{\rho}$	density
ω	variable in successive overrelaxation method given in equation (12)

Superscripts:

k	iteration number
n	time step number

Subscripts:

i	step in x-direction
j	step in y-direction

t differentiation with respect to time

x,y differentiation with respect to x or y

Bars over symbols denote dimensional quantities.

METHOD OF ANALYSIS

The nondimensional viscous incompressible flow equations in primitive variables are

$$u_x + v_y = 0 \tag{1}$$

$$u_t + uu_x + vu_y + p_x = \frac{1}{R}(u_{xx} + u_{yy}) \tag{2}$$

$$v_t + uv_x + vv_y + p_y = \frac{1}{R}(v_{xx} + v_{yy}) \tag{3}$$

The variables have been nondimensionalized with respect to $\overline{U}$ and $\overline{l}$; that is,

$$\left.\begin{aligned} p &= \frac{\overline{p}}{\overline{\rho}\overline{U}^2} & t &= \frac{\overline{t}\overline{U}}{\overline{l}} \\ u &= \frac{\overline{u}}{\overline{U}} & v &= \frac{\overline{v}}{\overline{U}} \\ x &= \frac{\overline{x}}{\overline{l}} & y &= \frac{\overline{y}}{\overline{l}} \end{aligned}\right\} \tag{4}$$

The boundary conditions are as follows:

at $y = 0$ $\quad u = v = 0$

at $y = 1$ $\quad u = 1$ and $v = 0$

at $x = 0$ $\quad u = v = 0$

at $x = 1$ $\quad u = v = 0$

The Crocco method (ref. 1) was applied to the x- and y-momentum equations (eq. (2) and (3), respectively) to solve for velocities u and v. The method presented by Crocco

is actually an iteration procedure which avoids the difficulties associated with numerical solution of the steady Navier-Stokes equations by considering the steady flow as the asymptotic form of a time-dependent flow. These transient flow calculations, although both inaccurate and inconsistent, are used only as an iteration procedure and permit freedom in choosing numerical differencing schemes which best fit the desired stability requirements. In the Crocco method, the convective terms are redefined in terms of their values at time steps n and $n - 1$ by means of a variable Γ which can be chosen to account for various differencing schemes (e.g., for $\Gamma = 0$, the differencing scheme is simply forward time and centered space, whereas for $\Gamma = 1/2$, the method becomes the well-known Adams-Bashforth method). As an illustration of the redefinition, the convective terms in the x-momentum equation (2) become

$$uu_x = (1 + \Gamma)u^n u_x^n - \Gamma u^{n-1} u_x^{n-1} \tag{5}$$

$$vu_y = (1 + \Gamma)v^n u_y^n - \Gamma v^{n-1} u_y^{n-1} \tag{6}$$

Modified forward time and centered space differencing (i.e., the values of $u_{i,j}$ and $v_{i,j}$ in the spatial derivatives are evaluated at time $n + 1$ instead of n) is applied to the appropriate derivatives. Values of Γ between 0 and 1.0 are chosen depending on the desired stability requirements. (For stability, the Crocco method requires that $\Gamma > 1/2$.)

Application of the Crocco method to equations (2) and (3) gives the following difference equations:

x-momentum

$$\left[1 + \frac{4\,\Delta t}{R(\Delta \ell)^2}\right] u_{i,j}^{n+1} = \frac{\Delta t}{R(\Delta \ell)^2}\left(u_{i+1,j}^n + u_{i-1,j}^n + u_{i,j+1}^n - u_{i,j-1}^n\right) - \frac{(1 + \Gamma)u_{i,j}^n\,\Delta t}{2\,\Delta \ell}\left(u_{i+1,j}^n - u_{i-1,j}^n\right)$$

$$- \frac{(1 + \Gamma)v_{i,j}^n\,\Delta t}{2\,\Delta \ell}\left(u_{i,j+1}^n - u_{i,j-1}^n\right) + \frac{\Gamma u_{i,j}^{n-1}\,\Delta t}{2\,\Delta \ell}\left(u_{i+1,j}^{n-1} - u_{i-1,j}^{n-1}\right)$$

$$+ \frac{\Gamma v_{i,j}^{n-1}\,\Delta t}{2\,\Delta \ell}\left(u_{i,j+1}^{n-1} - u_{i,j-1}^{n-1}\right) - \frac{\Delta t}{2\,\Delta \ell}\left(p_{i+1,j}^n - p_{i-1,j}^n\right) \tag{7}$$

y-momentum

$$\left[1 + \frac{4\,\Delta t}{R(\Delta \ell)^2}\right] v_{i,j}^{n+1} = \frac{\Delta t}{R(\Delta \ell)^2}\left(v_{i+1,j}^{n} + v_{i-1,j}^{n} + v_{i,j+1}^{n} + v_{i,j-1}^{n}\right) - \frac{(1+\Gamma)u_{i,j}^{n}\,\Delta t}{2\,\Delta \ell}\left(v_{i+1,j}^{n} - v_{i-1,j}^{n}\right)$$

$$- \frac{(1+\Gamma)v_{i,j}^{n}\,\Delta t}{2\,\Delta \ell}\left(v_{i,j+1}^{n} - v_{i,j-1}^{n}\right) + \frac{\Gamma u_{i,j}^{n-1}\,\Delta t}{2\,\Delta \ell}\left(v_{i+1,j}^{n-1} - v_{i-1,j}^{n-1}\right)$$

$$+ \frac{\Gamma v_{i,j}^{n-1}\,\Delta t}{2\,\Delta \ell}\left(v_{i,j+1}^{n-1} - v_{i,j-1}^{n-1}\right) - \frac{\Delta t}{2\,\Delta \ell}\left(p_{i,j+1}^{n} - p_{i,j-1}^{n}\right) \tag{8}$$

with the spatial increments in x and y being equal and defined by $\Delta \ell$.

The Spalding SIMPLE procedure (ref. 2) was used to solve the pressure-linked Poisson equation. The SIMPLE procedure is:

(1) Assume an initial value p_o for pressure.

(2) Calculate u and v based on the assumed p_o by any method.

(3) Let the calculated velocity vector be q^*.

(4) Assume that the actual velocity vector is

$$q = q^* + \nabla \hat{p} \tag{9}$$

The divergence of both sides of equation (9), along with the continuity equation, gives

$$\nabla \cdot q = 0 = \nabla \cdot q^* + \nabla^2 \hat{p} \tag{10}$$

The surface normal pressure gradients are assumed to be zero.

(5) The actual pressure p is then defined as

$$p = p_o + \hat{p} \tag{11}$$

The successive overrelaxation method is applied to equation (10) and the differencing gives

$$\hat{p}_{i,j}^{k+1,n+1} = \hat{p}_{i,j}^{k,n+1} + \frac{\omega}{4}\left[\hat{p}_{i+1,j}^{k,n+1} + \hat{p}_{i-1,j}^{k+1,n+1} + \hat{p}_{i,j+1}^{k,n+1} + \hat{p}_{i,j-1}^{k+1,n+1} - 4\hat{p}_{i,j}^{k,n+1} - \frac{\Delta\ell}{2}\left(u_{i+1,j}^{n+1}\right.\right.$$

$$\left.\left. - u_{i-1,j}^{n+1} + v_{i,j+1}^{n+1} - v_{i,j-1}^{n+1}\right)\right] \tag{12}$$

RESULTS

The results presented in table I and figures 1 and 2 are representative of the more accurate solutions obtained in the present study for the square cavity flow problem. The solution presented was obtained for $\Delta t = 0.035$, $\Delta\ell = 0.0714$, optimum $\omega = 1.5456$, and $\Gamma = 0.6$. Comparing the velocity profiles at the vortex center with those of reference 3 shows the inaccuracy of the present solution. The present predictions for velocities u and v disagree with reference 3 by as much as 10 to 12 percent and 30 to 35 percent, respectively. Furthermore, examination of table I indicates significant oscillations in the calculated pressures throughout the cavity. Despite these inadequacies the present solution does predict the correct overall recirculation and vortex center in the cavity. (See fig. 1.)

Attempts to improve the accuracy and convergence of the steady-state solution were unsuccessful in computing times up to 3000 sec on the CDC 6600 computer. Varying the time step by a factor of 2, varying Γ from 0 to 1.0, and using forward time and centered space differencing instead of modified forward time and centered space differencing on the viscous terms did not significantly affect the accuracy or convergence of the present solutions. In reference 3, Mills obtained accurate solutions by solving the equations for the cavity flow in terms of stream function and vorticity; therefore, the need to calculate pressure directly was eliminated. The present solutions using primitive variables require the pressures to be calculated, and hence the accuracy of the overall solution is dependent on the accuracy of the pressure calculation. Therefore, the relatively poor accuracy of the present solutions and the oscillations in predicted pressures are probably attributable to use of primitive variables and inaccurate solutions to the pressure-linked equations.

CONCLUDING REMARKS

Solutions of the steady Navier-Stokes equations using the Crocco method along with the Spalding SIMPLE procedure have been obtained for two-dimensional flow in a square

driven cavity. The results for the axial and normal velocities did not agree with those of another accurate method, and significant pressure oscillations were noted. These inadequacies were probably due to use of primitive variables and to inaccurate solutions to the pressure-linked equations. The solution did correctly predict the overall recirculation and vortex center.

REFERENCES

1. Crocco, Luigi: A Suggestion for the Numerical Solutions of the Steady Navier-Stokes Equations. AIAA J., vol. 3, no. 10, Oct. 1965, pp. 1824-1832.

2. Caretto, L. S.; Gosman, A. D.; Patanker, S. V.; and Spalding, D. B.: Two Calculation Procedures for Steady, Three-Dimensional Flows With Recirculation. Rep. No. EF/TN/A/47, Dep. Mech. Eng., Imperial College Sci. & Technol., June 1972.

3. Mills, Ronald D.: Numerical Solutions of the Viscous Flow Equations for a Class of Closed Flows. J. Roy. Aeronaut. Soc., vol. 69, no. 658, Oct. 1965, pp. 714-718; Correction, vol. 69, no. 660, Dec. 1965, p. 880.

TABLE I.- THEORETICAL PRESSURE DISTRIBUTION IN SQUARE CAVITY

y	Pressures at x of –														
	0	0.071	0.143	0.214	0.286	0.357	0.429	0.500	0.571	0.643	0.714	0.786	0.857	0.929	1.000
1.000	0.581	0.570	0.622	0.626	0.638	0.640	0.628	0.637	0.613	0.648	0.631	0.731	0.758	0.972	1.000
.929	.562	.520	.628	.604	.624	.628	.598	.636	.565	.655	.554	.749	.645	1.058	.998
.857	.612	.619	.626	.627	.624	.627	.610	.591	.619	.590	.661	.668	.668	.807	.863
.786	.614	.584	.623	.606	.616	.619	.595	.623	.570	.633	.566	.680	.640	.796	.804
.714	.639	.633	.635	.633	.629	.629	.616	.621	.602	.615	.606	.634	.660	.679	.725
.643	.638	.611	.633	.618	.625	.624	.612	.627	.600	.634	.608	.659	.652	.684	.700
.571	.653	.644	.647	.643	.642	.640	.635	.635	.631	.634	.639	.641	.661	.639	.670
.500	.650	.625	.644	.628	.638	.632	.632	.637	.630	.644	.639	.653	.656	.549	.666
.429	.661	.651	.656	.650	.653	.649	.651	.648	.651	.648	.656	.648	.661	.637	.659
.357	.656	.630	.650	.633	.647	.636	.644	.640	.645	.645	.650	.647	.657	.640	.659
.286	.665	.654	.661	.654	.660	.654	.659	.654	.659	.654	.662	.651	.662	.644	.660
.214	.657	.631	.652	.633	.650	.636	.649	.639	.650	.641	.653	.641	.657	.636	.659
.143	.666	.656	.664	.655	.662	.656	.662	.657	.663	.657	.664	.655	.664	.650	.664
.071	.658	.628	.652	.630	.649	.633	.648	.636	.650	.638	.653	.637	.656	.634	.661
0	.673	.657	.664	.656	.662	.657	.662	.659	.664	.661	.666	.661	.667	.655	.673

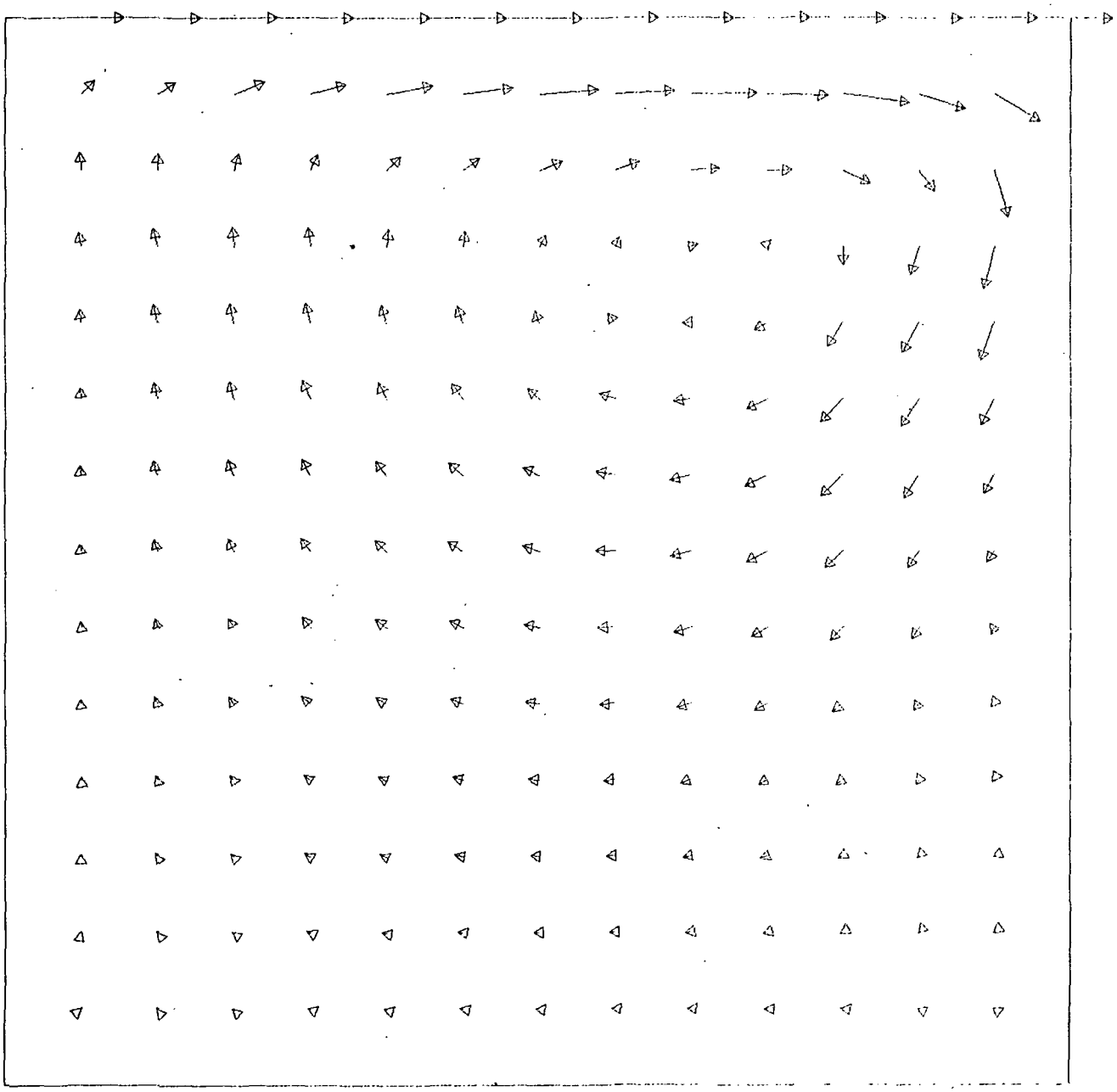

Figure 1.- Theoretical flow-field predictions for square cavity.

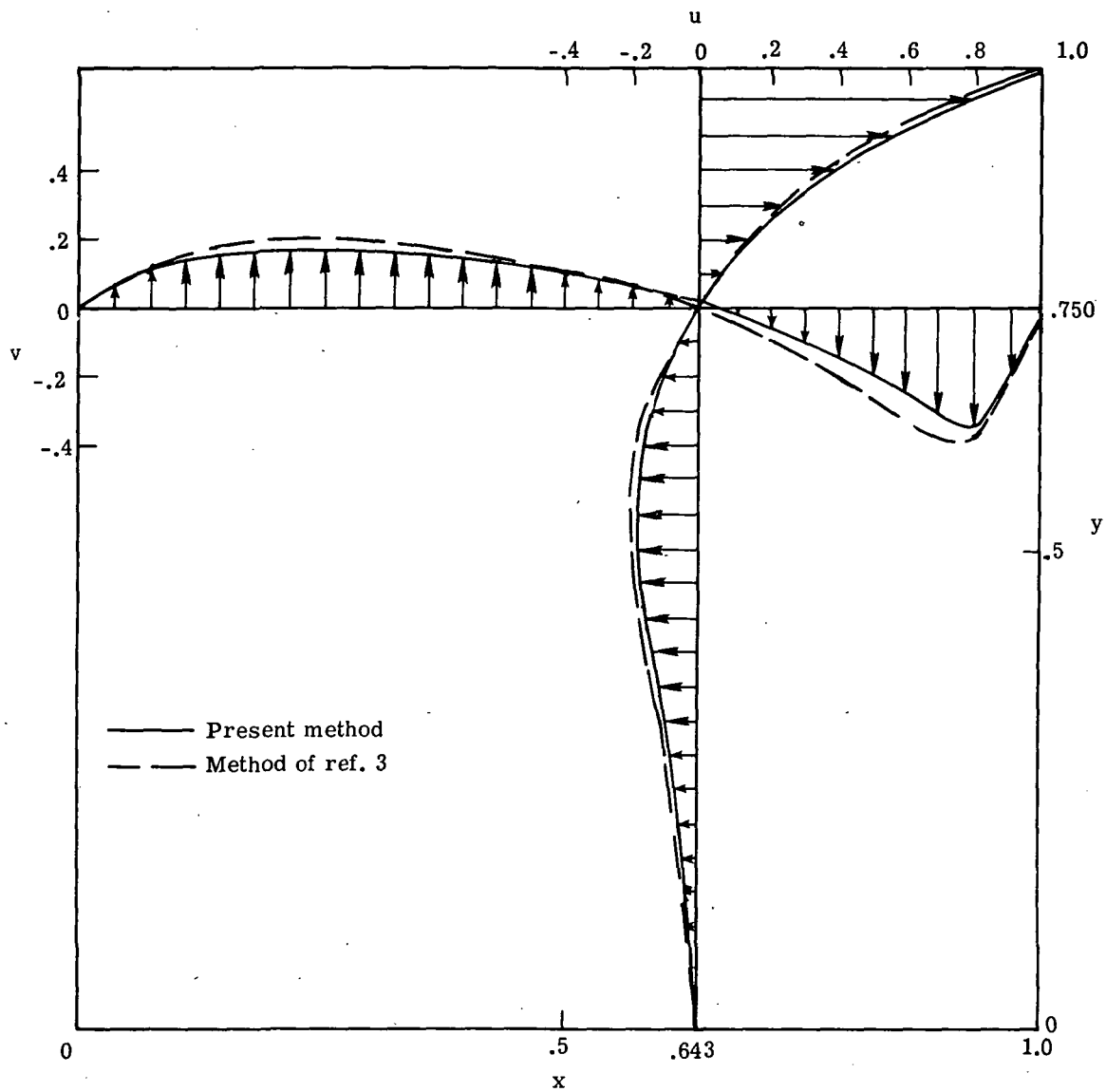

Figure 2. - Theoretical velocity profiles through center of vortex for square cavity.

4. SOLUTION OF THE DRIVEN CAVITY PROBLEM IN PRIMITIVE VARIABLES USING THE SMAC METHOD

Richard S. Hirsh
Langley Research Center

SUMMARY

The equations of two-dimensional incompressible fluid flow in the driven cavity have been solved in terms of primitive variables. The Simplified Marker-and-Cell method was used with forward time and centered space (FTCS) differencing and with modified forward time and centered space (MFTCS) differencing. The problem could not be solved for a Reynolds number of 100 with FTCS differencing because of stability limitations. For a Reynolds number of 10, the results were found to be inaccurate because of the inability of the pressure solver to converge to small tolerances. The MFTCS differencing seemed to relax the stability restriction on time step, but the limit on cell Reynolds number was retained. A lower order boundary condition on pressure resulted in marginal improvement.

INTRODUCTION

The equations of two-dimensional incompressible fluid flow can be integrated by either of two general procedures. The equations can be utilized as they are, written expressing conservation of mass and momentum in terms of axial and normal velocity and pressure, that is, the so-called primitive variables (PV); or the continuity equation can be satisfied by a stream function, and the pressure can be eliminated by taking the curl of the momentum equations to yield the vorticity—stream-function (VSF) system.

The VSF system is attractive since it reduces the number of equations from three to two and eliminates the troublesome continuity equation. This gain is offset somewhat by the difficulties encountered when dealing with the unknown boundary conditions on vorticity. In some problems, such as aerodynamic flows, for which knowledge of the pressure is desired, the VSF system must be supplemented by additional relations for the pressure. The PV system, on the other hand, yields the pressure directly and has little difficulty with the boundary conditions. The present study considers the solution of the driven cavity problem with a method which solves the PV system, and results are compared with a solution of the VSF system. See paper no. 1 by Rubin and Harris for details of the driven cavity problem.

SYMBOLS

n	unit surface normal
p	pressurelike variable
q	correct velocity vector
q^*	approximate velocity vector
R	Reynolds number
R_c	cell Reynolds number
t	time
Δt	time step
u	axial velocity
v	normal velocity
x,y	axial and normal coordinate, respectively
$\Delta x, \Delta y$	spatial increments in x- and y-directions
Δ	dilatation
ϵ	convergence factor in SOR pressure solver

Superscripts:

n	time level
$*$	intermediate time level

Subscripts:

i,j	index of grid points in x- and y-direction, respectively
x,y,t	differentiation with respect to x, y, or t

Abbreviations:

ADI	alternating direction implicit
FTCS	forward time and centered space
MAC	Marker and Cell
MFTCS	modified forward time and centered space
SMAC	Simplified Marker and Cell
SOR	successive overrelaxation

METHOD OF SOLUTION

The momentum equations in two-dimensional incompressible flow, written in dimensionless divergence form, are (ref. 1)

$$u_t + \left(u^2\right)_x + (uv)_y = -p_x + \frac{1}{R}\left(u_{xx} + u_{yy}\right) \tag{1}$$

$$v_t + (uv)_x + \left(v^2\right)_y = -p_y + \frac{1}{R}\left(v_{xx} + v_{yy}\right) \tag{2}$$

The continuity equation is

$$\Delta = u_x + v_y = 0 \tag{3}$$

These three equations constitute the governing equations of the driven cavity problem.

The method of solution used is the Simplified Marker-and-Cell (SMAC) method originally proposed by Amsden and Harlow. (See ref. 2.) Although this method does not yield the true pressure from the solution, it gives an indication of the accuracy which can

be achieved with the equations in terms of primitive variables since the velocity is correct, as pointed out in reference 2.

The methodology of the SMAC method is as follows:

(1) Integrate the momentum equations one time step to generate an approximate vector solution q^*.

(2) Knowing this to be incorrect since in general, it does not satisfy zero dilatation, assume that a pressurelike variable p corrects q^* to the actual value q such that $\text{div } q = 0$. Thus, say

$$q = q^* + \text{grad } p \tag{4}$$

(3) Since $\text{div } q = 0$, equation (4) gives

$$\nabla^2 p = -\text{div } q^* \tag{5}$$

(4) Since $q = q^*$ on the boundaries, equation (4) gives for boundary conditions,

$$\frac{\partial p}{\partial n} = 0 \tag{6}$$

(5) Once the Poisson equation (5) for the "pressure" is solved, the correct value of q at this particular time step can be found from equation (4). Then, the whole process is begun again at step (1) and continued in time until two consecutive time steps have velocities which differ by no more than some small convergence factor.

Note that the variable p is not the real fluid pressure, since the boundary condition (eq. (6)) is not correct. The true normal conditions on the pressure can be derived from equations (1) and (2) written at the wall.

The spatial differencing used in the numerical solution of equations (1), (2), and (5) is based on the staggered grid originally used in the MAC method (ref. 1), that is,

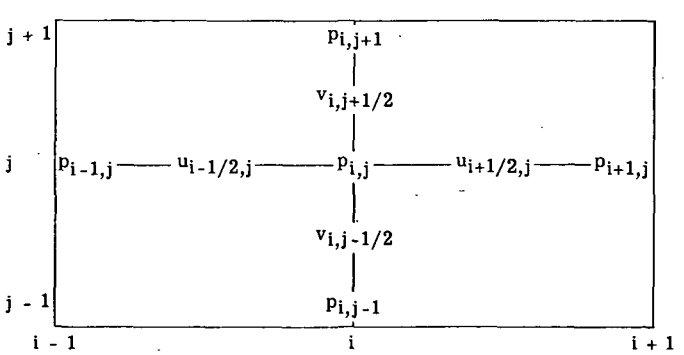

With forward time and centered space (FTCS) differencing, equations (1) and (2) are written

$$\frac{u^{*}_{i+1/2,j} - u^{n}_{i+1/2,j}}{\Delta t} + \frac{\left(u^2\right)^{n}_{i+1,j} - \left(u^2\right)^{n}_{i,j}}{\Delta x} + \frac{(uv)^{n}_{i+1/2,j+1/2} - (uv)^{n}_{i+1/2,j-1/2}}{\Delta y} =$$

$$- \frac{p^{n}_{i+1,j} - p^{n}_{i,j}}{\Delta x} + \frac{1}{R}\left[\frac{u^{n}_{i+3/2,j} - \left\{2u^{n}_{i+1/2,j}\right\} + u^{n}_{i-1/2,j}}{(\Delta x)^2}\right]$$

$$+ \frac{1}{R}\left[\frac{u^{n}_{i+1/2,j+1} - \left\{2u^{n}_{i+1/2,j}\right\} + u^{n}_{i+1/2,j-1}}{(\Delta y)^2}\right] \qquad (7)$$

$$\frac{v^{*}_{i,j+1/2} - v^{n}_{i,j+1/2}}{\Delta t} + \frac{(uv)^{n}_{i+1/2,j+1/2} - (uv)^{n}_{i-1/2,j+1/2}}{\Delta x} + \frac{\left(v^2\right)^{n}_{i,j+1} - \left(v^2\right)^{n}_{i,j}}{\Delta y} =$$

$$- \frac{p^{n}_{i,j+1} - p^{n}_{i,j}}{\Delta x} + \frac{1}{R}\left[\frac{v^{n}_{i+1,j+1/2} - \left\{2v^{n}_{i,j+1/2}\right\} + v^{n}_{i-1,j+1/2}}{(\Delta x)^2}\right]$$

$$+ \frac{1}{R}\left[\frac{v^{n}_{i,j+3/2} - \left\{2v^{n}_{i,j+1/2}\right\} + v^{n}_{i,j-1/2}}{(\Delta y)^2}\right] \qquad (8)$$

where

$$u_{i+1,j} = \frac{1}{2}\left(u_{i+3/2,j} + u_{i+1/2,j}\right)$$

$$u_{i,j} = \frac{1}{2}\left(u_{i+1/2,j} + u_{i-1/2,j}\right)$$

$$v_{i,j+1} = \frac{1}{2}\left(v_{i,j+3/2} + v_{i,j+1/2}\right)$$

$$v_{i,j} = \frac{1}{2}\left(v_{i,j+1/2} + v_{i,j-1/2}\right)$$

$$(uv)_{i+1/2,j+1/2} = \frac{1}{4}\left(u_{i+1/2,j+1} + u_{i+1/2,j}\right)\left(v_{i+1,j+1/2} + v_{i,j+1/2}\right)$$

$$(uv)_{i+1/2,j-1/2} = \frac{1}{4}\left(u_{i+1/2,j} + u_{i+1/2,j-1}\right)\left(v_{i+1,j-1/2} + v_{i,j-1/2}\right)$$

$$(uv)_{i-1/2,j+1/2} = \frac{1}{4}\left(u_{i-1/2,j+1} + u_{i-1/2,j}\right)\left(v_{i,j+1/2} + v_{i-1,j+1/2}\right)$$

The difference equation used in the solution of the Poisson equation is

$$\frac{p_{i+1,j} - 2p_{i,j} + p_{i-1,j}}{(\Delta x)^2} + \frac{p_{i,j+1} - 2p_{i,j} + p_{i,j-1}}{(\Delta y)^2} = -\frac{u^*_{i+1/2,j} - u^*_{i-1/2,j}}{\Delta x} - \frac{v^*_{i,j+1/2} - v^*_{i,j-1/2}}{\Delta y} \tag{9}$$

A simple successive overrelaxation (SOR) routine using optimal relaxation parameters was written to solve this equation rather than an alternating-direction implicit (ADI) technique since the efficiencies of these two methods are equivalent if no acceleration is used with the ADI method. The SOR routine was assumed to be converged when two successive iterations differed by no more than a prescribed convergence factor.

The use of FTCS differencing imposes stability restrictions on the time step, as well as on the cell Reynolds number. These three restrictions, given in reference 1, are (with equal mesh spacing)

$$\left.\begin{aligned} \beta &= \frac{\Delta t}{R(\Delta x)^2} \leqq \frac{1}{4} \\ c_x + c_y &= (|u| + |v|)\frac{\Delta t}{\Delta x} \leqq 1 \\ R_c &= (|u| + |v|)R\,\Delta x \leqq 4 \end{aligned}\right\} \tag{10}$$

If the maximum cell Reynolds number is assumed to occur at the upper moving wall of the driven cavity, the maximum flow Reynolds number which could be expected to be stable for a 15×15 grid is 56. Thus the test case of $R = 100$ could not be calculated with FTCS differencing. A value of $R = 10$ was chosen as the test case for runs using FTCS differencing in order to be on the conservative side of the stability limit. At these low values of R, the β-restriction in equation (10) is more severe than the c-restriction, so the test case was first run at an again conservative value of $\beta = 0.1$. After these runs proved to be successful, the values of β, R, Δx, and the convergence factor in the SOR solver were varied. The results of these runs are described in the next section.

In an attempt to overcome the restriction on β, a modified time integration scheme (MFTCS differencing) was used. In this approach the braced terms of the viscous expressions in equations (7) and (8) are evaluated at time $*$ instead of time n. This differencing scheme has been analyzed by Rubin and Lin (ref. 3) in their appendix for the one-dimensional case. Generalizing to two dimensions gives for stability when $R_c > 4$,

$$\beta \leqq \frac{4}{R_c^2 - 16} \tag{11}$$

and gives unconditional stability for β when $R_c \leqq 4$. Thus the restrictions (eq. (10)) are somewhat relaxed. Runs duplicating the calculations with FTCS differencing were made with MFTCS differencing and are discussed in the following section.

DISCUSSION OF RESULTS

The standard problem with $R = 10$ was first run on a 15×15 grid with a crude convergence factor in the SOR pressure solver ($\epsilon = 10^{-3}$). The flow in this and all other runs was assumed to be converged to a steady state when the velocities at two consecutive time steps differed by less than 10^{-6}. As with all the results to follow, this first run gave a flow pattern which was qualitatively correct, a one-cell circulation within the cavity. (See fig. 1.) However, the final answer generated values for the dilatation $\Delta = \text{div } q$ which were not close to zero. Values in excess of 0.2 were generated close to the boundaries, and the entire Δ field did not give the appearance of a quantity which should be identically zero.

In order to have a standard of comparison, the ADI solution of the next paper by Morris (paper no. 5), which agreed exactly with the published results of Mills (ref. 4) for $R = 100$ (and was therefore presumed to generate the correct result) was run for $R = 10$ on a 15×15 grid. The SMAC results and the ADI results for the axial velocity u at the first row of grid points from the moving wall are shown in figure 2. The difference between the maximum values of u is about 7 percent. It was felt that the crude

convergence for the pressure might lead to inaccuracies in the velocities (through the pressure gradients in the momentum equations), so the convergence factor for pressure was lowered an order of magnitude to $\epsilon = 10^{-4}$, and the identical problem was run again. The computation time was increased by a factor of 2.5, but the converged dilatation field, listed in table I, was considerably improved. There was a favorable change in all the velocities as shown in figure 2. Now the difference between maxima was only 4.5 percent.

Since the accuracy of the pressure calculation seemed crucial, the SOR convergence factor was decreased another order of magnitude to $\epsilon = 10^{-5}$. With this value the SOR pressure solver would not converge. It was then decided to use $\epsilon = 10^{-5}$ but to cut off the iteration at a large arbitrary limit (1000 iterations) if the convergence was not fulfilled and proceed to the next time step. The result was a significantly more uniform dilatation field. However the typical value of dilatation computed, 0.0040, was no better than the value for $\epsilon = 10^{-4}$ (table I). Thus, it seems that in addition to being the most time-consuming segment of the calculation, the method used for the pressure solver controls the overall accuracy of the computation. A plot of the velocity vector field for $\epsilon = 10^{-4}$ is presented in figure 1. The calculated velocities through the vortex center are compared with those of paper no. 5 in figure 3.

Attempts were made to solve the standard problem (i.e., $R = 100$) with FTCS differencing. As expected, the calculation diverged. At $R = 50$, the solution also diverged, but at $R = 40$, the computation did converge and gave a dilatation field comparable to that computed for $R = 10$. This behavior seemed to confirm the stability criteria of equation (10).

The MFTCS differencing was tested on the 15×15 grid. For $R = 10$, time steps 20 times larger than those used with FTCS differencing and 8 times larger than those indicated by the stability restriction (eq. (10)) were used. The results with MFTCS and FTCS differencing were identical. This was also true for $R = 40$. Although better stability was expected with MFTCS differencing (see eq. (11)), the solution for $R = 50$ diverged, even for a very small β. No explanation for this behavior could be found. The MFTCS method did require less total computer time than the FTCS computations, so all further runs were made with MFTCS differencing and a time step larger than the β stability limit of equation (10).

In an attempt to improve the accuracy for $R = 10$, the grid size was halved, and the computation was performed on a 29×29 grid. With $\epsilon = 10^{-3}$, the results (at comparable points) were essentially the same as those on the 15×15 grid at $\epsilon = 10^{-4}$. Computer time required was 6 times as much. Decreasing the convergence to $\epsilon = 10^{-4}$ for the fine grid did affect the velocity field at a location $y = 1/14$ away from the upper wall as shown in figure 2. Now the difference between the maxima of the ADI results and

the SMAC results was only 2.3 percent; however, the dilatation remained around 0.1 for most points. It must be remembered, however, that these comparative points in the 29×29 grid are no longer the ones adjacent to the boundary walls, so any wall effects felt by the first line of the 15×15 grid may be damped in the 29×29 grid by intervening points.

Some simple experiments with the normal gradients used at the boundaries in the pressure solver were performed to see the effects of different orders of accuracy. The previous results were all obtained with a second-order accurate end difference for the gradient; that is,

$$\left.\frac{\partial p}{\partial y}\right|_{i,1} = \frac{3p_{i,1} - 4p_{i,2} + p_{i,3}}{2\,\Delta y} = 0$$

A first-order accurate difference at the wall is

$$\left.\frac{\partial p}{\partial y}\right|_{i,1} = \frac{p_{i,2} - p_{i,1}}{\Delta y} = 0$$

which was inserted into the SOR routine, and all the previous runs were repeated. No substantial changes due to this new boundary condition were noticed. The velocities seemed higher in some instances, but in others the dilatation field seemed a bit lower.

CONCLUDING REMARKS

The Simplified Marker-and-Cell method using primitive variables did not give accurate results for flow in the driven cavity because of the inability of the pressure solver to converge to small tolerances. Perhaps, instead of correcting the velocity vector only once at each time step, additional pressure corrections could be made until the dilatation is reduced to a small level. Then a new time step could be calculated. This might also produce a more consistent scheme.

Modified forward time and centered space differencing seems to relax the stability restriction on the time step but still retains a limit on cell Reynolds number. The lower order boundary condition on the pressure gave marginal improvement in the dilatation, but the computed values of velocity were slightly higher.

REFERENCES

1. Roache, Patrick J.: Computational Fluid Dynamics. Hermosa Publ., c.1972.

2. Amsden, Anthony A.; and Harlow, Francis H.: The SMAC Method: A Numerical Techniques for Calculating Incompressible Fluid Flows. LA-4370, Los Alamos Sci. Lab., Univ. of California, Feb. 17, 1970.

3. Rubin, S. G.; and Lin, T. C.: Numerical Methods for Two- and Three-Dimensional Viscous Flow Problems: Application to Hypersonic Leading Edge Equations. AFOSR-TR-71-0778, U.S. Air Force, Apr. 1971. (Available from DDC as AD 726 547.)

4. Mills, Ronald D.: Numerical Solutions of the Viscous Flow Equations for a Class of Closed Flows. J. Roy. Aeronaut. Soc., vol. 69, no. 658, Oct. 1965, pp. 714-718; Correction, vol. 69, no. 660, Dec. 1965, p. 880.

TABLE I. - DILATATION AT INTERIOR MESH POINTS FOR $R = 10$, $\epsilon = 10^{-4}$, AND 15×15 GRID

[Each value computed at a grid point (i,j); columns correspond to i = 2, 3, 4, . . ., 14 and lines to j = 14, 13, 12, . . ., 2]

Dilatation, Δ												
.0253	.0051	.0043	.0035	.0028	.0021	.0015	.0011	.0008	.0005	.0004	.0004	.0005
.0253	.0052	.0043	.0035	.0028	.0021	.0015	.0011	.0007	.0005	.0004	.0004	.0005
.0252	.0052	.0043	.0035	.0028	.0021	.0016	.0011	.0008	.0005	.0004	.0004	.0005
.0252	.0053	.0044	.0036	.0028	.0022	.0016	.0011	.0008	.0006	.0004	.0004	.0005
.0251	.0053	.0045	.0037	.0029	.0022	.0017	.0012	.0009	.0006	.0005	.0005	.0006
.0251	.0054	.0046	.0038	.0030	.0023	.0018	.0013	.0010	.0007	.0006	.0006	.0007
.0249	.0055	.0047	.0039	.0031	.0025	.0019	.0014	.0011	.0009	.0007	.0007	.0008
.0246	.0056	.0048	.0040	.0033	.0026	.0021	.0016	.0013	.0010	.0009	.0009	.0010
.0244	.0057	.0049	.0041	.0034	.0028	.0022	.0018	.0014	.0012	.0011	.0011	.0012
.0241	.0058	.0050	.0043	.0036	.0030	.0024	.0020	.0016	.0014	.0013	.0013	.0014
.0239	.0058	.0051	.0044	.0038	.0031	.0026	.0022	.0019	.0016	.0015	.0015	.0016
.0236	.0059	.0052	.0046	.0039	.0033	.0028	.0024	.0021	.0019	.0017	.0017	.0018
.0401	.0222	.0208	.0192	.0174	.0157	.0139	.0123	.0109	.0097	.0088	.0083	.0080

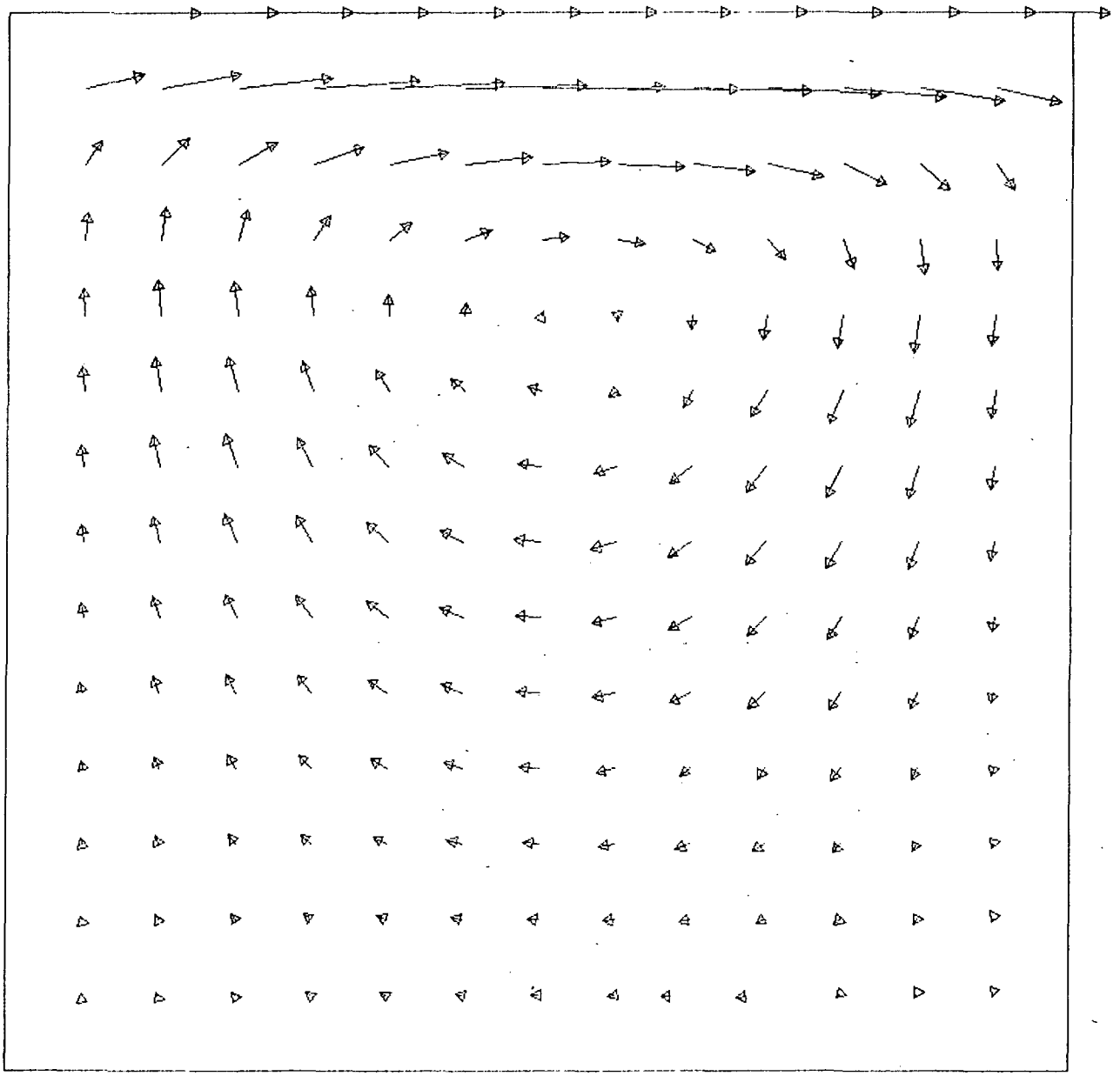

Figure 1.- Computed velocity vectors inside cavity. 15×15 grid; $R = 10$; $\epsilon = 10^{-4}$.

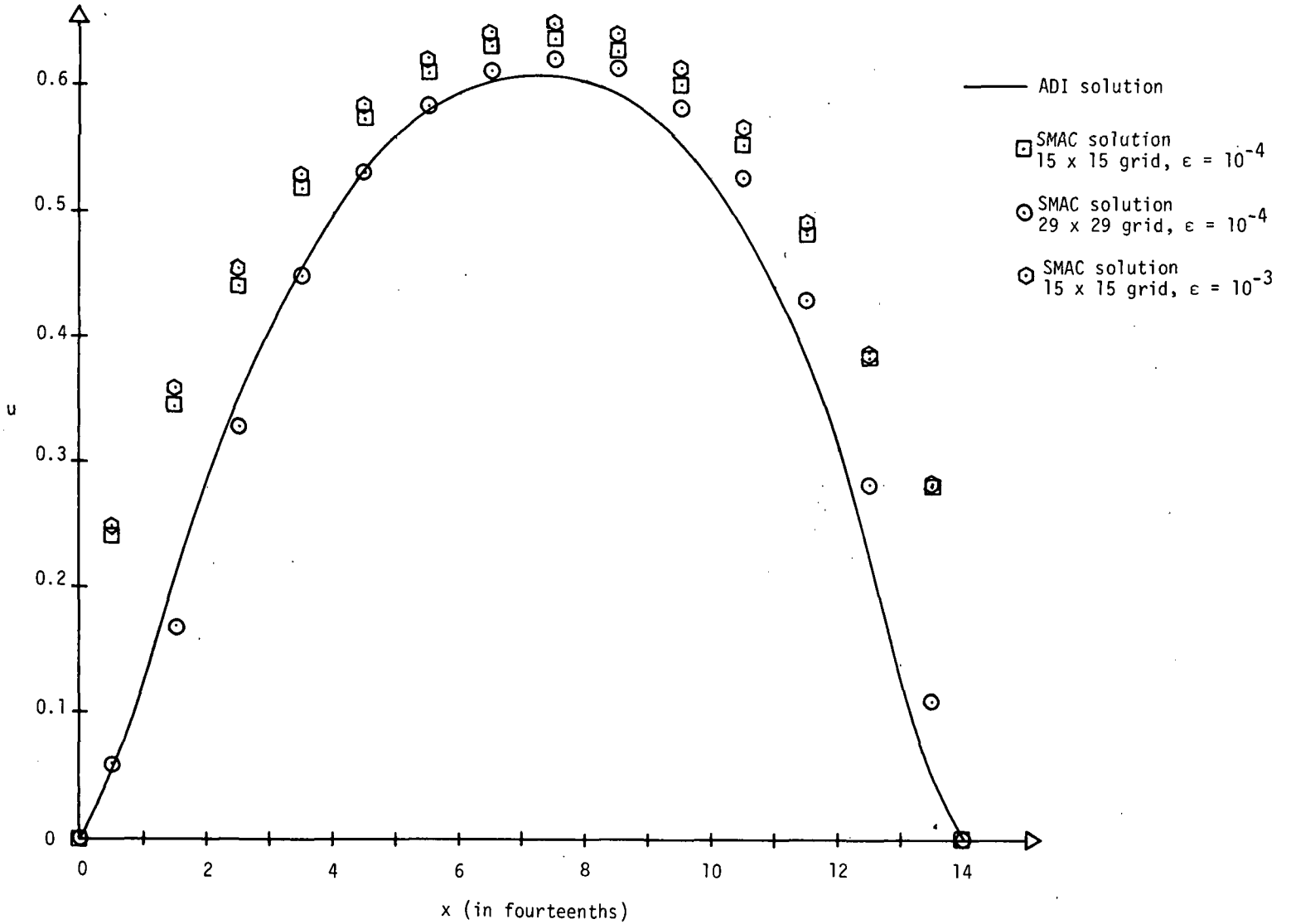

Figure 2.- Velocity u at y = 1/14 from moving wall for SMAC and ADI methods. R = 10.

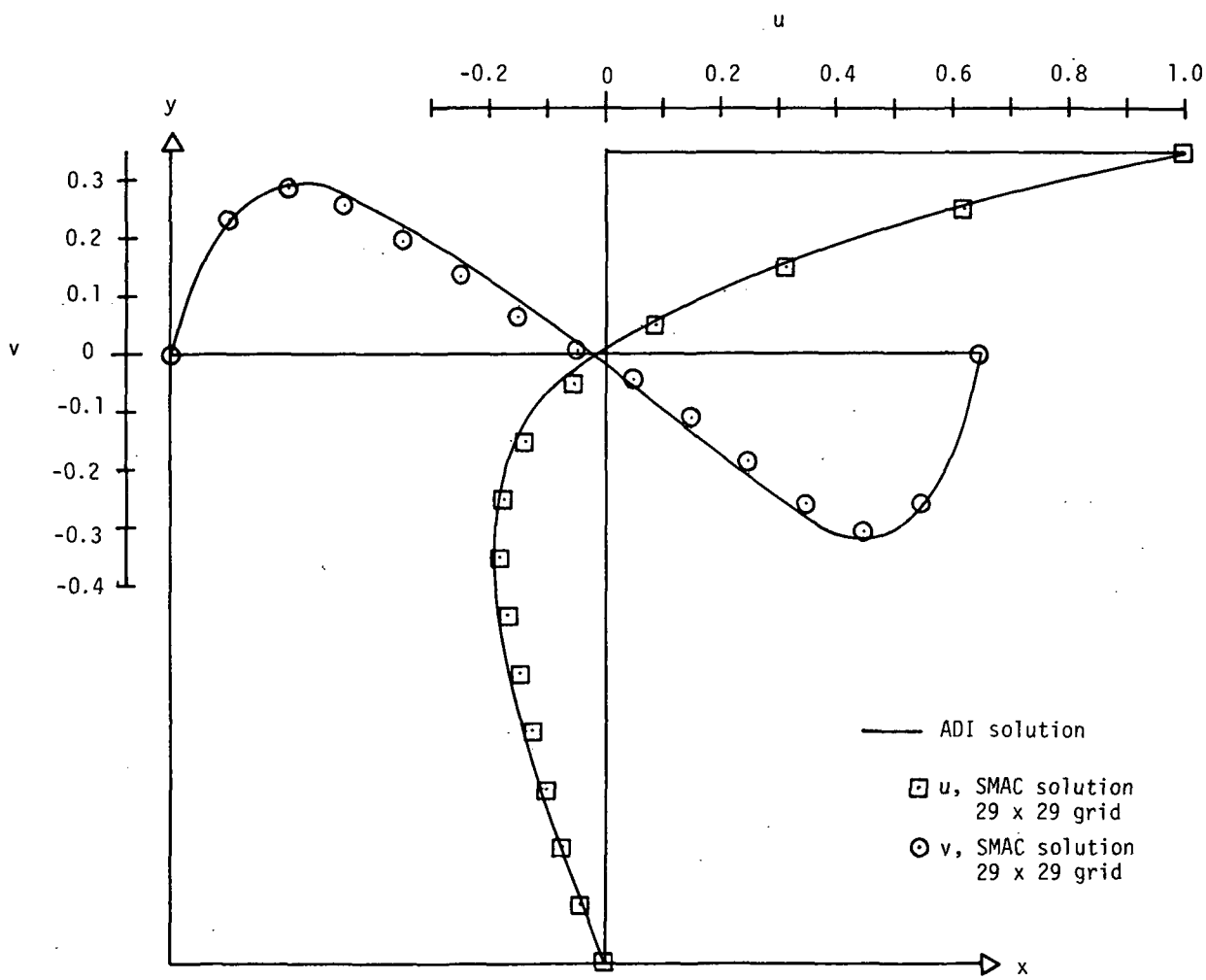

Figure 3.- Velocities through closest grid point to vortex center for SMAC and ADI methods.

5. SOLUTION OF THE INCOMPRESSIBLE DRIVEN CAVITY PROBLEM BY THE ALTERNATING-DIRECTION IMPLICIT METHOD

Dana J. Morris
Langley Research Center

SUMMARY

A second-order accurate alternating-direction implicit (ADI) method has been used to solve the two-dimensional incompressible Navier-Stokes equations for flow in a square driven cavity. Calculations were made at a Reynolds number of 100 with equally spaced 15×15, 17×17, 33×33, and 57×57 grids and at a Reynolds number of 10 with a 15×15 grid. The ADI results agreed well with other solutions. Choosing a criterion for convergence which was too strict was found to result in no steady-state solution being reached. A study of the maximum allowable time step for a Reynolds number of 100 indicated that time steps many times larger than those used for most consistent explicit methods could be used for the ADI method.

INTRODUCTION

A second-order accurate efficient implicit method is used to solve the two-dimensional incompressible Navier-Stokes equations for flow in a square driven cavity. (See paper no. 1 by Rubin and Harris for details of the driven cavity problem.) This problem was previously solved by Mills (ref. 1) using an explicit method.

Alternating-direction implicit (ADI) methods were introduced by Peaceman and Rachford (ref. 2) and take advantage of a splitting of the time step for multidimensional problems to obtain an implicit method which requires only the inversion of a tridiagonal matrix. The expected unconditional stability of the method allowed larger time steps than explicit methods without the complexity of a full matrix reduction routine required by one-step implicit methods.

SYMBOLS

K	constant
Δl	$= \Delta x = \Delta y$
N	number of grid points in one direction

R	Reynolds number
Δt	time step
u	axial velocity component
v	normal velocity component
x,y	axial and normal coordinate, respectively
$\Delta x, \Delta y$	spatial increments in x- and y-directions
ζ	vorticity
ν	kinematic viscosity
ψ	stream function

Superscripts:

n	index of time step
*	intermediate time level

Subscripts:

i,j	index of grid point in x- and y-direction, respectively
t	differentiation with respect to time
w	value at wall
x,y	differentiation with respect to x or y

METHOD OF SOLUTION

The nondimensional equations for viscous incompressible two-dimensional flow in vorticity—stream-function form which describe the flow field under investigation are

$$\zeta_t = -u\zeta_x - v\zeta_y + \nu\zeta_{xx} + \nu\zeta_{yy} \tag{1}$$

$$\nabla^2\psi = \zeta \tag{2}$$

and $u = \psi_y$, $v = -\psi_x$, and $\nu = 1/R$.

Applied to the vorticity transport equation (eq. (1)), the Peaceman-Rachford (ref. 2) alternating-direction implicit (ADI) method advances one time level in the following two steps.

Step 1

$$\frac{\zeta^*_{i,j} - \zeta^n_{i,j}}{\Delta t/2} = -u\zeta^*_x - v\zeta_y{}^n + \nu\zeta^*_{xx} + \nu\zeta^n_{yy}$$

Step 2

$$\frac{\zeta^{n+1}_{i,j} - \zeta^*_{i,j}}{\Delta t/2} = -u\zeta^*_x - v\zeta^{n+1}_y + \nu\zeta^*_{xx} + \nu\zeta^{n+1}_{yy}$$

The value ζ^* has no physical meaning.

The method applied to the linear equation has a formal error of order $O\left[(\Delta t)^2,(\Delta x)^2,(\Delta y)^2\right]$. It is unconditionally stable and consistent. The full second-order accuracy of the method can be deteriorated by the nonlinear terms which should be evaluated as u^* and v^n for step 1 and as u^* and v^{n+1} for step 2. If the old values u^n and v^n are used, the formal error is $O\left[\Delta t,(\Delta x)^2,(\Delta y)^2\right]$. Briley (ref. 3) calculated u^n and v^n and, from the previous values u^{n-1} and v^{n-1}, linearly extrapolated forward to u^* and v^*. This procedure is stable and appeared second-order accurate; however, additional storage is required for ψ^{n-1}. Another procedure (refs. 4 and 5) is to iterate on the entire time step, either to convergence or for a predictor-corrector method. In either case the error is $O\left[(\Delta t)^2\right]$ and additional storage is required for ψ^{n+1}. It is also possible to calculate ψ^* after step 1 and to use u^* and v^* in step 2. Aziz and Hellums (ref. 5) examined these alternatives and found iteration on the full two steps to be the most accurate. The iteration required to obtain full second-order accuracy of the nonlinear terms may not be undesirable since some iteration is an advantage in achieving accurate boundary values for ζ.

Although a linear Von Neumann analysis shows the ADI procedure to be unconditionally stable, a survey of the literature indicates that the procedure may not be unconditionally stable for flows with high Reynolds numbers because of the Δt time lag of ζ_w. (See ref. 6.) The degree of convergence for ζ_w to obtain stability is problem dependent. For large Δt, convergence may be prohibited by nonlinear effects. Also, the program-

ing involved with complex boundaries effectively restricts the use of this method to rectangular regions.

The tridiagonal nature of the matrix to be solved, although much simpler than that in fully implicit one-step methods, requires diagonal dominance if error buildup is to be avoided in the matrix inversion. This is equivalent to imposing a restriction on cell Reynolds number.

In the present study, the ADI procedure was applied to the vorticity transport equation. Central differencing was used with equal mesh spacing and nonlinear terms were lagged a full time step. After completing a full time step calculation on vorticity, the stream-function equation was solved by a successive overrelaxation (SOR) routine and the boundary conditions were updated. (The SOR routine was identical with the one used in the previous paper by Hirsh (paper no. 4).) The vorticity was then calculated for a new time step, rather than being iterated at each time level to achieve a solution which was second-order accurate in time, since the interest in this study was in the steady-state solution.

BOUNDARY CONDITIONS

The no-slip condition requires that both u and v (the normal and tangential gradients of ψ) are zero at the stationary walls whereas at the moving wall u is unity. These conditions are treated by taking a row of image points at a distance $\Delta l = \Delta x = \Delta y$ outside the boundaries. These values can be related to the interior points by taking derivatives at the boundaries. Thus, the boundary conditions for ζ are:

on the stationary walls,

$$\zeta_w = \frac{2\psi_{\text{interior}}}{(\Delta l)^2}$$

at the moving wall,

$$\zeta_w = \frac{2(\Delta l + \psi_{\text{interior}})}{(\Delta l)^2}$$

The boundary value of ψ is zero on all boundaries. Initial conditions are zero everywhere except on the moving wall.

RESULTS

These calculations were made at a Reynolds number of 100 for a square $N \times N$ cavity for $N = 15$, 17, 33, and 57 and at a Reynolds number of 10 for $N = 15$. For $N = 17$, the problem was also computed with the conservation form of the equations and the values were found to be much more accurate, although the computer time to achieve a converged solution was approximately 2 times longer. As shown in table I, the maximum value of the stream function increases with the number of grid points toward the value 0.101 published by Burggraf (ref. 7). The vorticity ζ at the midpoint of the moving wall is also shown. For $N = 15$, the solution was identical with the one published by Mills (ref. 1) with a maximum stream function of 0.08742. Machine plots of the velocity vectors and the streamlines of this flow field are shown in figure 1. The calculated values of vorticity ζ and stream function ψ for $N = 57$ are presented in table II. In figure 2 the axial component of velocity u is depicted along a vertical line passing through the vortex center, and the calculated values are shown in table III for the three cases, $N = 15$ and 57 in nondivergence form and $N = 17$ in divergence form. Attempts to increase the accuracy of the nonconservation form by increasing the number of nodal points resulted in solutions which did not converge because of a convergence criterion which was too strict. The percentage difference between time levels $n + 1$ and n was used to check convergence. For $N = 15$ and 17, solutions were achieved with the convergence requirement set at 0.00005. For $N = 33$, this requirement was repeatedly made less stringent and was set at 0.001 before a converged solution was reached. Solutions for $N = 57$ did not require further weakening of this convergence criterion. This study was made for a time step $\Delta t = \Delta x$, the Courant-Friedrichs-Lewy condition for explicit methods. Decreasing the Reynolds number to 10 for $N = 15$ also forced the convergence requirement to be set at 0.001 and the time step to be decreased. No attempt was made to find the maximum allowable time step for this Reynolds number. For a Reynolds number of 100, however, such a study was made with the nonconservation form of the equations and the results are shown in figure 3. For $N = 15$, no solution would converge for Δt greater than $7\,\Delta x$. An N of 17 required that Δt be lowered to $5\,\Delta x$. Increasing N to 33 with $\Delta t = 5\,\Delta x$ resulted in the solution iterating in the SOR routine until the time limit on the computer was reached. Lowering the time step to $3\,\Delta x$ allowed the solution to converge. For $N = 57$, convergence in the SOR routine required that $\Delta t = \Delta x$. Thus the maximum allowable time step appears to vary not only as a function of Δx but also with the number of grid points used.

CONCLUSIONS

An alternating-direction implicit (ADI) method has been used to solve the two-dimensional incompressible Navier-Stokes equations for flow in a square driven cavity. The following conclusions may be drawn:

(1) The ADI technique, although not unconditionally stable as a linear Von Neumann analysis indicates, does allow time steps many times larger than most consistent explicit methods.

(2) Choosing a criterion for convergence which is too strict may result in no steady-state solution being reached.

REFERENCES

1. Mills, Ronald D.: Numerical Solutions of the Viscous Flow Equations for a Class of Closed Flows. J. Roy. Aeronaut. Soc., vol. 69, no. 658, Oct. 1965, pp. 714-718; Correction, vol. 69, no. 660, Dec. 1965, p. 880.

2. Peaceman, D. W.; and Rachford, H. H., Jr.: The Numerical Solution of Parabolic and Elliptic Differential Equations. J. Soc. Ind. & Appl. Math., vol. 3, no. 1, Mar. 1955, pp. 28-41.

3. Briley, W. Roger: A Numerical Study of Laminar Separation Bubbles Using the Navier-Stokes Equations. J. Fluid Mech., vol. 47, pt. 4, June 1971, pp. 713-736.

4. Pearson, Carl E.: A Computational Method for Viscous Flow Problems. J. Fluid Mech. vol. 21, pt. 4, Apr. 1965, pp. 611-622.

5. Aziz, K.; and Hellums, J. D.: Numerical Solution of the Three-Dimensional Equations of Motion for Laminar Natural Convection. Phys. Fluids, vol. 10, no. 2, Feb. 1967, pp. 314-324.

6. Roache, Patrick J.: Computational Fluid Dynamics. Hermosa Publ., c.1972.

7. Burggraf, Odus R.: Analytical and Numerical Studies of the Structure of Steady Separated Flows. J. Fluid Mech., vol. 24, pt. 1, Jan. 1966, pp. 113-151.

TABLE I.- RESULTS FOR R = 100

N	Vorticity at midpoint of moving wall	Maximum stream function
15	8.9160	-0.08742
17	8.4646	-.09098
[a]17	7.3756	-.09867
33	6.9919	-.10038
57	6.6960	-.10128

[a]Divergence form.

TABLE II.- CALCULATED VORTICITY AND STREAM FUNCTION FOR SQUARE CAVITY WITH $R = 100$ AND EQUALLY SPACED 57×57 GRID

(a) Stream function

y	Stream function at x of –													
	0	0.0714	0.1428	0.2143	0.2857	0.3571	0.4286	0.5000	0.5714	0.6428	0.7143	0.7857	0.8571	0.9286	1.0
1.0000	0	0	0	0	0	0	0	0	0	0	0	0	0	0	0
.9286	0	-1.555×10^{-2}	-2.985×10^{-2}	-3.863×10^{-2}	-4.455×10^{-2}	-4.888×10^{-2}	-5.213×10^{-2}	-5.448×10^{-2}	-5.589×10^{-2}	-5.619×10^{-2}	-5.506×10^{-2}	-5.189×10^{-2}	-4.512×10^{-2}	-2.856×10^{-2}	0
.8571	0	-1.037×10^{-2}	-2.759×10^{-2}	-4.316×10^{-2}	-5.604×10^{-2}	-6.659×10^{-2}	-7.509×10^{-2}	-8.156×10^{-2}	-8.571×10^{-2}	-8.695×10^{-2}	-8.429×10^{-2}	-7.604×10^{-2}	-5.876×10^{-2}	-3.713×10^{-2}	0
.7857	0	-7.670×10^{-3}	-2.361×10^{-2}	-4.101×10^{-2}	-5.726×10^{-2}	-7.156×10^{-2}	-8.358×10^{-2}	-9.290×10^{-2}	-9.880×10^{-2}	-1.002×10^{-1}	-9.549×10^{-2}	-8.223×10^{-2}	-5.724×10^{-2}	-2.180×10^{-2}	0
.7143	0	-6.410×10^{-3}	-2.088×10^{-2}	-3.810×10^{-2}	-5.553×10^{-2}	-7.097×10^{-2}	-8.442×10^{-2}	-9.476×10^{-2}	-1.009×10^{-1}	-1.013×10^{-1}	-9.402×10^{-2}	-7.683×10^{-2}	-4.876×10^{-2}	-1.634×10^{-2}	0
.6428	0	-5.600×10^{-3}	-1.860×10^{-2}	-3.465×10^{-2}	-5.115×10^{-2}	-6.656×10^{-2}	-7.976×10^{-2}	-8.959×10^{-2}	-9.467×10^{-2}	-9.334×10^{-2}	-8.378×10^{-2}	-6.476×10^{-2}	-3.789×10^{-2}	-1.156×10^{-2}	0
.5714	0	-4.850×10^{-3}	-1.618×10^{-2}	-3.041×10^{-2}	-4.522×10^{-2}	-5.911×10^{-2}	-7.083×10^{-2}	-7.908×10^{-2}	-8.243×10^{-2}	-7.932×10^{-2}	-6.853×10^{-2}	-5.014×10^{-2}	-2.737×10^{-2}	-7.770×10^{-3}	0
.5000	0	-4.020×10^{-3}	-1.348×10^{-2}	-2.542×10^{-2}	-3.790×10^{-2}	-4.952×10^{-2}	-5.905×10^{-2}	-6.524×10^{-2}	-6.676×10^{-2}	-6.247×10^{-2}	-5.189×10^{-2}	-3.608×10^{-2}	-1.859×10^{-2}	-4.970×10^{-3}	0
.4286	0	-3.130×10^{-3}	-1.057×10^{-2}	-2.002×10^{-2}	-2.988×10^{-2}	-3.894×10^{-2}	-4.610×10^{-2}	-5.025×10^{-2}	-5.037×10^{-2}	-4.579×10^{-2}	-3.662×10^{-2}	-2.434×10^{-2}	-1.194×10^{-2}	-3.030×10^{-3}	0
.3571	0	-2.250×10^{-3}	-7.680×10^{-3}	-1.464×10^{-2}	-2.191×10^{-2}	-2.849×10^{-2}	-3.347×10^{-2}	-3.599×10^{-2}	-3.535×10^{-2}	-3.126×10^{-2}	-2.415×10^{-2}	-1.542×10^{-2}	-7.230×10^{-3}	-1.740×10^{-3}	0
.2857	0	-1.440×10^{-3}	-5.030×10^{-3}	-9.720×10^{-3}	-1.464×10^{-2}	-1.905×10^{-2}	-2.225×10^{-2}	-2.365×10^{-2}	-2.281×10^{-2}	-1.968×10^{-2}	-1.473×10^{-2}	-9.050×10^{-3}	-4.050×10^{-3}	-9.100×10^{-4}	0
.2143	0	-7.700×10^{-4}	-2.820×10^{-3}	-5.600×10^{-3}	-8.550×10^{-3}	-1.117×10^{-2}	-1.304×10^{-2}	-1.375×10^{-2}	-1.308×10^{-2}	-1.104×10^{-2}	-8.020×10^{-3}	-4.720×10^{-3}	-1.980×10^{-3}	-3.900×10^{-4}	0
.1428	0	-3.000×10^{-4}	-1.210×10^{-3}	-2.510×10^{-3}	-3.930×10^{-3}	-5.200×10^{-3}	-6.100×10^{-3}	-6.420×10^{-3}	-6.040×10^{-3}	-5.010×10^{-3}	-3.520×10^{-3}	-1.950×10^{-3}	-7.200×10^{-4}	-1.000×10^{-4}	0
.0714	0	-4.000×10^{-5}	-2.700×10^{-4}	-6.200×10^{-4}	-1.020×10^{-3}	-1.380×10^{-3}	-1.630×10^{-3}	-1.730×10^{-3}	-1.620×10^{-3}	-1.310×10^{-3}	-8.900×10^{-4}	-4.400×10^{-4}	-1.200×10^{-4}	-1.000×10^{-5}	0
0	0	0	0	0	0	0	0	0	0	0	0	0	0	0	0

TABLE II.- CALCULATED VORTICITY AND STREAM FUNCTION FOR SQUARE CAVITY WITH R = 100 AND EQUALLY SPACED 57 × 57 GRID – Concluded

(b) Vorticity

y	Vorticity at x of –														
	0	0.0714	0.1428	0.2143	0.2857	0.3571	0.4286	0.5000	0.5714	0.6428	0.7143	0.7857	0.8571	0.9286	1.0
1.0000			$2.099 \times 10^{+1}$	$1.495 \times 10^{+1}$	$1.159 \times 10^{+1}$	$9.338 \times 10^{+0}$	$7.749 \times 10^{+0}$	$6.696 \times 10^{+0}$	$6.187 \times 10^{+0}$	$6.317 \times 10^{+0}$	$7.254 \times 10^{+0}$	$9.314 \times 10^{+0}$	$1.345 \times 10^{+1}$	$2.537 \times 10^{+1}$	
.9286	$-1.291 \times 10^{+1}$	$2.644 \times 10^{+0}$	$6.096 \times 10^{+0}$	$6.718 \times 10^{+0}$	$6.603 \times 10^{+0}$	$6.287 \times 10^{+0}$	$5.937 \times 10^{+0}$	$5.624 \times 10^{+0}$	$5.393 \times 10^{+0}$	$5.296 \times 10^{+0}$	$5.418 \times 10^{+0}$	$5.969 \times 10^{+0}$	$7.587 \times 10^{+0}$	$9.314 \times 10^{+0}$	$-1.784 \times 10^{+1}$
.8571	$-5.622 \times 10^{+0}$	$-1.630 \times 10^{+0}$	4.408×10^{-1}	$1.520 \times 10^{+0}$	$2.198 \times 10^{+0}$	$2.683 \times 10^{+0}$	$3.072 \times 10^{+0}$	$3.421 \times 10^{+0}$	$3.764 \times 10^{+0}$	$4.128 \times 10^{+0}$	$4.561 \times 10^{+0}$	$5.184 \times 10^{+0}$	$5.861 \times 10^{+0}$	$1.160 \times 10^{+0}$	$-1.650 \times 10^{+1}$
.7857	$-3.662 \times 10^{+0}$	$-1.808 \times 10^{+0}$	-4.909×10^{-1}	3.429×10^{-1}	9.494×10^{-1}	$1.466 \times 10^{+0}$	$1.960 \times 10^{+0}$	$2.463 \times 10^{+0}$	$2.989 \times 10^{+0}$	$3.544 \times 10^{+0}$	$4.118 \times 10^{+0}$	$4.574 \times 10^{+0}$	$3.743 \times 10^{+0}$	$-2.257 \times 10^{+0}$	$-1.176 \times 10^{+1}$
.7143	$-2.955 \times 10^{+0}$	$-1.625 \times 10^{+0}$	-5.830×10^{-1}	1.401×10^{-1}	6.891×10^{-1}	$1.180 \times 10^{+0}$	$1.673 \times 10^{+0}$	$2.191 \times 10^{+0}$	$2.729 \times 10^{+0}$	$3.262 \times 10^{+0}$	$3.674 \times 10^{+0}$	$3.538 \times 10^{+0}$	$1.563 \times 10^{+0}$	$-3.278 \times 10^{+0}$	$-7.588 \times 10^{+0}$
.6428	$-2.565 \times 10^{+0}$	$-1.429 \times 10^{+0}$	-5.405×10^{-1}	9.230×10^{-2}	5.837×10^{-1}	$1.036 \times 10^{+0}$	$1.499 \times 10^{+0}$	$1.981 \times 10^{+0}$	$2.448 \times 10^{+0}$	$2.817 \times 10^{+0}$	$2.876 \times 10^{+0}$	$2.133 \times 10^{+0}$	-7.014×10^{-2}	$-3.180 \times 10^{+0}$	$-4.996 \times 10^{+0}$
.5714	$-2.218 \times 10^{+0}$	$-1.235 \times 10^{+0}$	-4.834×10^{-1}	4.798×10^{-2}	4.615×10^{-1}	8.450×10^{-1}	$1.235 \times 10^{+0}$	$1.620 \times 10^{+0}$	$1.941 \times 10^{+0}$	$2.074 \times 10^{+0}$	$1.795 \times 10^{+0}$	7.996×10^{-1}	-9.464×10^{-1}	$-2.610 \times 10^{+0}$	$-3.164 \times 10^{+0}$
.5000	$-1.836 \times 10^{+0}$	$-1.035 \times 10^{+0}$	-4.318×10^{-1}	-1.229×10^{-2}	3.092×10^{-1}	6.012×10^{-1}	8.847×10^{-1}	$1.134 \times 10^{+0}$	$1.281 \times 10^{+0}$	$1.209 \times 10^{+0}$	7.721×10^{-1}	-1.050×10^{-1}	$-1.199 \times 10^{+0}$	$-1.931 \times 10^{+0}$	$-1.921 \times 10^{+0}$
.4286	$-1.421 \times 10^{+0}$	-8.311×10^{-1}	-3.863×10^{-1}	-8.093×10^{-2}	1.470×10^{-1}	3.443×10^{-1}	5.181×10^{-1}	6.401×10^{-1}	6.516×10^{-1}	4.793×10^{-1}	7.067×10^{-2}	-5.260×10^{-1}	$-1.091 \times 10^{+0}$	$-1.325 \times 10^{+0}$	$-1.112 \times 10^{+0}$
.3571	$-1.004 \times 10^{+0}$	-6.322×10^{-1}	-3.435×10^{-1}	-1.462×10^{-1}	-3.450×10^{-3}	1.126×10^{-1}	2.018×10^{-1}	2.388×10^{-1}	1.865×10^{-1}	1.356×10^{-2}	-2.761×10^{-1}	-6.029×10^{-1}	-8.463×10^{-1}	-8.533×10^{-1}	-6.003×10^{-1}
.2857	-6.233×10^{-1}	-4.492×10^{-1}	-3.008×10^{-1}	-1.995×10^{-1}	-1.298×10^{-1}	-7.603×10^{-1}	-4.025×10^{-2}	-4.022×10^{-2}	-9.653×10^{-2}	-2.169×10^{-1}	-3.807×10^{-1}	-5.323×10^{-1}	-5.961×10^{-1}	-5.159×10^{-1}	-2.831×10^{-1}
.2143	-3.115×10^{-1}	-2.927×10^{-1}	-2.572×10^{-1}	-2.367×10^{-1}	-2.292×10^{-1}	-2.241×10^{-1}	-2.203×10^{-1}	-2.275×10^{-1}	-2.572×10^{-1}	-3.114×10^{-1}	-3.745×10^{-1}	-4.146×10^{-1}	-3.950×10^{-1}	-2.900×10^{-1}	-9.135×10^{-2}
.1428	-9.455×10^{-2}	-1.711×10^{-1}	-2.124×10^{-1}	-2.567×10^{-1}	-3.051×10^{-1}	-3.453×10^{-1}	-3.685×10^{-1}	-3.755×10^{-1}	-3.722×10^{-1}	-3.632×10^{-1}	-3.464×10^{-1}	-3.127×10^{-1}	-2.504×10^{-1}	-1.481×10^{-1}	1.013×10^{-2}
.0714	-6.710×10^{-3}	-8.313×10^{-2}	-1.608×10^{-1}	-2.579×10^{-1}	-3.635×10^{-1}	-4.559×10^{-1}	-5.163×10^{-1}	-5.328×10^{-1}	-5.029×10^{-1}	-4.331×10^{-1}	-3.375×10^{-1}	-2.339×10^{-1}	-1.339×10^{-1}	-5.867×10^{-2}	2.978×10^{-2}
0	0	6.610×10^{-3}	-8.180×10^{-2}	-2.378×10^{-1}	-4.141×10^{-1}	-5.763×10^{-1}	-6.946×10^{-1}	-7.403×10^{-1}	-6.929×10^{-1}	-5.532×10^{-1}	-3.528×10^{-1}	-1.498×10^{-1}	-8.960×10^{-3}	2.866×10^{-2}	0

TABLE III. - RESULTS FOR VELOCITY COMPONENT u THROUGH POINT OF MAXIMUM STREAM FUNCTION FOR R = 100

y	u through point of maximum ψ with –		
	15 × 15 grid, nondivergence form	57 × 57 grid, nondivergence form	17 × 17 grid, divergence form
0	0	0	0
.0625	----------	----------	-3.509×10^{-2}
.0714	-2.612×10^{-2}	-3.556×10^{-2}	----------
.1250	----------	----------	-6.513×10^{-2}
.1428	-5.018×10^{-2}	-6.774×10^{-2}	----------
.1875	----------	----------	-9.419×10^{-2}
.2143	-7.583×10^{-2}	-1.019×10^{-1}	----------
.2500	----------	----------	-1.245×10^{-1}
.2857	-1.054×10^{-1}	-1.409×10^{-1}	----------
.3125	----------	----------	-1.563×10^{-1}
.3571	-1.388×10^{-1}	-1.834×10^{-1}	----------
.3750	----------	----------	-1.868×10^{-1}
.4286	-1.724×10^{-1}	-2.215×10^{-1}	----------
.4375	----------	----------	-2.107×10^{-1}
.5000	-1.968×10^{-1}	-2.404×10^{-1}	-2.198×10^{-1}
.5625	----------	----------	-2.057×10^{-1}
.5714	-1.980×10^{-1}	-2.233×10^{-1}	----------
.6250	----------	----------	-1.622×10^{-1}
.6429	-1.616×10^{-1}	-1.606×10^{-1}	----------
.6875	----------	----------	-8.745×10^{-2}
.7143	-7.891×10^{-2}	-5.416×10^{-2}	----------
.7500	----------	----------	1.782×10^{-2}
.7857	5.022×10^{-2}	9.200×10^{-2}	----------
.8125	----------	----------	1.578×10^{-1}
.8571	2.445×10^{-1}	2.929×10^{-1}	----------
.8750	----------	----------	3.519×10^{-1}
.9286	5.470×10^{-1}	5.905×10^{-1}	----------
.9375	----------	----------	6.315×10^{-1}
1.0000	1.0	1.0	1.0

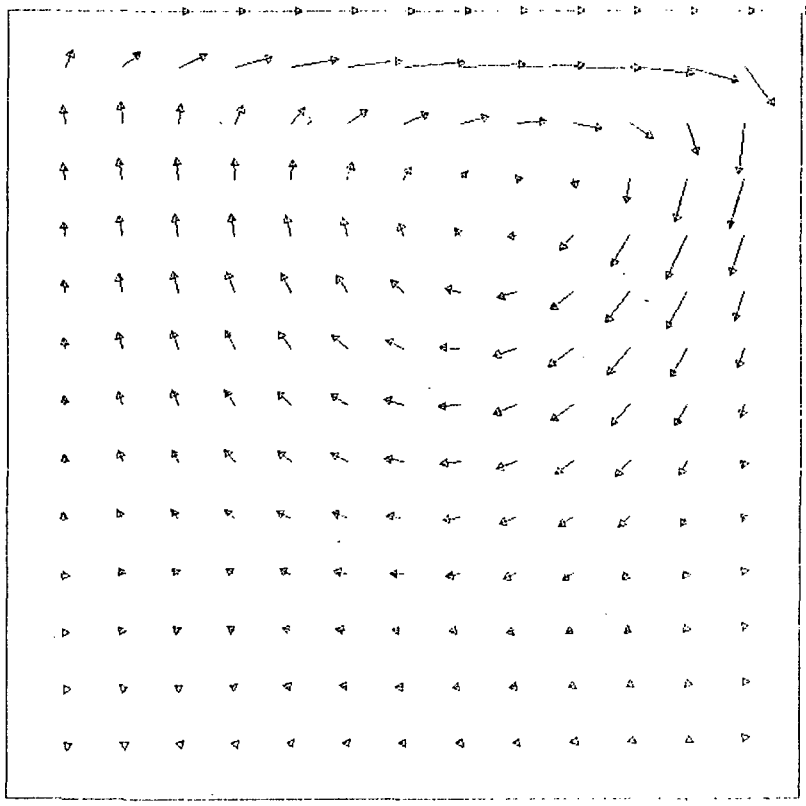

(a) Velocity vectors.

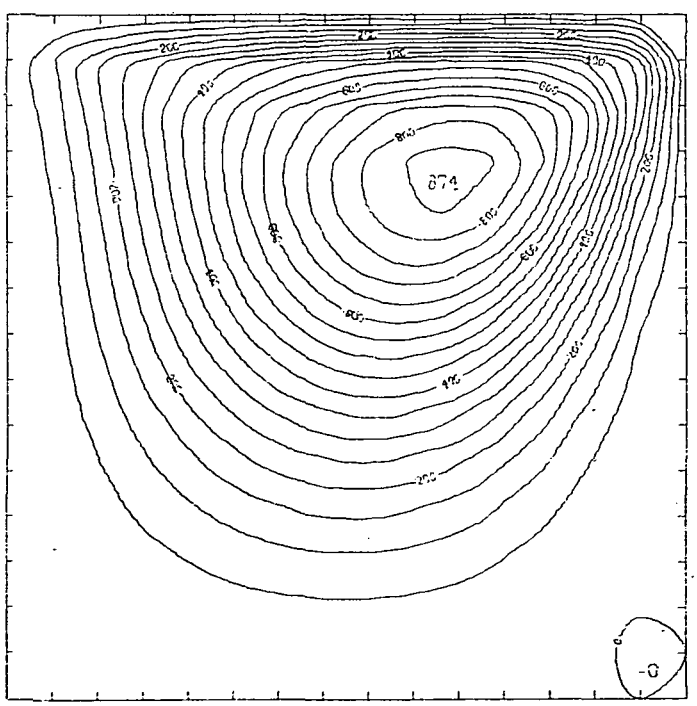

(b) Streamlines.

Figure 1.- Machine plots of flow field. N = 15; R = 100.

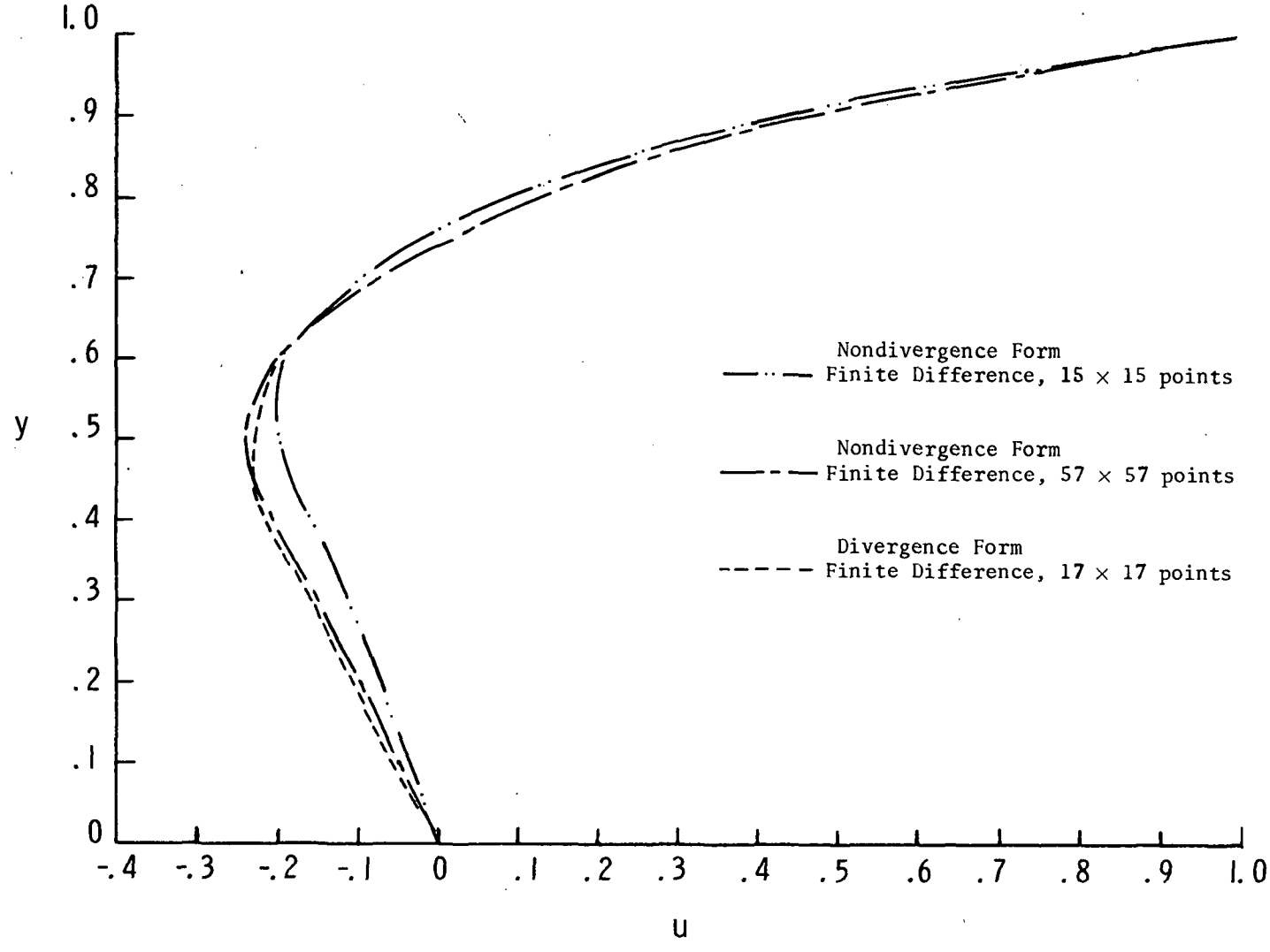

Figure 2.- Calculated velocity component u through point of maximum ψ. R = 100.

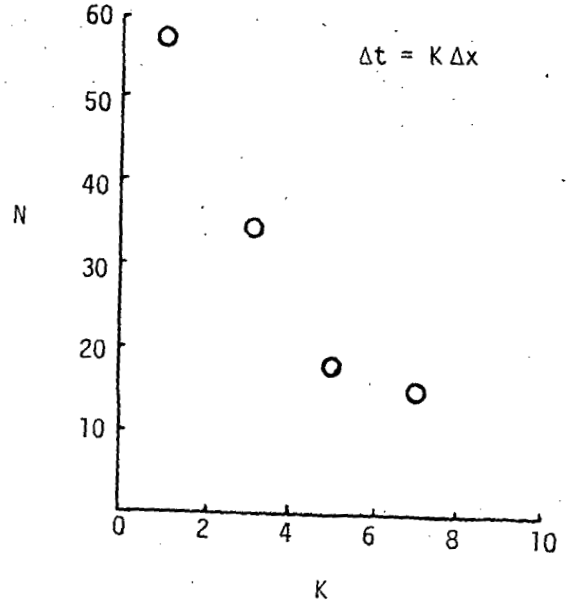

Figure 3.- Effect of number of nodal points (N × N) on time step.

Page intentionally left blank

6. COMPARATIVE STUDY OF TWO NUMERICAL TECHNIQUES FOR THE SOLUTION OF VISCOUS FLOW IN A DRIVEN CAVITY

Robert E. Smith, Jr., and Amy Kidd*
Langley Research Center

SUMMARY

Numerical solutions have been obtained for the steady two-dimensional flow of a viscous incompressible fluid in a rectangular cavity. The Reynolds number has been varied from 100 to 5000. The conservative stream-function—vorticity form of the two-dimensional incompressible Navier-Stokes equations was solved. Two techniques (alternating-direction implicit and hopscotch) have been applied to the vorticity equation. The stream-function equation has been solved by successive overrelaxation and by the Buneman direct method. The investigation assesses which combination of these techniques, applied to the stream-function—vorticity form of the Navier-Stokes equations, is the most computationally efficient. Width-depth ratios of 1, 2, and 4 have been used in this numerical experiment. Relative efficiency has been based on the central processing time of each technique run on the same computer. The results indicate that the alternating-direction implicit technique for solving the vorticity equation and the Buneman direct method for solving the stream-function equation yield the most efficient combination of the techniques studied. In addition, solutions have been obtained at Reynolds numbers of 100, 1000, and 5000 with a second-order accurate approximation.

INTRODUCTION

Numerical solutions of the stream-function—vorticity form of the Navier-Stokes equations describing two-dimensional flow have been the subject of many investigations. In particular, the flow properties of a viscous incompressible fluid within a rectangular cavity whose upper surface is translating with uniform velocity have been established for low Reynolds numbers. (See paper no. 1 by Rubin and Harris.) This study has attempted to increase understanding of optimum solution techniques for solving the two-dimensional Navier-Stokes equations at low Reynolds numbers. The optimum solution technique is taken to be the one which provides a steady-state solution in minimum computer time with the least complex program. It is recognized that optimum in this sense is computer dependent. However, the results should hold for any third generation computer. Two techniques which appear to be near optimum for solving the vorticity equation are the alternating-direction implicit (ADI) and hopscotch (HS) procedures. Reference 1 should be referred to for the ADI technique and reference 2 is adequate for the HS technique.

*Computer Sciences Corporation, Hampton, Va.

For solving the stream-function equation the successive overrelaxation (SOR) technique and the Buneman direct method (BDM) are candidates for being optimum solution procedures. Reference 3 should be consulted for the BDM and reference 2 is adequate for the SOR technique.

The two-dimensional Navier-Stokes equations have been described in conservation form and approximate boundary conditions established. A computer program with the option of using the ADI or HS technique for the solution of the vorticity equation has been written. In addition, the HS technique is applied in two ways. The first approach (HS1) is direct application of the difference equations at the even and odd grid points. The second approach (HS2) is application of a combined difference equation when the iteration plus the grid point is even. The second approach should reduce the number of operations by approximately 40 percent. The computer program has the option of solving the stream-function equation by either SOR or BDM. The BDM subroutine used in the computer program is one written by Buzbee. (See ref. 3.) The Buneman algorithm is much more complex than the SOR algorithm; however, once the algorithm is written into a computer program, it is easily applied. Note that if the domain of interest is not rectangular, the Buzbee routine and the BDM are not directly applicable. The computer program has been written with the ability to vary time step, grid size, Reynolds number, and initial conditions. With this program as an experimental tool, many runs varying time step, grid size, Reynolds number, and width-depth ratio with each of the combination techniques – ADI-SOR, ADI-BDM, HS1-SOR, HS1-BDM, HS2-SOR, and HS2-BDM – have been made on a CDC 6400 computer and appropriate statistics recorded.

SYMBOLS

N,M	dimensions of grid (see fig. 1)
R	Reynolds number
t	time
Δt	time step
U	uniform velocity at upper surface (see fig. 1)
u	axial velocity
v	normal velocity

x,y	axial and normal coordinate, respectively
$\Delta x, \Delta y$	spatial increments in x- and y-directions
β	$= \Delta x/\Delta y$
ζ	vorticity
ψ	stream function
ω	convergence parameter in SOR approximation

Superscripts:

k	index of iteration
n	index of time step

Subscripts:

i,j	index of grid point in x- and y-direction, respectively
in	grid point inside surface
out	grid point outside surface
s	grid point on surface
t	differentiation with respect to t
x,y	differentiation with respect to x or y

Abbreviations:

ADI	alternating direction implicit
BDM	Buneman direct method
HS1	hopscotch method 1

HS2 hopscotch method 2

SOR successive overrelaxation

GOVERNING EQUATIONS AND BOUNDARY CONDITIONS

The normalized stream-function—vorticity conservation form of the two-dimensional incompressible Navier-Stokes equations is:

$$\zeta_t = -(\psi_y)\zeta_x + (\psi_x)\zeta_y + \frac{1}{R}(\zeta_{xx} + \zeta_{yy}) \tag{1}$$

$$\psi_{xx} + \psi_{yy} = -\zeta \tag{2}$$

The boundary conditions on the stream-function equation (eq. (2)) for flow in a cavity with the upper surface translating to the left with uniform velocity $U = 1$ and with no flow at the other boundaries are (see fig. 1):

at upper surface (moving to left),

$$\psi_y = -1 \qquad \psi_x = 0 \qquad \psi = 0$$

at bottom, left, and right surfaces,

$$\psi_y = 0 \qquad \psi_x = 0 \qquad \psi = 0$$

The boundary conditions on the vorticity equation are obtained by central differencing equation (2), by applying the boundary conditions for the stream function, and by enforcing reflection at the boundary. They are:

at upper surface,

$$\frac{\psi_{out} - 2\psi_s + \psi_{in}}{(\Delta y)^2} = -\zeta_s$$

$$\psi_s = 0$$

$$\frac{\psi_{out} - \psi_{in}}{2\,\Delta y} = -1$$

or combining these conditions results in

$$\frac{2\psi_{in} - 2\,\Delta y}{(\Delta y)^2} = -\zeta_s$$

at bottom surface,

$$\frac{\psi_{out} - 2\psi_s + \psi_{in}}{(\Delta y)^2} = -\zeta_s$$

$$\psi_s = 0$$

$$\psi_{in} = \psi_{out}$$

or

$$\frac{2\psi_{in}}{(\Delta y)^2} = -\zeta_s$$

at left and right surfaces,

$$\frac{\psi_{out} - 2\psi_s + \psi_{in}}{(\Delta x)^2} = -\zeta_s$$

$$\psi_s = 0$$

$$\psi_{in} = \psi_{out}$$

or

$$\frac{2\psi_{in}}{(\Delta x)^2} = -\zeta_s$$

FINITE-DIFFERENCE APPROXIMATIONS

Because of the complexity of the BDM, an explanation of this method is not given. Details of the method are given by Buzbee, Golub, and Nielson in reference 3.

ADI Approximation for Vorticity Equation

The ADI algorithm is applied to the vorticity equation (eq. (1)) in the following two steps:

Step 1

$$-\left[\left(\psi_y\right)_{i-1,j}^{n+1/2}\gamma_x + \lambda_x\right]\zeta_{i-1,j}^{n+1/2} + \left(1 + 2\lambda_x\right)\zeta_{i,j}^{n+1/2} + \left[\left(\psi_y\right)_{i+1,j}^{n+1/2}\gamma_x - \lambda_x\right]\zeta_{i+1,j}^{n+1/2}$$

$$= \left[-\left(\psi_x\right)_{i,j-1}^{n}\gamma_y + \lambda_y\right]\zeta_{i,j-1}^{n} + \left(1 - 2\lambda_y\right)\zeta_{i,j}^{n} - \left[\left(\psi_x\right)_{i,j+1}^{n}\gamma_y + \lambda_y\right]\zeta_{i,j+1}^{n} \tag{3}$$

Step 2

$$\left[\left(\psi_x\right)_{i,j-1}^{n+1}\gamma_y - \lambda_y\right]\zeta_{i,j-1}^{n+1} + \left(1 + 2\lambda_y\right)\zeta_{i,j}^{n+1} + \left[-\left(\psi_x\right)_{i,j+1}^{n+1}\gamma_y + \lambda_y\right]\zeta_{i+1,j}^{n+1}$$

$$= \left[\left(\psi_y\right)_{i-1,j}^{n+1/2}\gamma_x + \lambda_x\right]\zeta_{i-1,j}^{n+1/2} + \left(1 - 2\lambda_x\right)\zeta_{i,j}^{n+1/2}$$

$$+ \left[-\left(\psi_y\right)_{i+1,j}^{n+1/2}\gamma_x + \lambda_x\right]\zeta_{i+1,j}^{n+1/2} \tag{4}$$

where

$$\gamma_x = \frac{\Delta t}{4\,\Delta x} \qquad \gamma_y = \frac{\Delta t}{4\,\Delta y}$$

$$\lambda_x = \frac{\Delta t}{2R(\Delta x)^2} \qquad \lambda_y = \frac{\Delta t}{2R(\Delta y)^2}$$

and

$$\Delta x = x_i - x_{i-1} \qquad \Delta y = y_j - y_{j-1} \qquad \Delta t = t^n - t^{n-1}$$

Steps 1 and 2 form tridiagonal systems of linear algebraic equations. Solving equations (3) and (4) in succession yields one time step.

Hopscotch Approximation for Vorticity Equation

The following three equations are used in the hopscotch techniques:

$$\zeta_{i,j}^{n+1} = \left[(\psi_y)_{i-1,j}^{n}\gamma_x' + \lambda_x'\right]\zeta_{i-1,j}^{n} + \left[-(\psi_y)_{i+1,j}^{n}\gamma_x' + \lambda_x'\right]\zeta_{i+1,j}^{n} + \left[-(\psi_x)_{i,j-1}^{n}\gamma_y' + \lambda_y'\right]\zeta_{i,j-1}^{n}$$

$$+ \left[(\psi_x)_{i,j-1}^{n}\gamma_y' + \lambda_y'\right]\zeta_{i,j+1}^{n} + \left(1 - 2\lambda_x' - 2\lambda_y'\right)\zeta_{i,j}^{n} \tag{5}$$

$$\zeta_{i,j}^{n+1} = \frac{1}{1 + 2\lambda_x' + 2\lambda_y'}\left\{\left[(\psi_y)_{i-1,j}^{n+1}\gamma_x' + \lambda_x'\right]\zeta_{i-1,j}^{n+1} + \left[-(\psi_y)_{i+1,j}^{n+1}\gamma_x' + \lambda_x'\right]\zeta_{i+1,j}^{n+1}\right.$$

$$\left. + \left[-(\psi_x)_{i,j-1}^{n+1}\gamma_y' + \lambda_y'\right]\zeta_{i,j-1}^{n} + \left[(\psi_x)_{i,j+1}^{n+1}\gamma_y' + \lambda_y'\right]\zeta_{i,j+1}^{n} + \zeta_{i,j}^{n}\right\} \tag{6}$$

and

$$\zeta_{i,j}^{n+1} = 2\zeta_{i,j}^{n} - \zeta_{i,j}^{n-1} \tag{7}$$

where

$$\lambda_x' = \frac{\Delta t}{R(\Delta x)^2} \qquad \lambda_y' = \frac{\Delta t}{R(\Delta y)^2}$$

$$\gamma_x' = \frac{\Delta t}{2\,\Delta x} \qquad \gamma_y' = \frac{\Delta t}{2\,\Delta y}$$

The HS technique is used in two ways to approximate the vorticity equation:

(1) In the first method (HS1), the difference equations are directly applied in two sweeps. First, equation (5) is computed at grid points for which $i + j + n$ is even. Then, equation (6) is computed at points for which $i + j + n$ is odd.

(2) The second approach (HS2) is a three-level method which results from a combination of equations (5) and (6). For $n \leq 2$, the equations are applied as for HS1. For $n \geq 3$, equation (7) is computed at points for which $i + j + n$ is even and equation (6) is applied at points for which $i + j + n$ is odd.

The hopscotch technique is conditionally stable for the vorticity equation according to the Courant-Friedrichs-Lewy (CFL) condition; that is, $U(\Delta t/\Delta x) \leq 1$. For HS1, 21 arithmetic operations are necessary for computing ζ at time level $n + 1$. Dimensional computer variables are stored and retrieved from memory at two time levels, n and $n + 1$. With HS2, 43 percent less arithmetic operations are necessary. However, HS2 requires 33 percent more storage than HS1. Since HS2 requires storage of two-dimensional arrays at three time levels, 43 percent less arithmetic operations does not necessarily imply 43 percent increase in computational efficiency.

SOR Approximation for Stream-Function Equation

The following equation is used in the SOR routine to approximate the stream function:

$$\psi^{k+1} = \psi^{k}_{i,j} + \frac{\omega}{2(1 + \beta^2)}\left[\psi^{k}_{i+1,j} + \psi^{k+1}_{i-1,j} + \beta^2\psi_{i,j+1} + \beta^2\psi^{k+1}_{i,j-1} - (\Delta x)^2\zeta_{i,j} - 2(1 + \beta^2)\psi^{k}_{i,j}\right]$$

where the convergence parameter ω is 1.67351.

ANALYSIS AND RESULTS

An analysis of the techniques discussed in the preceding section based on an experimental computer program designed to execute the ADI-SOR, ADI-BDM, HS1-SOR, HS1-BDM, HS2-SOR, or HS2-BDM combination has been performed. The results of computer runs made with this program on a CDC 6400 computer are summarized in table I. The Reynolds number has been varied from 100 to 5000 in cavities with width-depth of 1, 2, and 4. The basic grid size is 1/16. More accurate solutions were obtained with grid sizes of 1/32 and 1/64 for a Reynolds number of 100 and a width-depth ratio of 1. In order to save computer time with the 1/64 grid, initial conditions with the converged 1/32 grid were used. Linear interpolation was used to obtain initial conditions at the midpoints. The 1/64 grid required considerably more computer resources than any of the others. The initial conditions for all runs other than those with the 1/64 grid are $\psi = 0.1$ and $\zeta = 0$.

For the solution of flow in a cavity, the ADI-BDM combination was found to be the most computationally efficient of the techniques studied. The memory requirements are comparable with the HS1-BDM combination which is approximately 20 percent slower. In both the ADI-BDM and HS1-BDM combinations, only two levels of information must be stored simultaneously. The advantage of the ADI-BDM combination is due to the larger time steps that can be taken. The HS1-BDM and HS2-BDM combinations require fewer arithemetic operations per time step; however, hopscotch is stability limited by the

CFL condition ($\overline{U}(\Delta t/\Delta x) \leqq 1$). A linearized stability analysis indicates the ADI method is unconditionally stable. In practice, arbitrarily large time steps could not be used. It was necessary to make runs with a number of time steps to determine a satisfactorily large step which produced a stable solution for a particular Reynolds number and grid size.

The BDM is probably the fastest technique presently known for solving a Poisson equation over a rectangular domain. The particular routine of Buzbee (ref. 3) is partially written in COMPASS (machine language) to add additional speed to the routine. Since this routine yielded a 1/3 decrease in central processing time, it was used exclusively for more time-consuming runs.

The HS1 method was relatively easy to program and its storage requirements satisfactory (two simultaneous levels of information). It was not necessary to run this technique with $\Delta t = \Delta x$ since the velocity falls off from 1 to 0.6 (R = 100) in one grid step ($\Delta x = \Delta y = 1/16$). However, when $\Delta t > \Delta x$, some oscillation would occur near the moving boundary.

The HS2-BDM combination was the second most computationally efficient on the basis of these computer experiments. It was about 20 percent slower than ADI-BDM combination. According to the number of arithmetic operations, it should have required about 40 percent less computational time than HS1-BDM; however, because of the requirement of three simultaneous time levels of information, there are added machine operations associated with storing and retrieving this information. Table I shows the results of all the computer runs in order of ascending central processing time. Because of its explicit nature, it is believed that the hopscotch algorithm has a high potential for the STAR computer. It is 20 percent slower than the ADI method, but the machine efficiency of an explicit (vectorizable) technique has the potential of rendering HS1 superior to ADI when an inconsistent transient solution is acceptable.

REMARKS ON ACCURACY

Solutions calculated with the ADI technique of the stream-function—vorticity form of the Navier-Stokes equations are given in figures 2, 3, and 4 for Reynolds numbers of 100, 1000, and 5000, respectively. The results for a Reynolds number of 100 (fig. 2) agree well with Burggraf (ref. 4) and Bozeman (ref. 5). For a Reynolds number of 1000, the results for the stream function obtained in this study (figs. 3(a) and 3(b)) have the character of those obtained by Bozeman. Bozeman used a grid size of 1/50; however, his differencing of the convective terms of the vorticity equation for a Reynolds number of 1000 is first-order accurate, whereas the present solution is based on a central-difference approximation of the convective terms and is therefore second-order accurate. The contour plots of the vorticity solutions for Reynolds numbers of 1000 and 5000

(figs. 3(c) and 4(c)) are meaningless near the center of the cavity since the surface is nearly flat there. Probably the perspective plots (figs. 3(d) and 4(d)) are more meaningful. They show how the vorticity changes rapidly at the boundaries and is flat in the middle for high Reynolds numbers. The 1/16 grid size is too large for good accuracy at Reynolds numbers of 1000 and 5000 even though the solutions obtained show the expected character. A point of interest is that with the ADI procedure, which used central differencing of the convective terms in the vorticity equation, converged solutions could not be obtained at higher Reynolds numbers than Bozeman used. Bozeman was unable to obtain solutions with either central or upwind differencing for $R > 1000$.

CONCLUDING REMARKS

The primary conclusion of this study is that a combination of the alternating-direction implicit technique and the Buneman direct method is a rapid procedure for solving the Navier-Stokes stream-function and vorticity equations in a rectangular region. The combination of the hopscotch and Buneman direct methods is only 20 percent slower at low Reynolds numbers. The hopscotch technique was applied in two ways: (1) direct application of the difference equations at even and odd grid points and (2) application of a combined difference equation at points for which the iteration plus the grid point was even. With both hopscotch approaches combined with the Buneman direct method, the first is preferable to the second, because it is easier to program, requires less storage, and is only slightly slower. The first hopscotch approach appears to have potential for flow computations on vector machines such as the STAR computer.

It was possible to obtain converged solutions at Reynolds numbers of 1000 and above with the alternating-direction implicit technique which used central-difference approximations for the convective terms in the vorticity equation. The solutions obtained at higher Reynolds numbers are not necessarily accurate, but they do show the character of high vorticity gradients near the moving boundary and low vorticity gradients near the center.

REFERENCES

1. Peaceman, D. W.; and Rachford, H. H., Jr.: The Numerical Solution of Parabolic and Elliptic Differential Equations. J. Soc. Ind. & Appl. Math., vol. 3, no. 1, Mar. 1955, pp. 28-41.

2. Roach, Patrick J.: Computational Fluid Dynamics. Hermosa Publ., c.1972.

3. Buzbee, B. L.; Golub, G. H.; and Nielson, C. W.: On Direct Methods for Solving Poisson's Equations. SIAM J. Numerical Anal., vol. 7, no. 4, Dec. 1970, pp. 627-656.

4. Burggraf, Odus R.: Analytical and Numerical Studies of the Structure of Steady Separated Flows. J. Fluid Mech., vol. 24, pt. 1, Jan. 1966, pp. 113-151.

5. Bozeman, James D.; and Dalton, Charles: Numerical Study of Viscous Flow in a Cavity. J. Comput. Phys., vol. 12, no. 3, July 1973, pp. 348-363.

TABLE I.- RESULTS OF ANALYSIS OF TECHNIQUES ON CDC 6400 COMPUTER

[Convergence criterion was 0.0001]

Reynolds number	Width-depth ratio of cavity	Techniques used –		Grid size, $\Delta x = \Delta y$	Time step	Central processing time, sec	Number of iterations	Computer time ratio (a)
		For vorticity	For stream function					
100	1	ADI	BDM	1/16	0.2	56.85	119	1
100	1	HS2	BDM	1/16	.063	63.8	337	1.12
100	1	HS1	BDM	1/16	.063	65.4	339	1.14
100	1	ADI	SOR	1/16	.2	90.17	110	1.586
100	1	HS2	SOR	1/16	.063	117.8	325	2.07
100	1	HS1	SOR	1/16	.063	122.9	328	2.16
100	2	ADI	BDM	1/16	.2	260.9	136	4.58
100	4	ADI	BDM	1/16	.2	588.8	139	10.35
100	1	ADI	BDM	1/32	.075	478.7	322	8.42
100	1	ADI	BDM	1/64	.0097	16 783.0	2561	295.21
1000	1	ADI	BDM	1/16	.2	198.03	693	3.48
5000	1	ADI	BDM	1/16	.2	2 106.5	3469	37.05

[a]Ratio of central processing time to central processing time of first entry.

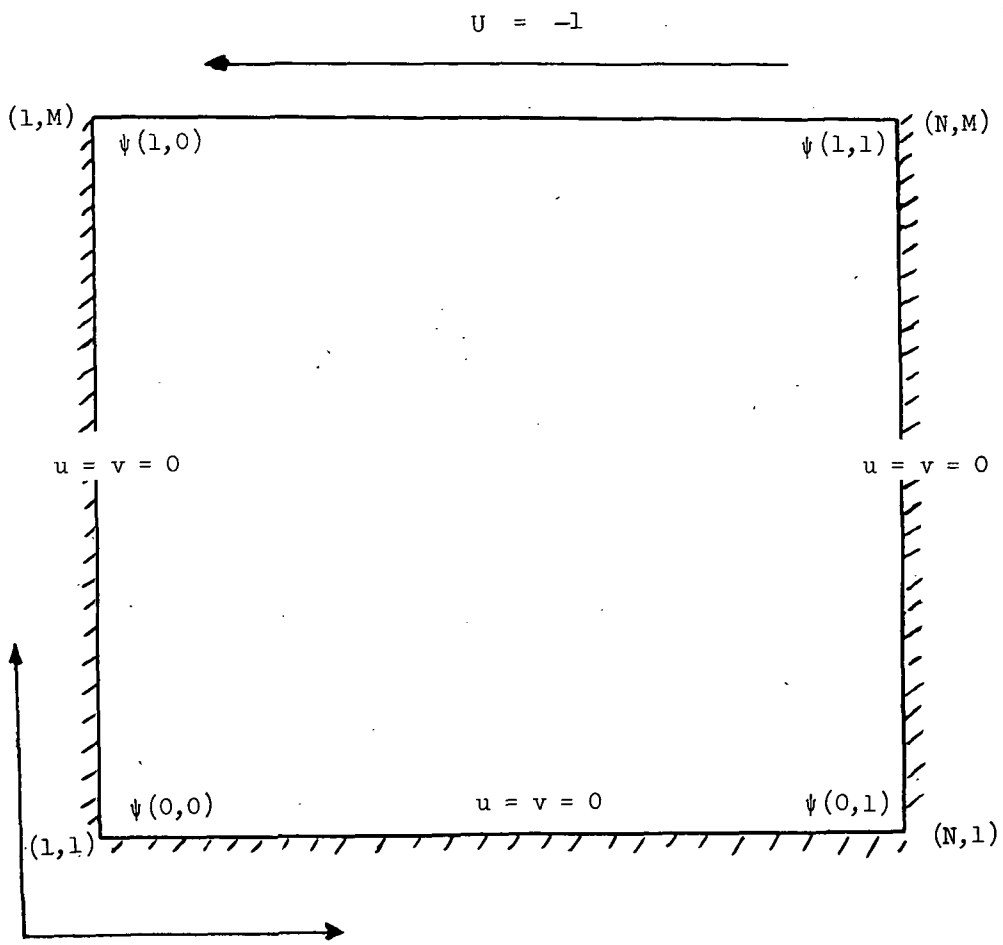

Figure 1.- Flow domain.

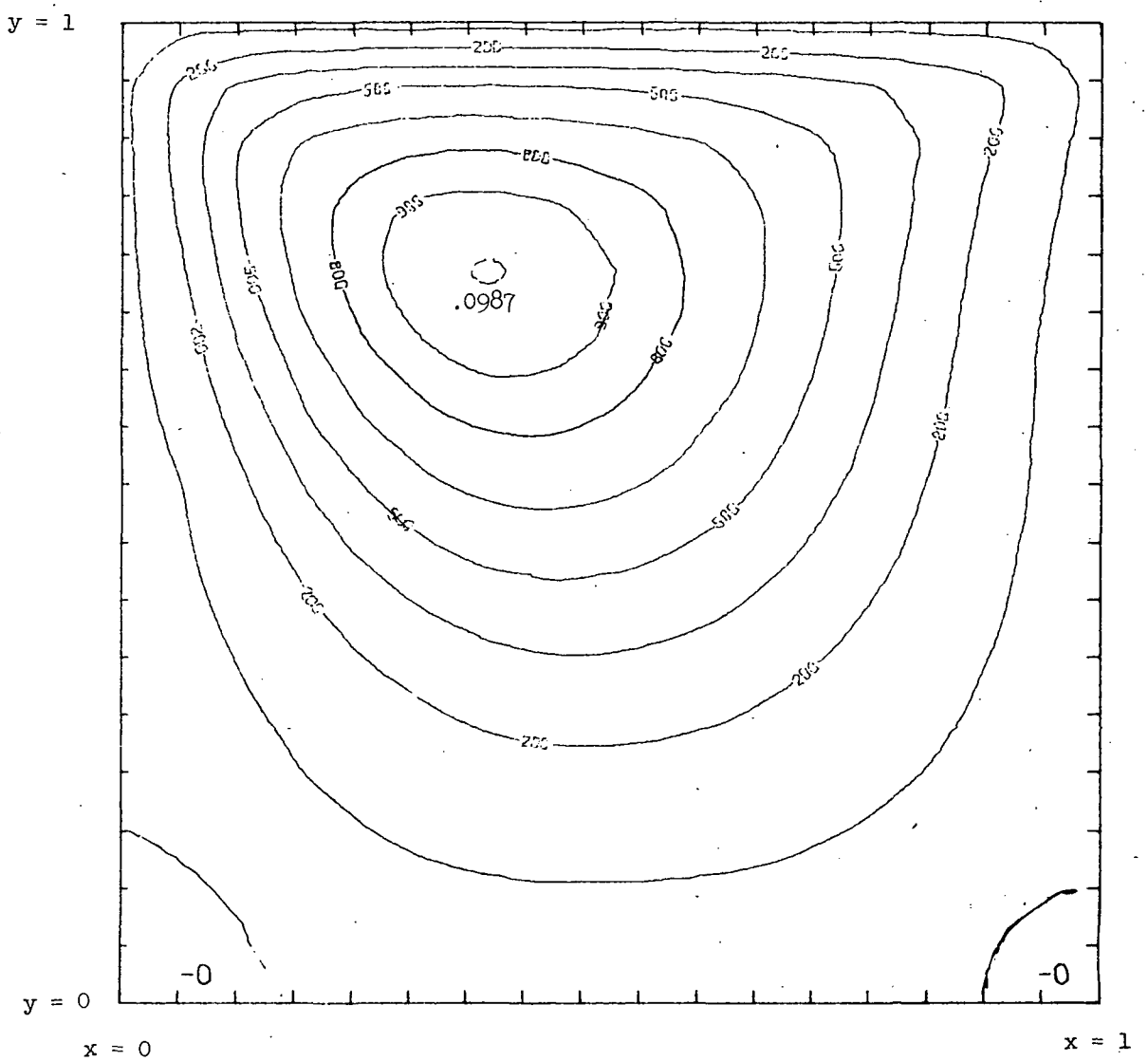

(a) Contour plot of stream function.

Figure 2.- ADI-BDM solutions for R = 100.

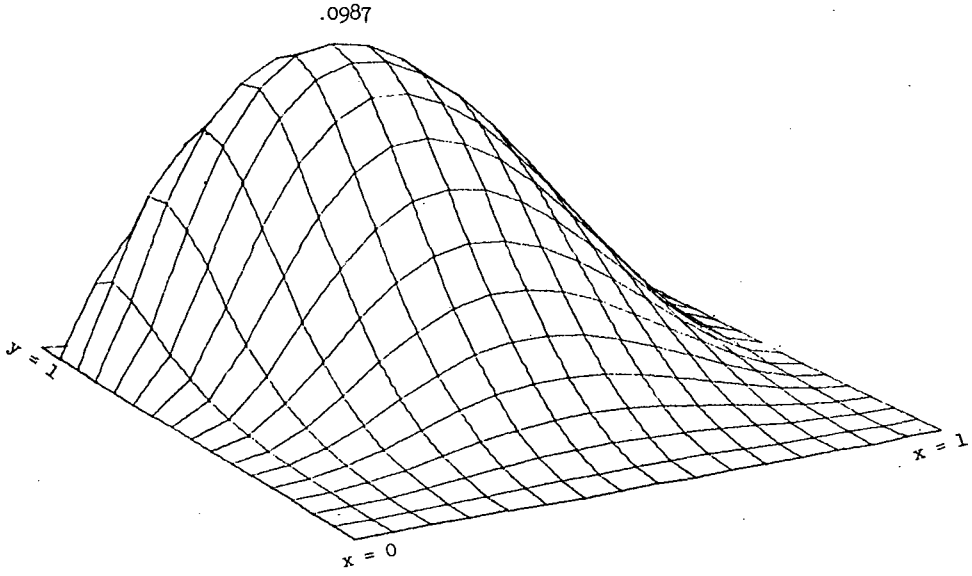

(b) Perspective view of stream function.

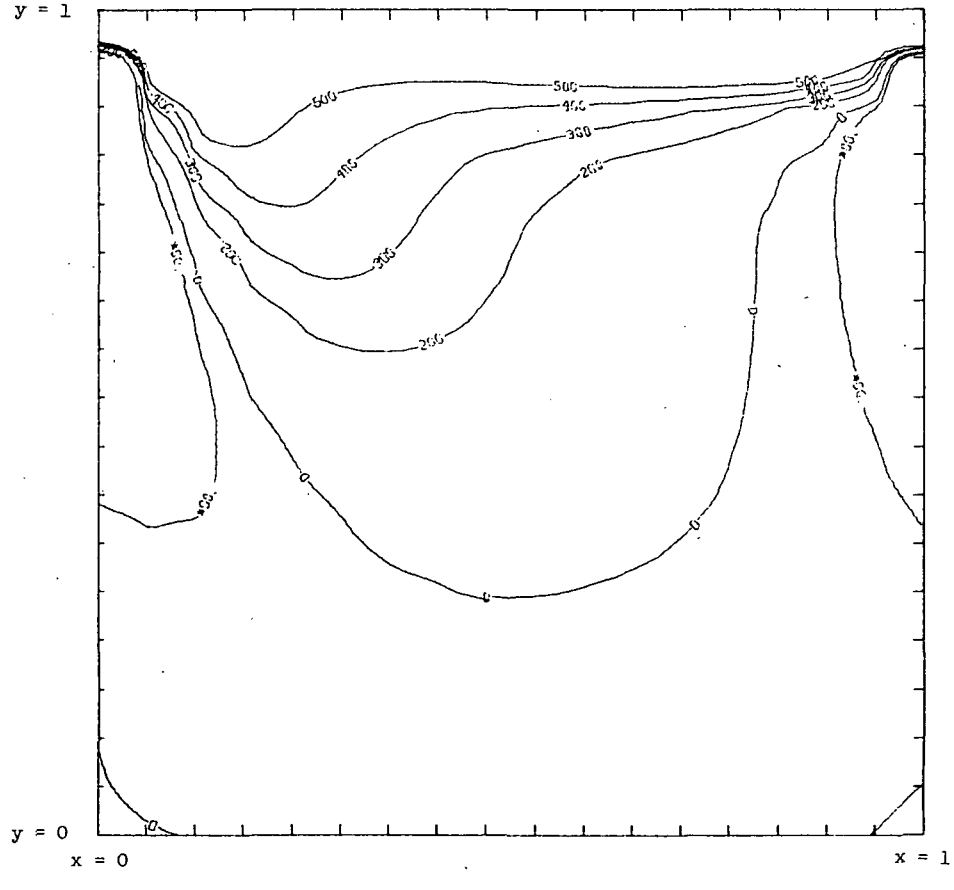

(c) Contour plot of vorticity.

Figure 2.- Continued.

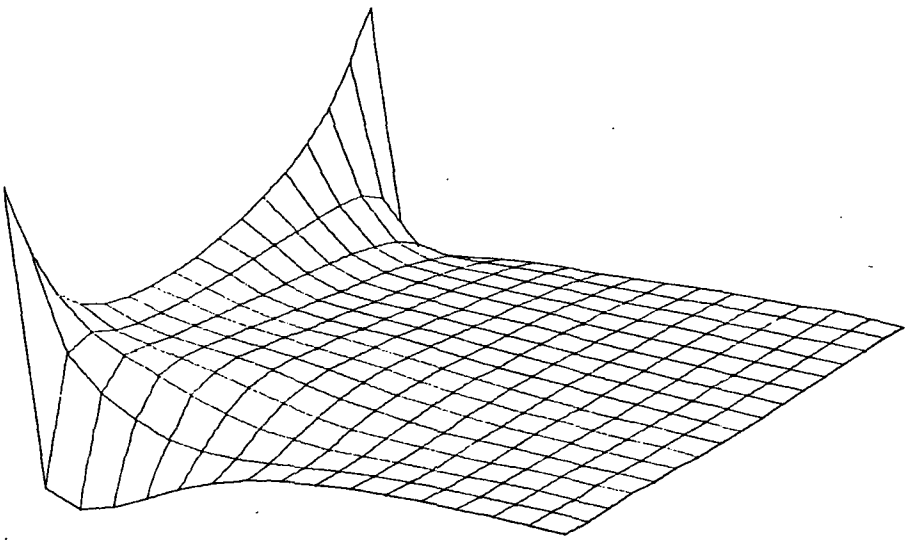

(d) Perspective view of vorticity.

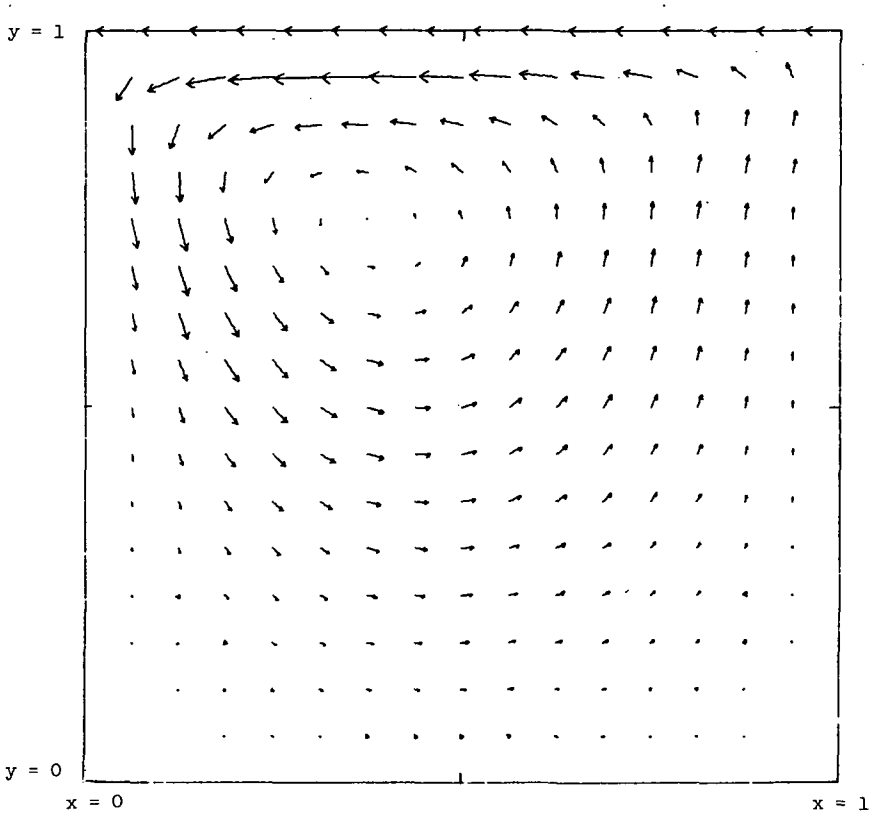

(e) Velocity field.

Figure 2.- Concluded.

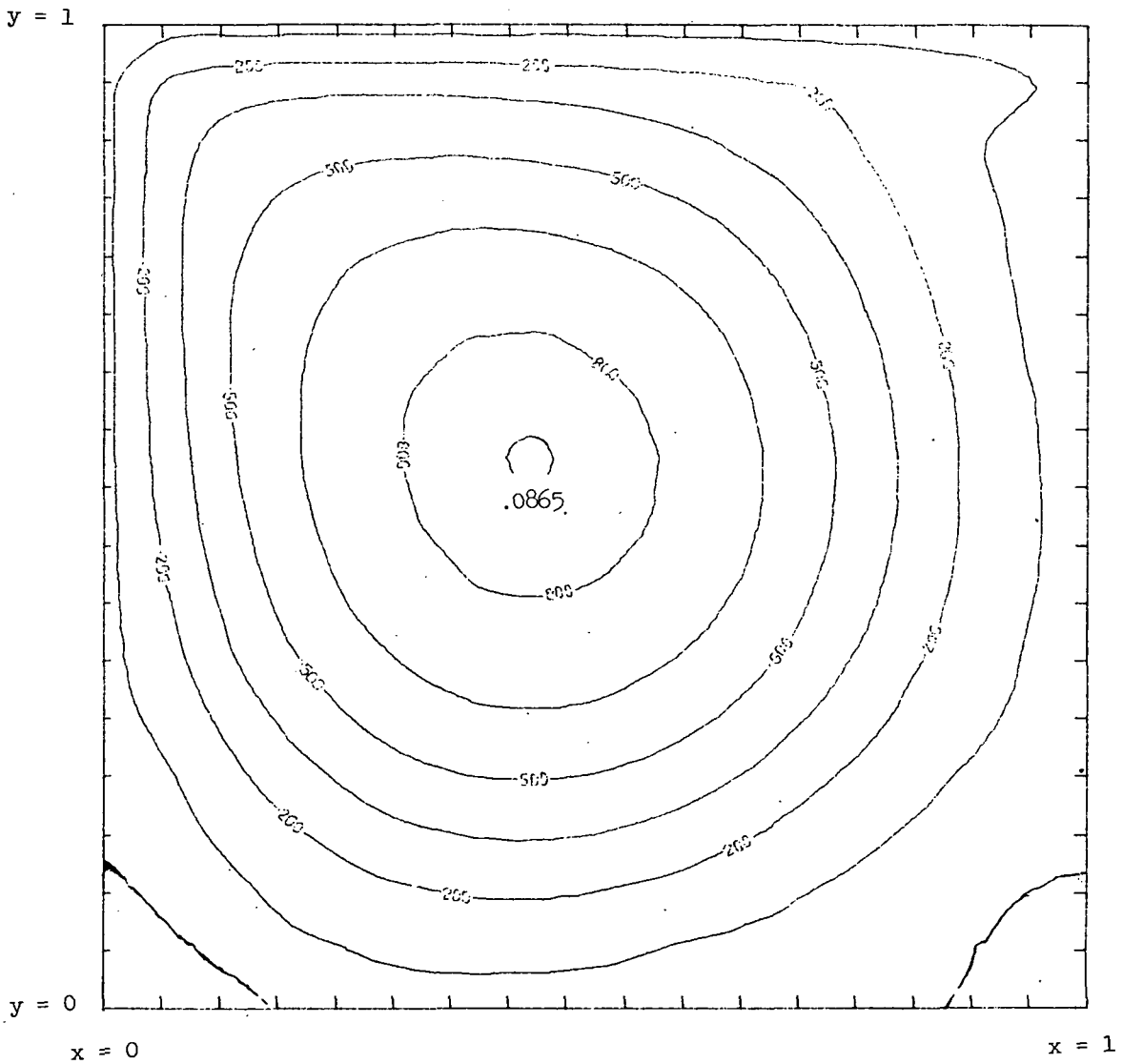

(a) Contour plot of stream function.

Figure 3.- ADI-BDM solutions for R = 1000.

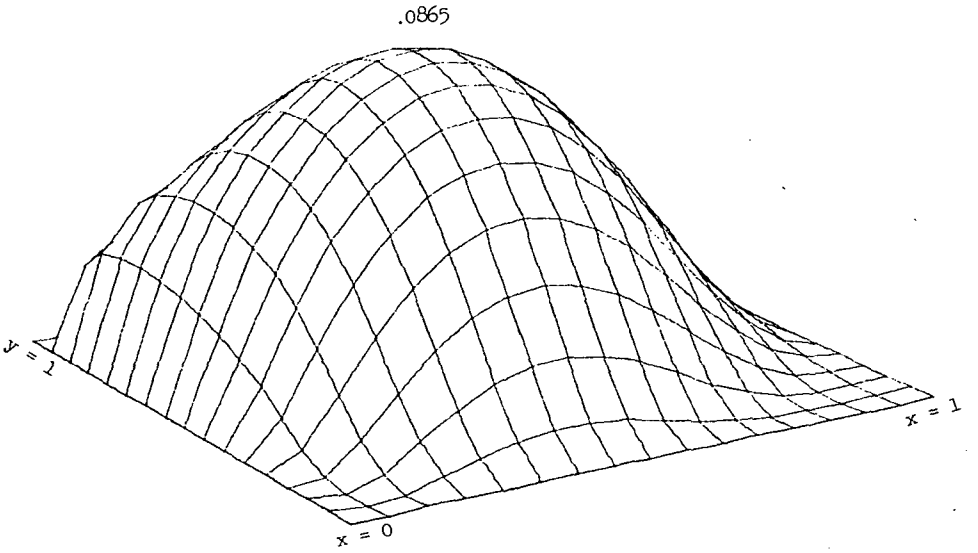

(b) Perspective view of stream function.

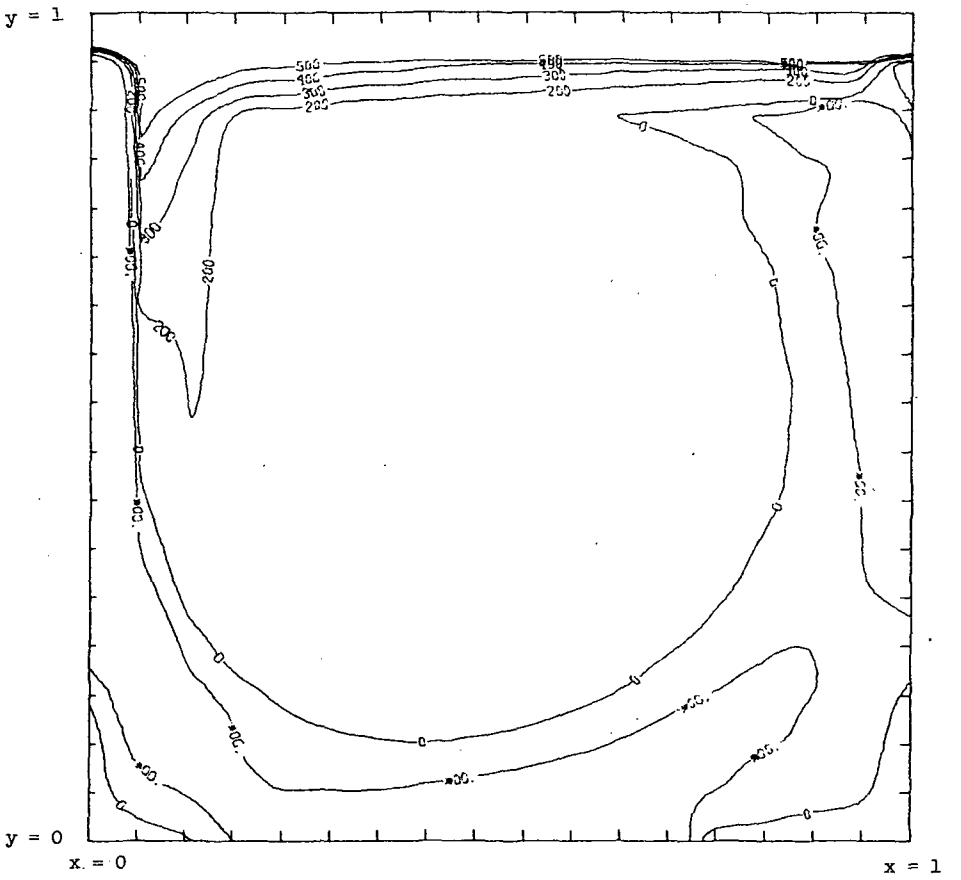

(c) Contour plot of vorticity.

Figure 3.- Continued.

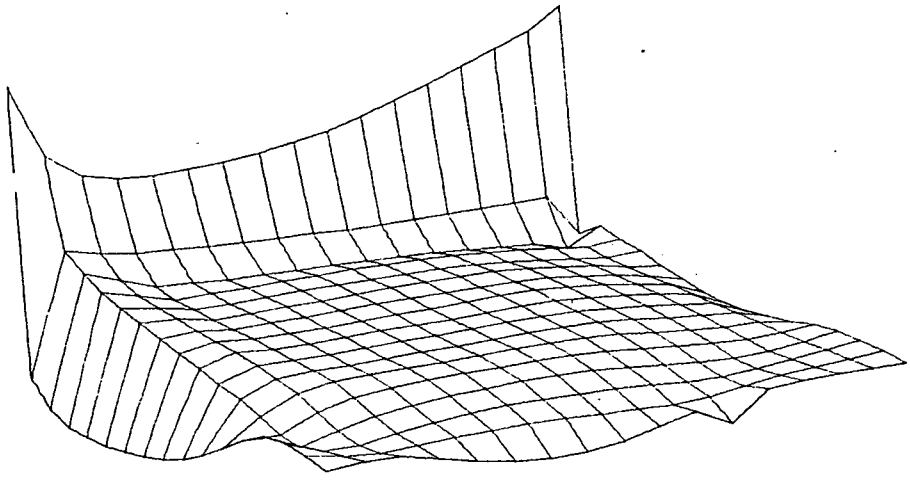

(d) Perspective view of vorticity.

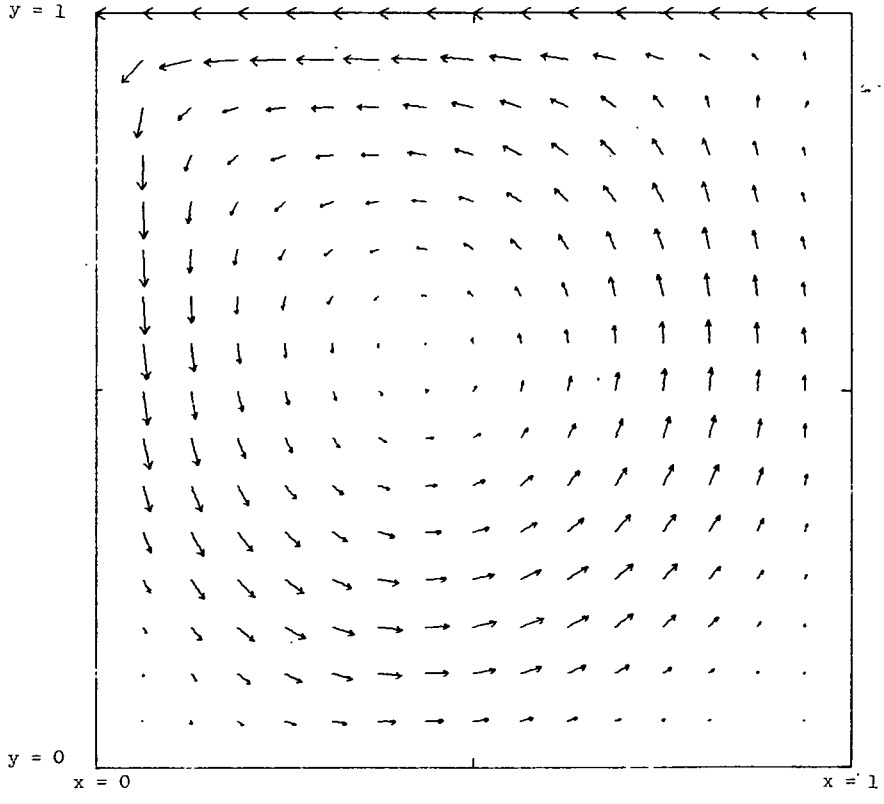

(e) Velocity field.

Figure 3.- Concluded.

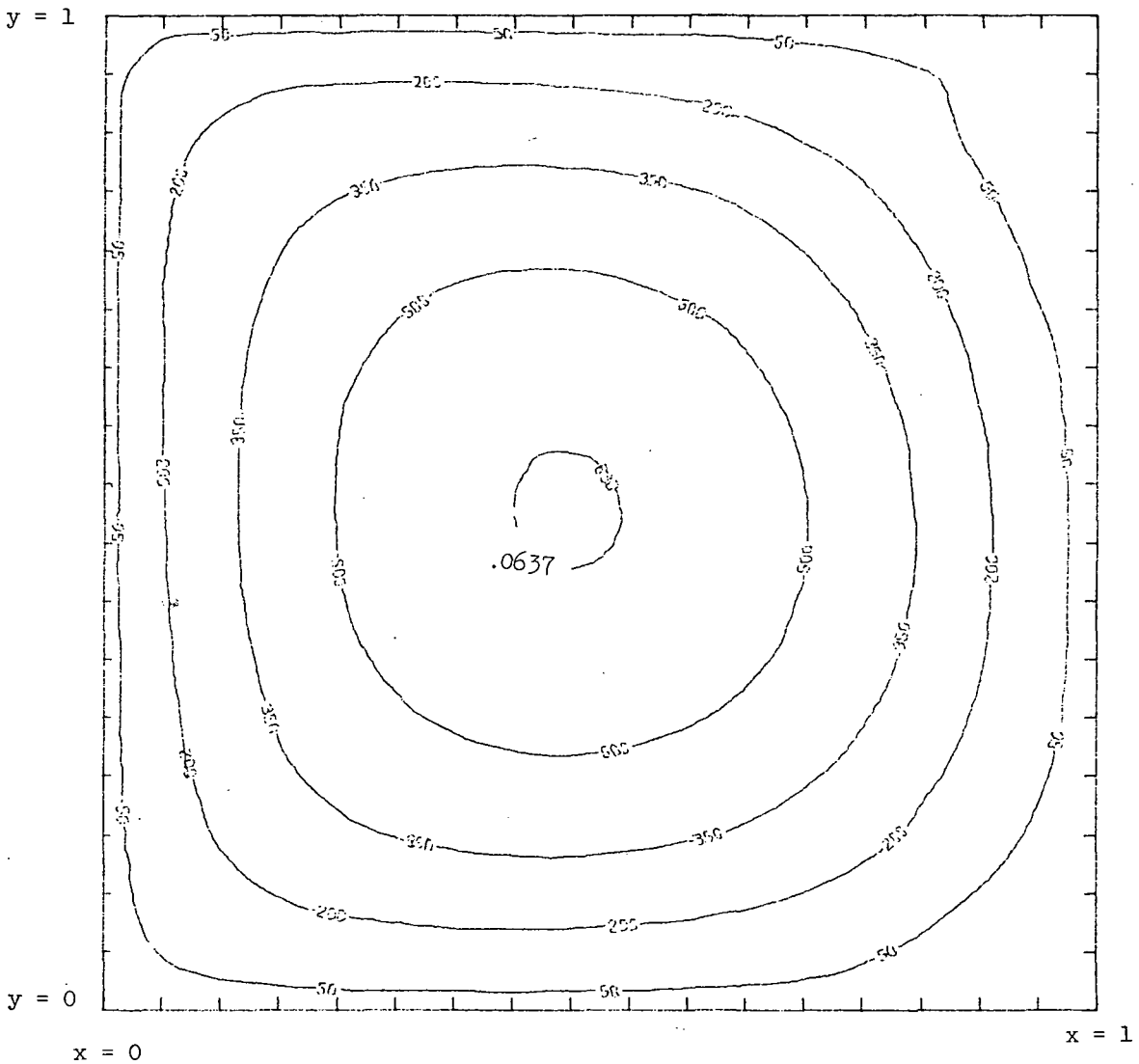

(a) Contour plot of stream function.

Figure 4.- ADI-BDM solutions for R = 5000.

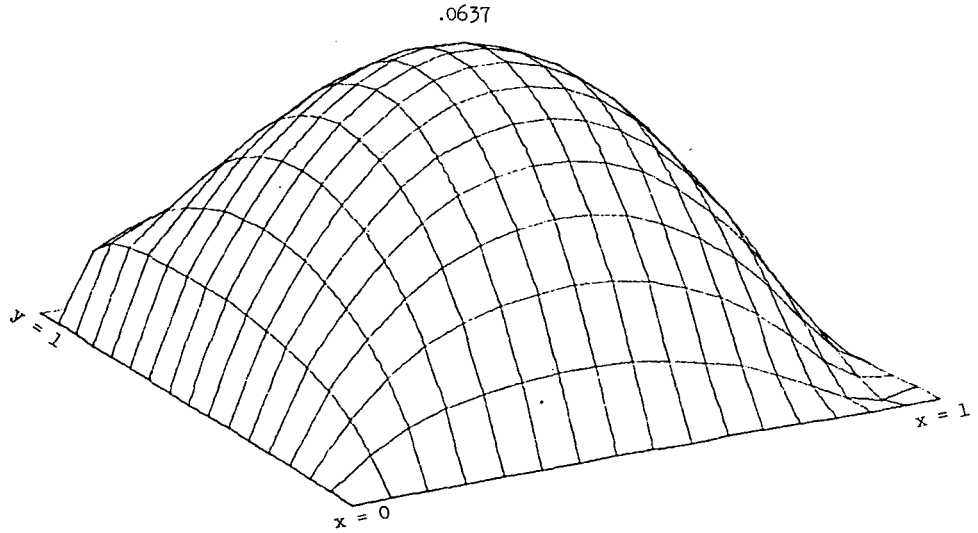

(b) Perspective view of stream function.

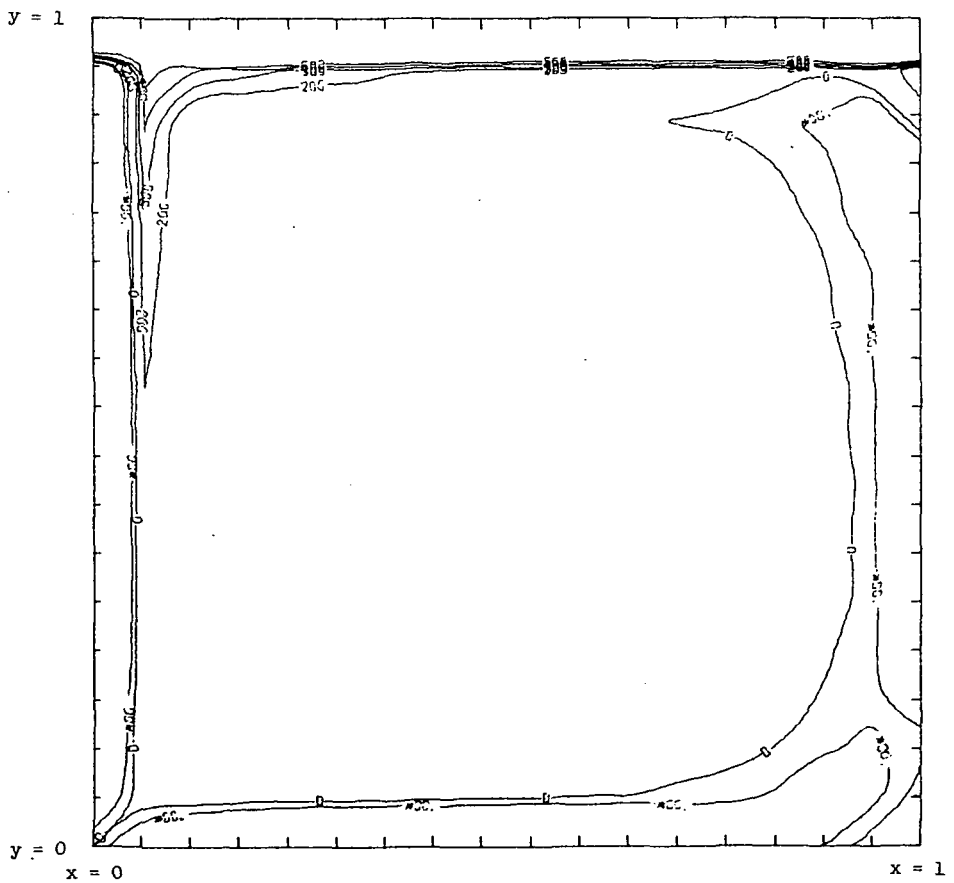

(c) Contour plot of vorticity.

Figure 4.- Continued.

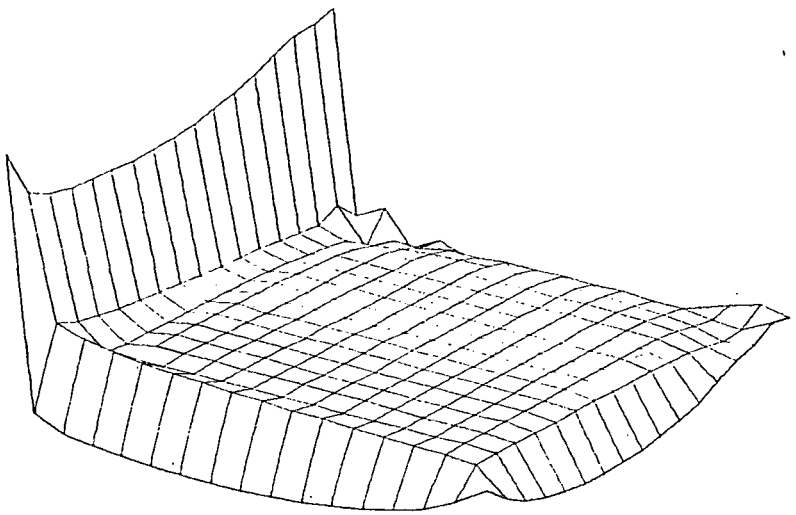

(d) Perspective view of vorticity.

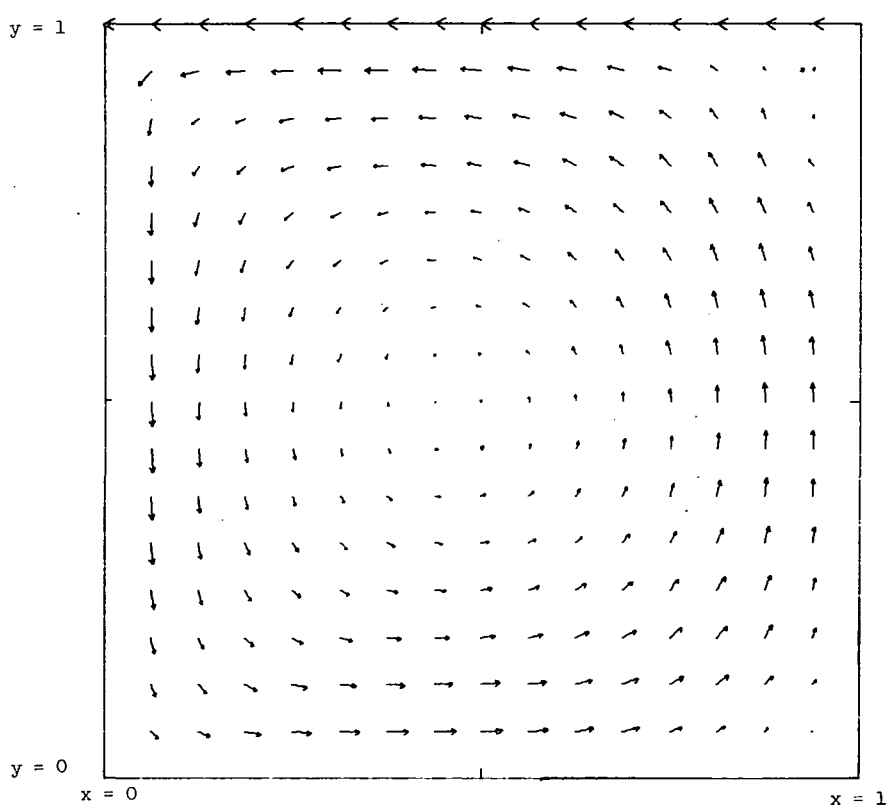

(e) Velocity field.

Figure 4.- Concluded.

7. CALCULATION OF STEADY VISCOUS FLOW IN A SQUARE DRIVEN CAVITY BY THE ARTIFICIAL COMPRESSIBILITY METHOD

John T. Suttles
Langley Research Center

SUMMARY

Numerical solutions of steady viscous flow in a two-dimensional cavity have been obtained by the method of artificial compressibility. The method, originally presented by A. J. Chorin, was programed for a computer solution and checked against a simple channel flow problem which has an analytical solution. The comparison indicated that the method was correctly programed. Results for a square cavity at a Reynolds number of 100 were then obtained and compared with published results. This comparison showed that the method produces good results for velocities but that the computed pressures are unreliable.

INTRODUCTION

The literature, in recent years, includes numerous studies of different numerical methods for obtaining finite-difference computer solutions to fluid mechanics problems. (See ref. 1, for examples.) Consequently, a study was undertaken to compare the ability of several reported methods to compute the motions of a viscous incompressible fluid in a two-dimensional square cavity which has one of its walls undergoing uniform translation. (See paper no. 1 by Rubin and Harris.) This problem was selected because it represents a simple example of a steady flow involving closed streamlines and it has been studied extensively in the literature. (See refs. 2 to 6.) The present paper is one of a series of papers dealing with this problem and reports the results of application of the method of artificial compressibility (ref. 7).

The method of artificial compressibility was proposed by A. J. Chorin (ref. 7) as an efficient approach to solving the steady-state problem of viscous incompressible flow. The principle of this method is to solve the steady incompressible problem by using an asymptotic time solution of the equations of motion. These are modified to contain an artificial compressibility that is designed to vanish as steady state is approached. Through a stability analysis and numerical experiments, Chorin showed that the approach involves two parameters (time step Δt and artificial compressibility δ) which may be adjusted within the constraints of the stability criteria to obtain a converged solution rapidly. In reference 7, a simple channel flow was used as a test problem, and the method was applied to the solution of thermal convection in a fluid layer heated from below.

Because of the analytical complexities involved, Chorin relied heavily on his numerical results to show the stability, convergence (to a steady state in time and to a unique solution as the grid size is reduced), and efficiency of the method.

In the present paper, the problem of steady viscous flow in a square cavity is formulated in primitive variables (as opposed to a stream-function—vorticity formulation), and the method of artificial compressibility is applied to obtain the solution. Therefore, these results provide further numerical evidence for evaluating the method and a consistent basis for comparing the accuracy and efficiency of this method with other approaches.

SYMBOLS

C_p	pressure coefficient
$\tilde{c}$	artificial speed of sound
l	characteristic length
Δl	$= \Delta x = \Delta y$
$\tilde{M}$	artificial Mach number
N	number of space dimensions
p	pressure
q	magnitude of velocity vector, $(u^2 + v^2)^{1/2}$
R	Reynolds number
t	time
Δt	time step
$\overline{U}$	characteristic velocity, velocity of translating wall of cavity
u	axial velocity

v	normal velocity
x,y	axial and normal coordinate, respectively
$\Delta x, \Delta y$	spatial increments in x- and y-directions
δ	artificial compressibility
$\overline{\nu}$	kinematic viscosity
ρ	density

Superscript:

n	index of time step

Subscripts:

c	center
i,j	index of grid point in x- and y-direction, respectively
max	maximum value
ref	reference

A bar over a symbol denotes a dimensional quantity.

METHOD

Governing Equations

The equations of motion of an incompressible viscous fluid in two-dimensional rectangular coordinates are:

Continuity

$$\frac{\partial \overline{u}}{\partial \overline{x}} + \frac{\partial \overline{v}}{\partial \overline{y}} = 0 \tag{1}$$

x-momentum

$$\frac{\partial \bar{u}}{\partial \bar{t}} + \bar{u}\frac{\partial \bar{u}}{\partial \bar{x}} + \bar{v}\frac{\partial \bar{u}}{\partial \bar{y}} = -\frac{1}{\bar{\rho}}\frac{\partial \bar{p}}{\partial \bar{x}} + \bar{\nu}\left(\frac{\partial^2 \bar{u}}{\partial \bar{x}^2} + \frac{\partial^2 \bar{u}}{\partial \bar{y}^2}\right) \tag{2}$$

y-momentum

$$\frac{\partial \bar{v}}{\partial \bar{t}} + \bar{u}\frac{\partial \bar{v}}{\partial \bar{x}} + \bar{v}\frac{\partial \bar{v}}{\partial \bar{y}} = -\frac{1}{\bar{\rho}}\frac{\partial \bar{p}}{\partial \bar{y}} + \bar{\nu}\left(\frac{\partial^2 \bar{v}}{\partial \bar{x}^2} + \frac{\partial^2 \bar{v}}{\partial \bar{y}^2}\right) \tag{3}$$

where bars over symbols denote dimensional quantities. These equations are nondimensionalized by defining:

$$u = \frac{\bar{u}}{\bar{U}} \qquad v = \frac{\bar{v}}{\bar{U}}$$

$$x = \frac{\bar{x}}{\bar{l}} \qquad y = \frac{\bar{y}}{\bar{l}}$$

$$p = \frac{\bar{l}}{\bar{\rho}\bar{\nu}\bar{U}}\bar{p} \qquad t = \frac{\bar{\nu}}{\bar{l}}\bar{t}$$

where $\bar{l}$ is a dimensional characteristic length and $\bar{U}$ is a dimensional characteristic velocity. Applying these relations in equations (1) to (3) and using the continuity equation to write the momentum equation in divergence form result in

$$\frac{\partial u}{\partial x} + \frac{\partial v}{\partial y} = 0 \tag{4}$$

$$\frac{\partial u}{\partial t} + R\left(\frac{\partial u^2}{\partial x} + \frac{\partial uv}{\partial y}\right) = -\frac{\partial p}{\partial x} + \left(\frac{\partial^2 u}{\partial x^2} + \frac{\partial^2 u}{\partial y^2}\right) \tag{5}$$

$$\frac{\partial v}{\partial t} + R\left(\frac{\partial uv}{\partial x} + \frac{\partial v^2}{\partial y}\right) = -\frac{\partial p}{\partial y} + \left(\frac{\partial^2 v}{\partial x^2} + \frac{\partial^2 v}{\partial y^2}\right) \tag{6}$$

where the Reynolds number R is defined by

$$R = \frac{\bar{l}\bar{U}}{\bar{\nu}} \tag{7}$$

To apply the method of artificial compressibility, the continuity equation (eq. (4)) is rewritten as

$$\frac{\partial \tilde{\rho}}{\partial \tilde{t}} + \frac{\partial u}{\partial x} + \frac{\partial v}{\partial y} = 0 \tag{8}$$

where $\tilde{\rho}$ is the artificial density and $\tilde{t}$ is an auxiliary time which is analogous to real time in a compressible flow problem. An artificial equation of state,

$$p = \frac{\tilde{\rho}}{\delta} \tag{9}$$

is introduced with δ being the artificial compressibility. Equation (8) may be solved with equations (5) and (6) to produce a pseudotransient solution. Note that in such a solution the time in equations (5) and (6) becomes the auxiliary time $\tilde{t}$. The solution thus obtained is meaningful only if a steady state is attained and the time derivatives in equations (5), (6), and (8) vanish so that $\tilde{\rho}$ and $\tilde{t}$ no longer influence the results. Thus, this approach is appropriate when a steady-state solution is desired.

Finite-Difference Equations

In applying the method of artificial compressibility, the governing equations may be written according to any of the known difference schemes. The schemes selected by Chorin (ref. 7) were used in the work reported herein. These are the leapfrog difference scheme, wherein central differencing is applied to first-order time and space derivatives, and the DuFort-Frankel method for the second-order space derivatives (viscous terms). The DuFort-Frankel approach treats the derivatives as follows:

$$\frac{\partial^2 u}{\partial x^2} = \frac{u^n_{i+1,j} + u^n_{i-1,j} - u^{n+1}_{i,j} - u^{n-1}_{i,j}}{(\Delta x)^2}$$

where

$$u(x,y,\tilde{t}) \equiv u^n_{i,j} = u(i\,\Delta x, j\,\Delta y, n\,\Delta \tilde{t})$$

and Δx, Δy, and $\Delta \tilde{t}$ are the space and time increments. This scheme is discussed in reference 1, in which it is shown that use of the DuFort-Frankel scheme results in a dis-

torted time scaling. However, since the method of artificial compressibility seeks only the steady-state solution, this difficulty with the DuFort-Frankel approach is of no consequence.

With the above schemes, the finite-difference form of equations (8), (5), and (6) becomes

$$\frac{\tilde{\rho}_{i,j}^{n+1} - \tilde{\rho}_{i,j}^{n-1}}{2\,\Delta\tilde{t}} = -\frac{u_{i+1,j}^{n} - u_{i-1,j}^{n}}{2\,\Delta x} - \frac{v_{i,j+1}^{n} - v_{i,j-1}^{n}}{2\,\Delta y}$$

$$\frac{u_{i,j}^{n+1} - u_{i,j}^{n-1}}{2\,\Delta\tilde{t}} = -R\,\frac{\left(u_{i+1,j}^{n}\right)^2 - \left(u_{i-1,j}^{n}\right)^2}{2\,\Delta x} - R\,\frac{u_{i,j+1}^{n}v_{i,j+1}^{n} - u_{i,j-1}^{n}v_{i,j-1}^{n}}{2\,\Delta y} - \frac{1}{\delta}\,\frac{\tilde{\rho}_{i+1,j}^{n} - \tilde{\rho}_{i-1,j}^{n}}{2\,\Delta x}$$

$$+\frac{u_{i+1,j}^{n} + u_{i-1,j}^{n} - u_{i,j}^{n+1} - u_{i,j}^{n-1}}{(\Delta x)^2} + \frac{u_{i,j+1}^{n} + u_{i,j-1}^{n} - u_{i,j}^{n+1} - u_{i,j}^{n-1}}{(\Delta y)^2}$$

$$\frac{v_{i,j}^{n+1} - v_{i,j}^{n-1}}{2\,\Delta\tilde{t}} = -R\,\frac{u_{i+1,j}^{n}v_{i+1,j}^{n} - u_{i-1,j}^{n}v_{i-1,j}^{n}}{2\,\Delta x} - R\,\frac{\left(v_{i,j+1}^{n}\right)^2 - \left(v_{i,j-1}^{n}\right)^2}{2\,\Delta y} - \frac{1}{\delta}\,\frac{\tilde{\rho}_{i,j+1}^{n} - \tilde{\rho}_{i,j-1}^{n}}{2\,\Delta y}$$

$$+\frac{v_{i+1,j}^{n} + v_{i-1,j}^{n} - v_{i,j}^{n+1} - v_{i,j}^{n-1}}{(\Delta x)^2} + \frac{v_{i,j+1}^{n} + v_{i,j-1}^{n} - v_{i,j}^{n+1} - v_{i,j}^{n-1}}{(\Delta y)^2}$$

where $u_{i,j}^{n} = u(i\,\Delta x, j\,\Delta y, n\,\Delta\tilde{t})$, $v_{i,j}^{n} = v(i\,\Delta x, j\,\Delta y, n\,\Delta\tilde{t})$, and $\rho_{i,j}^{n} = \rho(i\,\Delta x, j\,\Delta y, n\,\Delta\tilde{t})$ and equation (9) has been used to eliminate pressure from the system of equations. Assuming equal space increments $\Delta x = \Delta y = \Delta l$ and solving for the artificial density and velocities explicitly result in

$$\tilde{\rho}_{i,j}^{n+1} = \tilde{\rho}_{i,j}^{n-1} - \frac{\Delta\tilde{t}}{\Delta l}\left(u_{i+1,j}^{n} - u_{i-1,j}^{n} + v_{i,j+1}^{n} - v_{i,j-1}^{n}\right) \tag{10}$$

$$u_{i,j}^{n+1} = \alpha u_{i,j}^{n-1} - R\beta\left[\left(u_{i+1,j}^{n}\right)^2 - \left(u_{i-1,j}^{n}\right)^2 + u_{i,j+1}^{n}v_{i,j+1}^{n} - u_{i,j-1}^{n}v_{i,j-1}^{n}\right] - \frac{\beta}{\delta}\left(\tilde{\rho}_{i+1,j}^{n} - \tilde{\rho}_{i-1,j}^{n}\right)$$

$$+\frac{2\beta}{\Delta l}\left(u_{i+1,j}^{n} + u_{i-1,j}^{n} + u_{i,j+1}^{n} + u_{i,j-1}^{n}\right) \tag{11}$$

$$v_{i,j}^{n+1} = \alpha v_{i,j}^{n-1} - R\beta\left[u_{i+1,j}^{n} v_{i+1,j}^{n} - u_{i-1,j}^{n} v_{i-1,j}^{n} + \left(v_{i,j+1}^{n}\right)^2 - \left(v_{i,j-1}^{n}\right)^2\right] - \frac{\beta}{\delta}\left(\tilde{\rho}_{i,j+1}^{n} - \tilde{\rho}_{i,j-1}^{n}\right)$$

$$+ \frac{2\beta}{\Delta l}\left(v_{i+1,j}^{n} + v_{i-1,j}^{n} + v_{i,j+1}^{n} + v_{i,j-1}^{n}\right) \tag{12}$$

where

$$\alpha = \frac{1 - 4\dfrac{\Delta\tilde{t}}{(\Delta l)^2}}{1 + 4\dfrac{\Delta\tilde{t}}{(\Delta l)^2}} \tag{13}$$

and

$$\beta = \frac{\dfrac{\Delta\tilde{t}}{\Delta l}}{1 + 4\dfrac{\Delta\tilde{t}}{(\Delta l)^2}} \tag{14}$$

The boundary conditions consist of prescribed velocities on all boundaries; however, the artificial density given by equation (8) must be updated on the boundaries. In reference 7, Chorin used forward or backward space differences at the boundaries to update the artificial density in the continuity equation (eq. (8)). For example, at a point on the $y = 0$ $(j = 1)$ boundary

$$\tilde{\rho}_{i,1}^{n+1} = \tilde{\rho}_{i,1}^{n-1} - \frac{\Delta\tilde{t}}{\Delta l}\left(u_{i+1,1}^{n} - u_{i-1,1}^{n}\right) - 2\frac{\Delta\tilde{t}}{\Delta l}\left(v_{i,2}^{n} - v_{i,1}^{n}\right) \tag{15}$$

Points on other boundaries were treated similarly. This method of treating the boundary points was initially adopted in this work also. The approach was found to work quite satisfactorily for the duplication of the simple channel flow problem presented by Chorin; however, it was found to produce poor results near the boundaries for the cavity problem. An attempt to rectify this problem is described in the section entitled "Results and Discussion."

Stability

The stability conditions for the system of finite-difference equations (eqs. (10) to (12)) have been discussed by Chorin (ref. 7). The main points of that discussion are given in this section.

The artificial equation of state, equation (9), indicates the presence of an artificial sound speed

$$\tilde{c} = \frac{1}{R\delta^{1/2}} \tag{16}$$

where the Reynolds number has been introduced to allow $\tilde{c}$ to be nondimensionalized in the same manner as the other velocities. To ensure the stability of the system of equations, the artificial Mach number based on this sound speed must be less than unity. The required condition is

$$\tilde{M}_{max} = \frac{q_{max}}{\tilde{c}} = R\delta^{1/2} q_{max} < 1 \tag{17}$$

where q is the magnitude of the velocity vector; that is

$$q = \left(u^2 + v^2\right)^{1/2}$$

If this Mach-number condition is satisfied and if the boundary conditions consist of prescribed velocities, Chorin showed that the remaining stability requirement is satisfied by

$$\Delta t \leq \frac{2}{N^{1/2}\left(1 + 5^{1/2}\right)} \left(\min_k \Delta x_k\right) \delta^{1/2} \tag{18}$$

where N is the number of space dimensions and $\left(\min_k \Delta x_k\right)$ is the minimum spatial increment. Thus the method contains two parameters, δ and Δt, which may be adjusted within the stability criteria given by equations (17) and (18), respectively, to optimize the time required for obtaining a converged solution. Chorin states that the optimal value of δ must be determined by preliminary test computations and that his experience indicated that this value is not sharply defined. Therefore, no attempt to determine optimal values was made in this work. It was found, however, that a maximum Mach number of 0.5 produced satisfactory results in most instances.

RESULTS AND DISCUSSION

Simple Channel Problem

In reference 7, Chorin presented results of calculations for a simple two-dimensional channel flow problem which has a closed form solution, that is, a parabolic

axial velocity profile across the channel and a linear decay of pressure going down the channel. Calculations for this test problem have also been made in this work to gain confidence that the method has been correctly programed. Both a horizontal (channel axis parallel to x-direction) and a vertical (channel axis parallel to y-direction) channel flow, shown in figure 1, were computed. In these calculations, the boundary velocities were specified to be zero except for the axial velocities across the channel ends which were specified to have the correct parabolic distribution. The interior velocities and densities were initially set at zero, and the velocities and densities in the interior of the channel were computed. The calculations were done for a unit Reynolds number (R = 1) with 19 grid points in each coordinate direction and for $\delta = 0.000\,32$ and $\Delta t = 0.000\,596\,28$ as was done in reference 7. The computations for both channels converged to the correct parabolic axial velocity distributions (i.e., all velocities within 10^{-5} of known solution) and to the correct linear axial pressure gradient throughout the channel in approximately 500 iterations. This rate of convergence is in good agreement with Chorin's reported experience. It was, therefore, concluded that the method has been properly programed.

Square Cavity Problem

The square cavity problem considered in this work is illustrated in figure 2. The steady viscous flow in the cavity has been computed by Chorin's artificial compressibility method. Preliminary computations for this problem indicated that the velocity results near the boundaries were poor. The difficulty was found to be due to the use of conditions like equation (15) to update the artificial densities along the boundaries. This problem was eliminated by applying the governing equations at the boundary to derive a relationship for the pressure gradient normal to the boundary (and from the artificial equation of state, the artificial density gradient also) in terms of the normal velocity gradient. For example, along the boundary where $y = u = v = 0$, and hence $\partial u/\partial t = \partial v/\partial t = \partial u/\partial x = \partial v/\partial x = 0$, the relation is found from equation (6) to be

$$\left(\frac{\partial p}{\partial y}\right)_{i,1} = \left(\frac{\partial^2 v}{\partial y^2}\right)_{i,1} \tag{19}$$

Taylor's series expansions about the boundary point for the pressure and velocity gradient one grid point from the boundary result in

$$p(i,2) = p(i,1) + \left(\frac{\partial p}{\partial y}\right)_{i,1} \Delta y$$

$$\left(\frac{\partial v}{\partial y}\right)_{i,2} = \left(\frac{\partial v}{\partial y}\right)_{i,1} + \left(\frac{\partial^2 v}{\partial y^2}\right)_{i,1} \Delta y$$

Equation (19) can then be used along with these relations to obtain

$$p(i,1) = p(i,2) - \left(\frac{\partial v}{\partial y}\right)_{i,2} + \left(\frac{\partial v}{\partial y}\right)_{i,1}$$

Finally, with a central-difference expression for the velocity gradient, the boundary pressure is given by

$$p(i,1) = p(i,2) - \frac{v(i,3)}{2\,\Delta l} \tag{20}$$

when it is noted that

$$v(i,1) = 0$$

from the boundary condition and that

$$\left(\frac{\partial v}{\partial y}\right)_{i,1} = 0$$

from the boundary condition applied to the continuity equation. Thus, the appropriate equation for updating the artificial density on the $y = 0$ $(j = 1)$ boundary is found from equation (20) and the artificial equation of state (eq. (9)) to be

$$\tilde{\rho}(i,1) = \tilde{\rho}(i,2) - \frac{\delta\, v(i,3)}{2\,\Delta l} \tag{21}$$

Analogous equations for the remaining boundaries are:

for the $x = 0$ $(i = 1)$ boundary,

$$\tilde{\rho}(1,j) = \tilde{\rho}(2,j) - \frac{\delta\, u(3,j)}{2\,\Delta l} \tag{22}$$

for the $y = 1$ $(j = j_{max})$ boundary,

$$\tilde{p}(i,j_{max}) = \tilde{p}(i,j_{max} - 1) + \frac{\delta\, v(i,j_{max} - 2)}{2\,\Delta l} \tag{23}$$

for the $x = 1$ $(i = i_{max})$ boundary,

$$\tilde{p}(i_{max},j) = \tilde{p}(i_{max} - 1,j) + \frac{\delta\, u(i_{max} - 2,j)}{2\,\Delta l} \tag{24}$$

The use of equations (21) to (24) made a considerable improvement in the velocity results near the boundaries.

Calculations for a square cavity were made for a Reynolds number of 100 with 15×15, 29×29, and 43×43 grid points. Table I lists the stability parameters, δ and Δt, the number of iterations, required storage, and run time for the calculations. Although a large number of iterations were required (1500 to 3000), the computations only took computational times of approximately 1/2, 3, and 7 minutes for 15×15, 29×29, and 43×43 grid points, respectively. The results of these calculations are presented and compared with other results in figures 3 to 7.

In figure 3, the velocity vectors are shown for the steady-state solution by the method of artificial compressibility with 15×15 grid points. The flow direction vectors, which are obtained by normalizing each velocity vector to a unit magnitude, are shown in figure 4. These results illustrate the features of the vortical flow which occurs for the cavity problem. The features shown are in good agreement with the streamline patterns shown in reference 3 for this problem. The anomalous flow direction vector shown in the lower right corner of figure 4 is probably associated with a weak corner vortex flow which is described in references 3 and 5.

The velocity and pressure profiles through the vortex center (i.e., the nearest node point in the grid to the vortex center) for the present solutions are compared with the results of reference 3 in figures 5 and 6. The velocity results in figure 5 show that the present solutions for the various grid spacings vary only slightly and that the results for 15×15 grid points appear to be adequate. It is also seen that the present calculations of velocity are in good agreement with those of reference 3 which were obtained by a stream-function—vorticity method. The vortex center locations are apparent in these graphs and are compared with those of reference 3 in table II where it seems that the

values are in good agreement, that is, within about 4 percent. On the other hand, the pressure profiles through the vortex center shown in figure 6 are in substantial disagreement. Of particular concern is the fact that the pressure profiles for the various grid spacings of the artificial compressibility method are not smooth and are in disagreement with each other. This makes the pressure results of this method highly questionable.

In figure 7, the pressures along the boundaries are compared qualitatively with the results in reference 6. Note that the Reynolds numbers are not the same, that is, 100 compared with 64. Although there are relatively high frequency oscillations in the present results, the qualitative comparisons show good agreement with reference 6.

Thus, these results indicate that the method of artificial compressibility applied to the square cavity problem produces good results for velocity, but the pressure results are unreliable.

CONCLUDING REMARKS

The method of artificial compressibility has been applied to obtain numerical solutions of the steady viscous flow in a two-dimensional square cavity. The method, proposed by A. J. Chorin, was programed and checked against a simple channel flow problem which has an analytic solution. The comparison indicates that the method was correctly programed. Results for a square cavity with a Reynolds number of 100 were obtained and compared with published solutions for this problem. These comparisons indicated that good velocity results are obtained with the method, but that the pressure results are unreliable.

REFERENCES

1. Roache, Patrick J.: Computational Fluid Dynamics. Hermosa Publ., c.1972.

2. Burggraf, Odus R.: Analytical and Numerical Studies of the Structure of Steady Separated Flows. J. Fluid Mech., vol. 24, pt. 1, Jan. 1966, pp. 113-151.

3. Mills, Ronald D.: Numerical Solutions of the Viscous Flow Equations for a Class of Closed Flows. J. Roy. Aeronaut. Soc., vol. 69, no. 658, Oct. 1965, pp. 714-718; Correction, vol. 69, no. 660, Dec. 1965, p. 880.

4. Runchal, A. K.; and Wolfshtein, M.: Numerical Integration Procedure for the Steady State Navier-Stokes Equations. J. Mech. Eng. Sci., vol. 11, no. 5, Oct. 1969, pp. 445-453.

5. Pan, Frank; and Acrivos, Andreas: Steady Flows in Rectangular Cavities. J. Fluid Mech., vol. 28, pt. 4, June 22, 1967, pp. 643-655.

6. Kawaguti, Mitutosi: Numerical Solution of the Navier-Stokes Equations for the Flow in a Two-Dimensional Cavity. J. Phys. Soc. Jap., vol. 16, no. 11, Nov. 1961, pp. 2307-2315.

7. Chorin, Alexandre Joel: A Numerical Method for Solving Incompressible Viscous Flow Problems. J. Comput. Phys., vol. 2, no. 1, Aug. 1967, pp. 12-26.

TABLE I. - STABILITY AND COMPUTATIONAL PARAMETERS FOR SQUARE CAVITY CALCULATIONS

Number of grid points	δ	Δt	Number of iterations	Execution time,[a] sec	Execution storage[a]
15 × 15	0.000 025	0.000 21	1500	29	20624_8
29 × 29	.000 003 2	.000 038 33	3000	205	24314_8
43 × 43	.000 025	.000 071 4	3000	419	32234_8

[a]For CDC 6600 computer system which has a minimum storage of 40000_8 for compilation.

TABLE II. - COMPARISON OF VORTEX CENTER LOCATIONS

Vortex center at –	Results	
	Present	Mills (ref. 3)
x	0.61	0.63
y	.73	.75

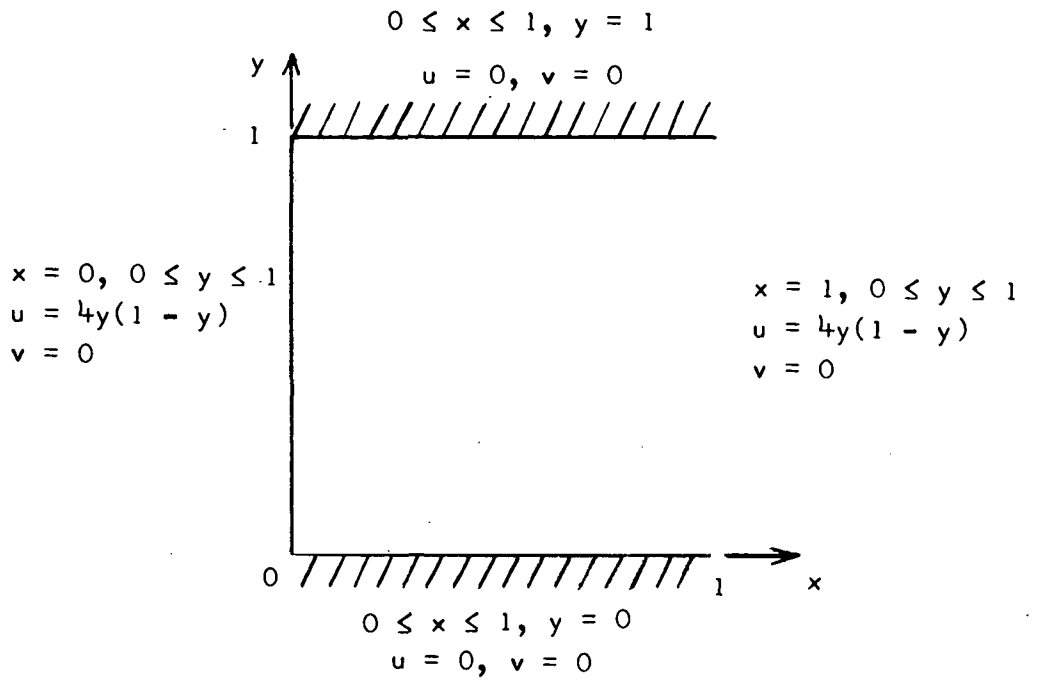

(a) Horizontal channel.

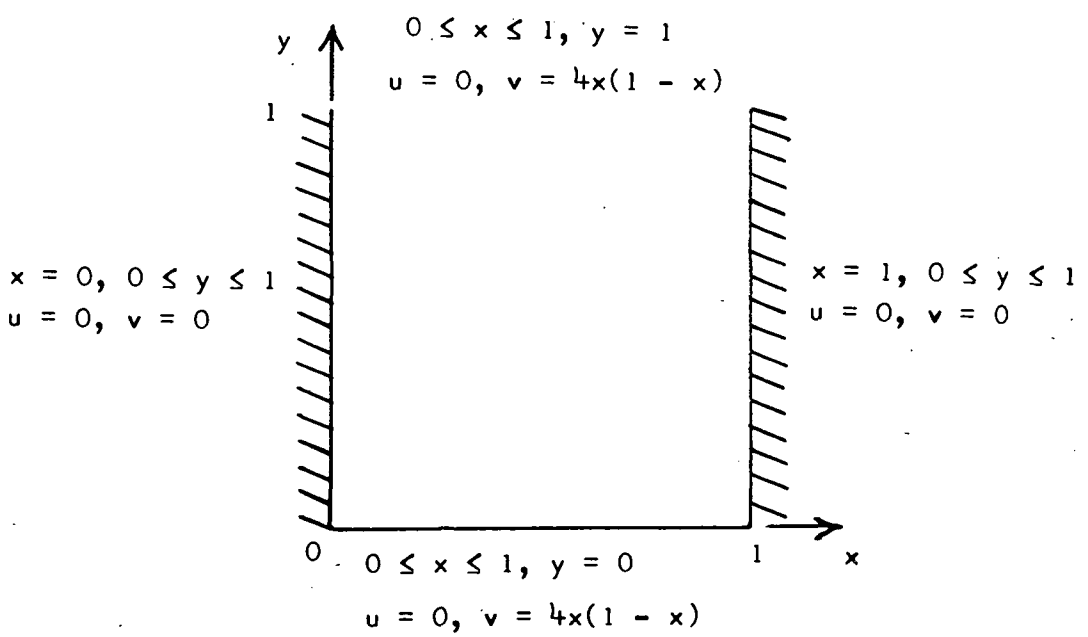

(b) Vertical channel.

Figure 1.- Geometry and boundary conditions for simple channel flow problems.

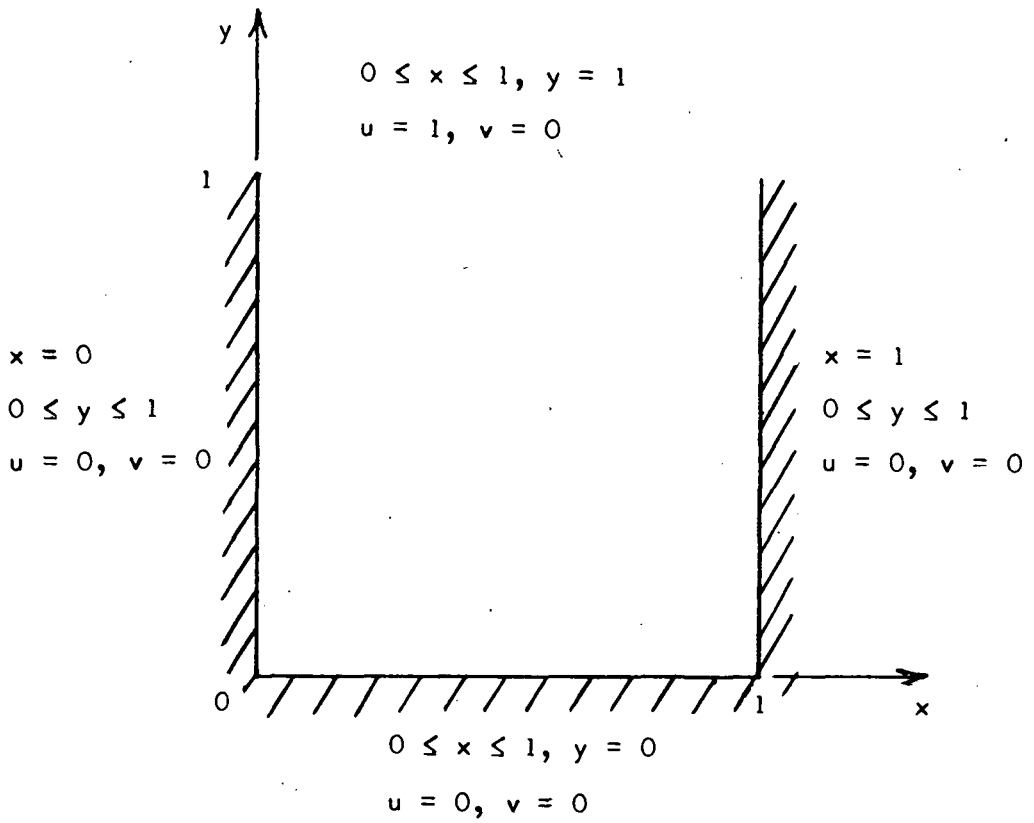

Figure 2.- Geometry and boundary conditions for square cavity problem.

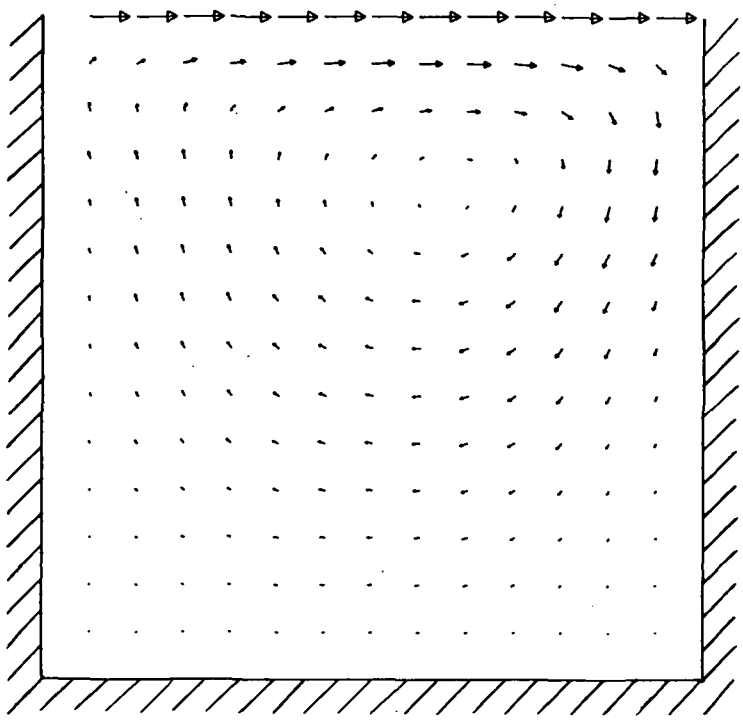

Figure 3.- Velocity vectors from solution of square cavity problem with $R = 100$ and 15×15 grid points.

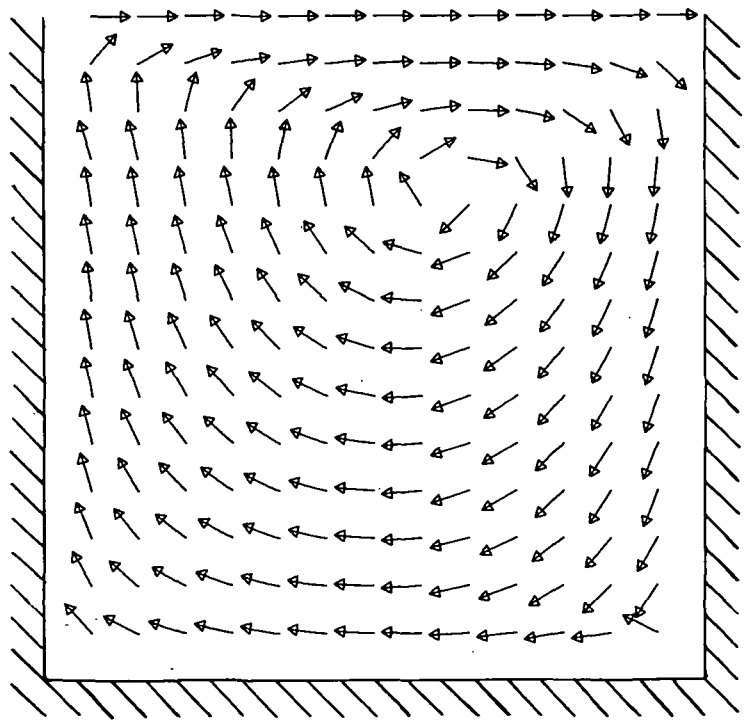

Figure 4.- Flow direction vectors from solution of square cavity problem with $R = 100$ and 15×15 grid points.

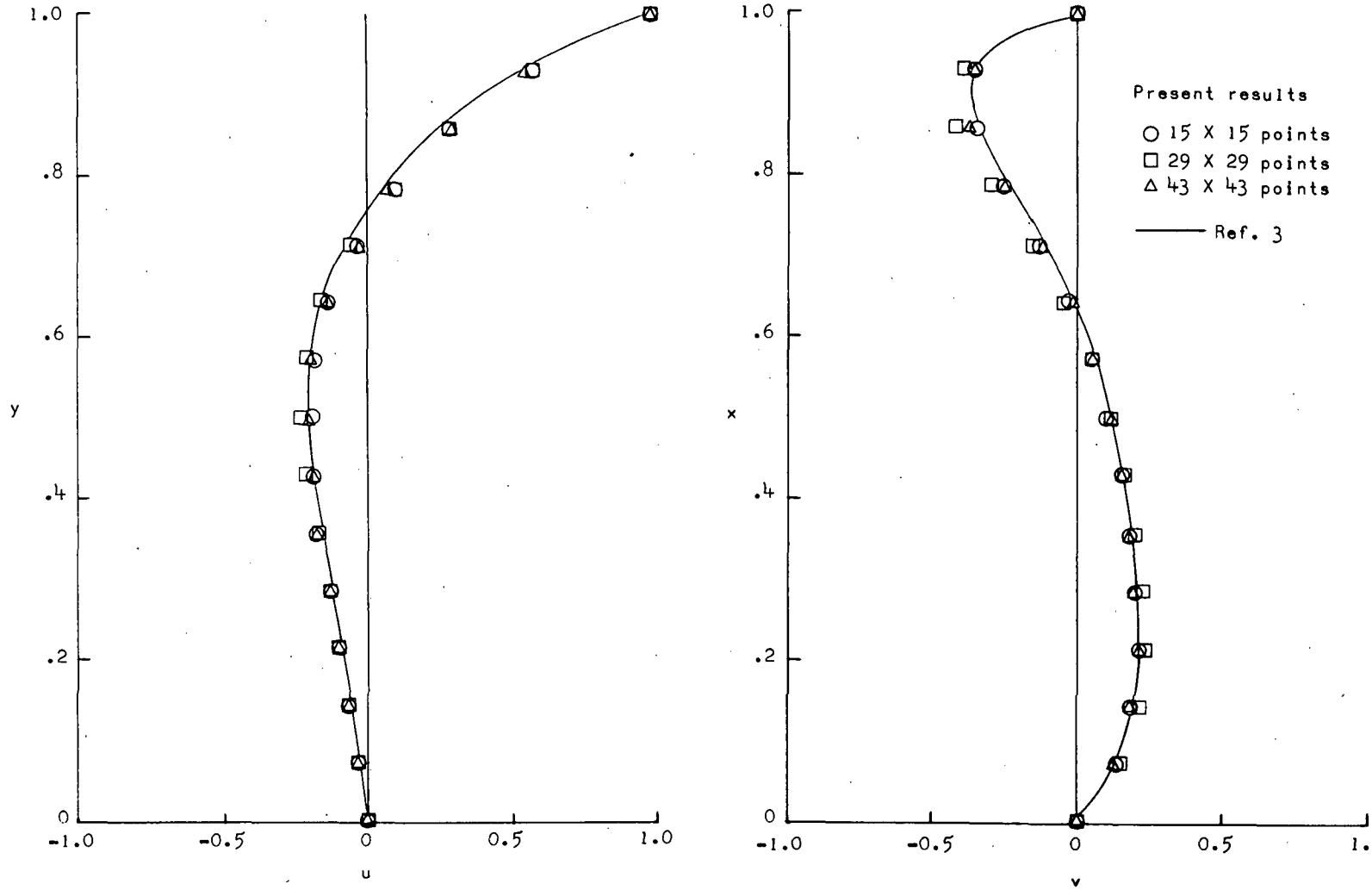

(a) Vertical velocity profile.

(b) Horizontal velocity profile.

Figure 5.- Velocity profiles through vortex center from present square cavity calculations and from reference 3.

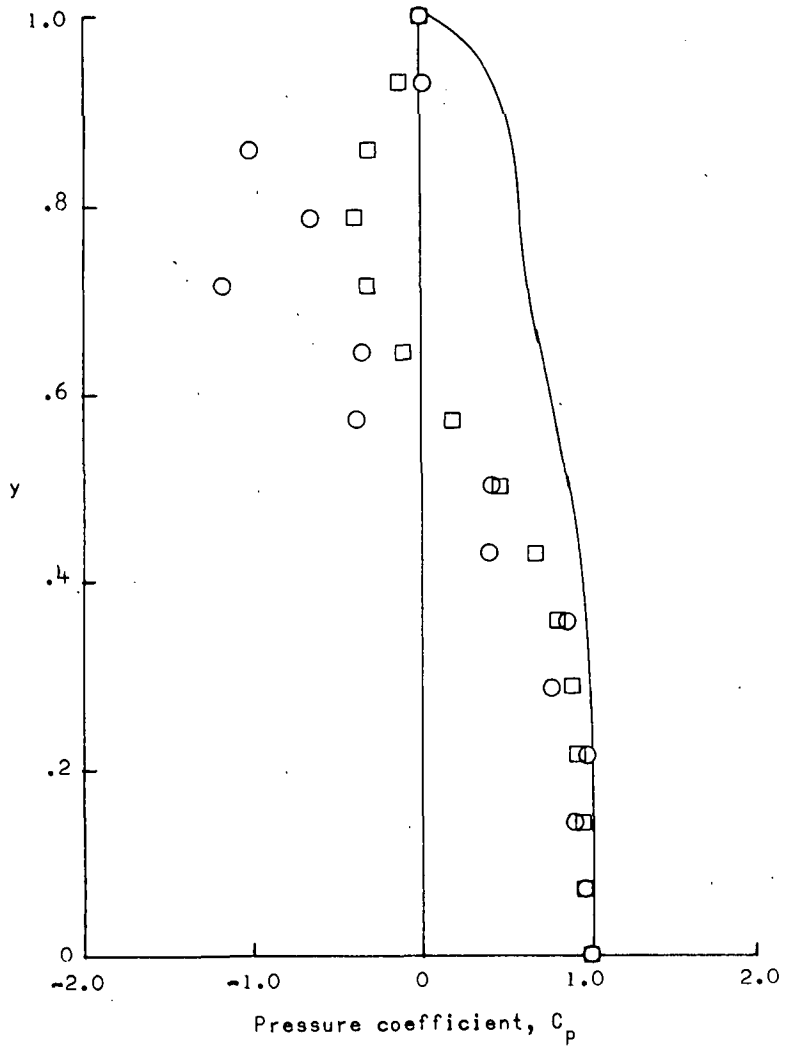

(a) Vertical profile. $C_p = \dfrac{p(i_c,j) - p(i_c,j_{max})}{p(i_c,1) - p(i_c,j_{max})}$.

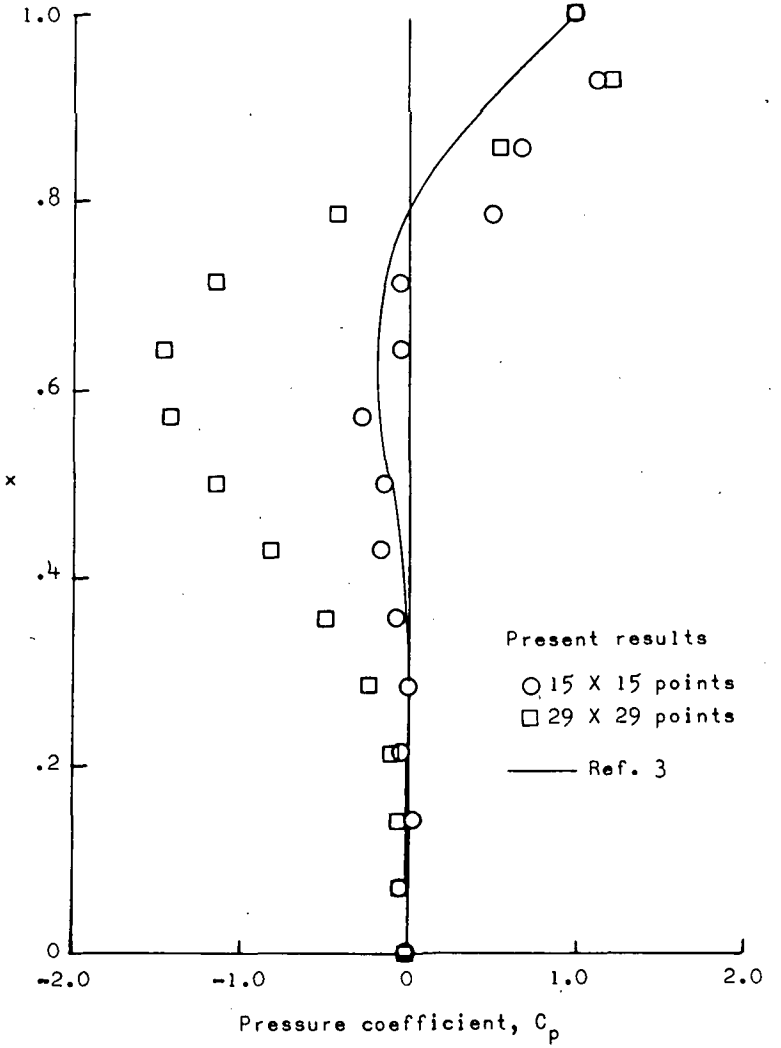

(b) Horizontal profile. $C_p = \dfrac{p(i,j_c) - p(1,j_c)}{p(i_{max},j_c) - p(1,j_c)}$.

Figure 6.- Profiles of pressure coefficient through vortex center from present calculations and from reference 3.

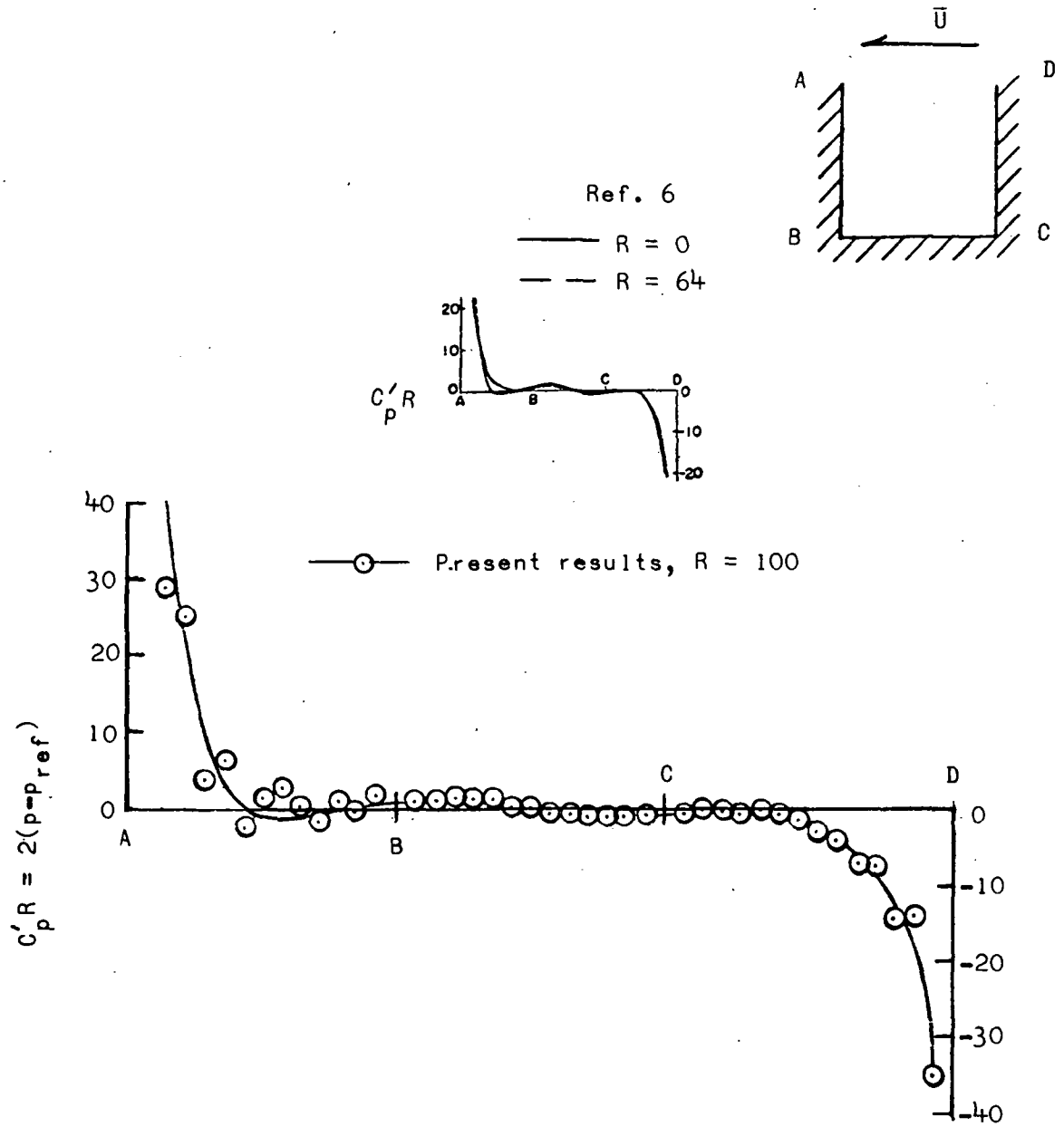

Figure 7.- Pressure along cavity walls from present calculations and from reference 6. Reference pressure p_{ref} is pressure at midpoint of side BC. $C'_p = \frac{\bar{p} - \bar{p}_{ref}}{1/2\rho\bar{U}^2} = \frac{2(p - p_{ref})}{R}$.

8. FINITE-DIFFERENCE SOLUTION FOR THE INCOMPRESSIBLE DRIVEN CAVITY FLOW PROBLEM

Ernest V. Zoby
Langley Research Center

SUMMARY

An alternating-direction implicit (ADI) finite-difference procedure has been employed to compute the two-dimensional viscous incompressible flow generated within a rectangular cavity by a moving surface at the cavity open end. The pressure through the cavity was computed by the Spalding SIMPLE procedure.

Although the present method does not predict axial and normal velocities as high as indicated by more exact methods, the values of the velocities through the vortex center are reasonably predicted and the overall velocity vector diagrams appear satisfactory. The pressure levels are generally in poor agreement with other predictions. However, the pressure gradients must be reasonably well predicted because of the accurate results obtained for the velocities.

INTRODUCTION

The solution of the Navier-Stokes equations easily provides a more than adequate test for the viability of various numerical techniques. For a rational assessment of these methods, a singular flow model and compatible test conditions are naturally desirable. Numerical as well as experimental results (e.g., ref. 1) exist for the two-dimensional incompressible flow field generated within a rectangular cavity by a moving surface at the open end. (See paper no. 1 by Rubin and Harris for details of driven cavity.) Consequently, the driven cavity problem was selected as the test model for an investigation to compare the accuracy and applicability of several numerical techniques.

As part of the aforementioned investigation, this paper presents numerical solutions based on an alternating-direction implicit (ADI) technique for the two-dimensional incompressible Navier-Stokes equations. The equations are programed in the rectangular Cartesian coordinate system. For an evaluation of the pressure, the Spalding SIMPLE procedure (ref. 2) is used. The Spalding method relates a perturbation in pressure at each time step to the continuity relation so that at steady state the pressure at each node point is determined and the continuity equation is satisfied. A discussion of

the present method and the results of calculated test cases are presented. Comparison with existing results is also included.

SYMBOLS

C_p	pressure coefficient
l	characteristic length (fig. 1)
p	pressure
$\hat{p}$	pressure correction
R	Reynolds number
t	time
Δt	time step
$\overline{U}$	velocity across open end of cavity
u	axial component of velocity
v	normal component of velocity
x,y	axial and normal distance, respectively
$\Delta x, \Delta y$	spatial increments in x- and y-directions
$\overline{\nu}$	kinematic viscosity
$\overline{\rho}$	density

Subscripts:

i,j	index of node points in x- and y-direction, respectively
max	maximum value

Superscripts:

k iteration counter

n index of time step

A bar over a symbol denotes a dimensional quantity.

ANALYSIS

The governing equations for an incompressible viscous fluid in two-dimensional rectangular coordinates are given as

$$\frac{\partial \bar{u}}{\partial \bar{t}} + \bar{u}\frac{\partial \bar{u}}{\partial \bar{x}} + \bar{v}\frac{\partial \bar{u}}{\partial \bar{y}} = -\frac{1}{\bar{\rho}}\frac{\partial \bar{p}}{\partial \bar{x}} + \bar{\nu}\left(\frac{\partial^2 \bar{u}}{\partial \bar{x}^2} + \frac{\partial^2 \bar{u}}{\partial \bar{y}^2}\right) \tag{1}$$

$$\frac{\partial \bar{v}}{\partial \bar{t}} + \bar{u}\frac{\partial \bar{v}}{\partial \bar{x}} + \bar{v}\frac{\partial \bar{v}}{\partial \bar{y}} = -\frac{1}{\bar{\rho}}\frac{\partial \bar{p}}{\partial \bar{y}} + \bar{\nu}\left(\frac{\partial^2 \bar{v}}{\partial \bar{x}^2} + \frac{\partial^2 \bar{v}}{\partial \bar{y}^2}\right) \tag{2}$$

and

$$\frac{\partial \bar{u}}{\partial \bar{x}} + \frac{\partial \bar{v}}{\partial \bar{y}} = 0 \tag{3}$$

Defining the dimensionless quantities to be

$$x = \frac{\bar{x}}{\bar{l}} \qquad y = \frac{\bar{y}}{\bar{l}}$$

$$u = \frac{\bar{u}}{\bar{U}} \qquad v = \frac{\bar{v}}{\bar{U}}$$

$$t = \frac{\bar{t}}{\bar{l}/\bar{U}} \qquad p = \frac{\bar{p}}{\bar{\rho}\bar{U}^2}$$

and substituting them into equations (1) to (3) result in

$$\frac{\partial u}{\partial t} + u\frac{\partial u}{\partial x} + v\frac{\partial u}{\partial y} = -\frac{\partial p}{\partial x} + \frac{1}{R}\left(\frac{\partial^2 u}{\partial x^2} + \frac{\partial^2 u}{\partial y^2}\right) \tag{4}$$

$$\frac{\partial v}{\partial t} + u\frac{\partial v}{\partial x} + v\frac{\partial v}{\partial y} = -\frac{\partial p}{\partial y} + \frac{1}{R}\left(\frac{\partial^2 v}{\partial x^2} + \frac{\partial^2 v}{\partial y^2}\right) \tag{5}$$

and

$$\frac{\partial u}{\partial x} + \frac{\partial v}{\partial y} = 0 \tag{6}$$

where $R = \overline{U}l/\nu$. The boundary conditions on u and v are

$$u(0,y) = u(1,y) = u(x,0) = 0 \qquad u(x,1) = 1$$

$$v(0,y) = v(1,y) = v(x,0) = v(x,1) = 0$$

However, with equations (4) to (6), there is no simple way to compute pressure. For this paper, a semi-implicit method of Spalding (ref. 2) has been employed. The equation for this method is

$$\frac{\partial \hat{p}}{\partial t} - \left(\frac{\partial^2 \hat{p}}{\partial x^2} + \frac{\partial^2 \hat{p}}{\partial y^2}\right) = \frac{\partial u}{\partial x} + \frac{\partial v}{\partial y} \tag{7}$$

where the $\partial\hat{p}/\partial t$ is a pseudotime term relating to the iterations and $\hat{p}$ is a pressure correction which is combined with the pressure p from the previous time step for a new pressure value at the new time step. The correction $\hat{p}$ continually updates p in the time marching procedure until convergence is obtained at steady state. At steady state, $\hat{p}$ is very small, so that the left side of equation (7) equals zero and continuity is satisfied. The boundary condition for equation (7) is that the normal pressure gradient is zero.

Equations (4), (5), and (7) are then applied to the square cavity (fig. 1) to determine the flow field generated within the cavity. The basic conditions for these calculations are that $R = 100$ and $\Delta x = \Delta y = 1/14$. For initial conditions, u, v, and p (and $\hat{p}$) were taken to be zero.

Equations (4), (5), and (7) are solved by an alternating-direction implicit (ADI) finite-difference procedure. With the first one-half time step implicit in the y-direction, equations (4) and (5) are given as

$$-\left[\frac{v_{i,j}^{n}\,\Delta t}{4\,\Delta y}+\frac{\Delta t}{2R(\Delta y)^2}\right]u_{i,j-1}^{n+1/2}+\left[1+\frac{\Delta t}{R(\Delta y)^2}\right]u_{i,j}^{n+1/2}+\left[\frac{v_{i,j}^{n}\,\Delta t}{4\,\Delta y}-\frac{\Delta t}{2R(\Delta y)^2}\right]u_{i,j+1}^{n+1/2}$$

$$=-\frac{\Delta t}{4\,\Delta x}\left(p_{i+1,j}^{n}-p_{i-1,j}^{n}\right)+\left[\frac{u_{i,j}^{n}\,\Delta t}{4\,\Delta x}+\frac{\Delta t}{2R(\Delta x)^2}\right]u_{i-1,j}^{n}+\left[1-\frac{\Delta t}{R(\Delta x)^2}\right]u_{i,j}^{n}$$

$$+\left[\frac{\Delta t}{2R(\Delta x)^2}-\frac{u_{i,j}^{n}\,\Delta t}{4\,\Delta x}\right]u_{i+1,j}^{n} \tag{8}$$

and

$$-\left[\frac{v_{i,j}^{n}\,\Delta t}{4\,\Delta y}+\frac{\Delta t}{2R(\Delta y)^2}\right]v_{i,j-1}^{n+1/2}+\left[1+\frac{\Delta t}{R(\Delta y)^2}\right]v_{i,j}^{n+1/2}+\left[\frac{v_{i,j}^{n}\,\Delta t}{4\,\Delta y}-\frac{\Delta t}{2R(\Delta y)^2}\right]v_{i,j+1}^{n+1/2}$$

$$=-\frac{\Delta t}{4\,\Delta y}\left(p_{i,j+1}^{n}-p_{i,j-1}^{n}\right)+\left[\frac{u_{i,j}^{n}\,\Delta t}{4\,\Delta x}+\frac{\Delta t}{2R(\Delta x)^2}\right]v_{i-1,j}^{n}+\left[1-\frac{\Delta t}{R(\Delta x)^2}\right]v_{i,j}^{n}$$

$$+\left[\frac{\Delta t}{2R(\Delta x)^2}-\frac{u_{i,j}^{n}\,\Delta t}{4\,\Delta x}\right]v_{i+1,j}^{n} \tag{9}$$

For the second one-half time step implicit in the x-direction, equations (4) and (5) are given as

$$-\left[\frac{u_{i,j}^{n+1/2}\,\Delta t}{4\,\Delta x}+\frac{\Delta t}{2R(\Delta x)^2}\right]u_{i-1,j}^{n+1}+\left[1+\frac{\Delta t}{R(\Delta x)^2}\right]u_{i,j}^{n+1}+\left[\frac{u_{i,j}^{n+1/2}\,\Delta t}{4\,\Delta x}-\frac{\Delta t}{2R(\Delta x)^2}\right]u_{i+1,j}^{n+1}$$

$$=-\frac{\Delta t}{4\,\Delta x}\left(p_{i+1,j}^{n}-p_{i-1,j}^{n}\right)+\left[\frac{v_{i,j}^{n+1/2}\,\Delta t}{4\,\Delta y}+\frac{\Delta t}{2R(\Delta y)^2}\right]u_{i,j-1}^{n+1/2}+\left[1-\frac{\Delta t}{R(\Delta y)^2}\right]u_{i,j}^{n+1/2}$$

$$+\left[\frac{\Delta t}{2R(\Delta y)^2}-\frac{v_{i,j}^{n+1/2}\,\Delta t}{4\,\Delta y}\right]u_{i,j+1}^{n+1/2} \tag{10}$$

and

$$-\left[\frac{u_{i,j}^{n+1/2}\,\Delta t}{4\,\Delta x}+\frac{\Delta t}{2R(\Delta x)^2}\right]v_{i-1,j}^{n+1}+\left[1+\frac{\Delta t}{R(\Delta x)^2}\right]v_{i,j}^{n+1}+\left[\frac{u_{i,j}^{n+1/2}\,\Delta t}{4\,\Delta x}-\frac{\Delta t}{2R(\Delta x)^2}\right]v_{i+1,j}^{n+1}$$

$$=-\frac{\Delta t}{4\,\Delta y}\left(p_{i,j+1}^{n}-p_{i,j-1}^{n}\right)+\left[\frac{v_{i,j}^{n+1/2}\,\Delta t}{4\,\Delta y}+\frac{\Delta t}{2R(\Delta y)^2}\right]v_{i,j-1}^{n+1/2}+\left[1-\frac{\Delta t}{R(\Delta x)^2}\right]v_{i,j}^{n+1/2}$$

$$+\left[\frac{\Delta t}{2R(\Delta y)^2}-\frac{v_{i,j}^{n+1/2}\,\Delta t}{4\,\Delta y}\right]v_{i,j+1}^{n+1/2} \tag{11}$$

Note that a simple linearization of the convection term is used by evaluating the velocity at the previous time step. Since there is interest in only the steady-state solution, this assumption should not have any effect on the results presented herein.

Equation (7) written implicitly in the x-direction and then in the y-direction is

$$-\frac{\Delta t}{(\Delta x)^2}\hat{p}_{i-1,j}^{k+1}+\left[1+\frac{\Delta t}{(\Delta x)^2}\right]\hat{p}_{i,j}^{k+1}-\frac{\Delta t}{(\Delta x)^2}\hat{p}_{i+1,j}^{k+1}=\Delta t\left[\frac{1}{2\,\Delta x}\left(u_{i+1,j}^{n+1}-u_{i-1,j}^{n+1}\right)+\frac{1}{2\,\Delta y}\left(v_{i,j+1}^{n+1}-v_{i,j-1}^{n+1}\right)\right]+\frac{\Delta t}{(\Delta y)^2}\left(\hat{p}_{i,j-1}^{k}+\hat{p}_{i,j+1}^{k}-2\hat{p}_{i,j}^{k}\right)+\hat{p}_{i,j}^{k} \tag{12}$$

and

$$-\frac{\Delta t}{(\Delta y)^2}\hat{p}_{i,j-1}^{k+2}+\left[1+\frac{\Delta t}{(\Delta y)^2}\right]\hat{p}_{i,j}^{k+2}-\frac{\Delta t}{(\Delta y)^2}\hat{p}_{i,j+1}^{k+2}=\Delta t\left[\frac{1}{2\,\Delta x}\left(u_{i+1,j}^{n+1}-u_{i-1,j}^{n+1}\right)+\frac{1}{2\,\Delta y}\left(v_{i,j+1}^{n+1}-v_{i,j-1}^{n+1}\right)\right]+\frac{\Delta t}{(\Delta x)^2}\left(\hat{p}_{i+1,j}^{k+1}+\hat{p}_{i-1,j}^{k+1}-2\hat{p}_{i,j}^{k+1}\right)+\hat{p}_{i,j}^{k+1} \tag{13}$$

where k represents the iteration and the u and v velocities from the last time step are used. The boundary conditions for equations (8) to (11) are

$$u(i,1) = u(1,j) = u(i_{max},j) = 0 \qquad u(i,j_{max}) = 1$$

$$v(i,1) = v(1,j) = v(i_{max},j) = v(i,j_{max}) = 0$$

The pressure correction $\hat{p}$ was computed at the boundaries by three methods. The first was to solve equations (12) and (13) on the boundaries. For this computation, reflection of the node points was used. The second method was to use three-point extrapolation utilizing the information that the normal derivative of $\hat{p}$ is 0. This extrapolation is

$$\hat{p}_i = \frac{1}{3}\left(4\hat{p}_{i+1} - \hat{p}_{i+2}\right) \tag{14}$$

The third method is to simply set the first interior pressure equal to the boundary value. Whether these assumptions are first- or second-order accurate is not material since $\hat{p}$ is zero at steady state.

APPLICATION

The procedure for solving equations (8) to (13) is as follows:

(1) With the initial conditions, u and v are computed first by equations (8) and (9) and then by equations (10) and (11). With the velocity of the upper moving surface equal to 1, the greater change is in the vertical direction and thus the reason for the order of solution.

(2) These velocities from equations (10) and (11) are used in equations (12) and (13) to compute $\hat{p}$. These two equations (eqs. (12) and (13)) are iterated until the current $\hat{p}$ at each node is within 10^{-3} of the corresponding previous value.

(3) The velocities u and v are then updated to correspond to the new $\hat{p}$ by

$$u_{i,j}^{n+1} = u_{i,j}^{n+1} + \frac{1}{2\,\Delta x}\left(\hat{p}_{i+1,j} - \hat{p}_{i-1,j}\right)$$

$$v_{i,j}^{n+1} = v_{i,j}^{n+1} + \frac{1}{2\,\Delta y}\left(\hat{p}_{i,j+1} - \hat{p}_{i,j-1}\right)$$

(4) These values of u and v at time level $n + 1$ are compared with u and v at time level n. If values are within 10^{-4} of one another, convergence is accepted. If not, $\hat{p}$ is combined with the previous pressure p for a new value. The pressure correction $\hat{p}$ is subtracted from p at each new time step. Adding $\hat{p}$ gives incorrect trends in the results.

(5) The velocities u and v are recomputed in the momentum equations and the procedure is continued until convergence is obtained.

(6) Before recomputing $\hat{p}$ the initial value of $\hat{p}$ is always reset to zero. At convergence, $\hat{p}$ should be near zero, so that continuity is satisfied.

RESULTS AND DISCUSSION

Solutions are presented for three test cases. For case 1, $R = 100$, $\Delta t = 0.01$, and $\hat{p}$ was calculated at boundaries with equations (12) and (13). Case 2 is the same except $R = 10$. For case 3, $R = 100$, $\Delta t = 0.005$, and $\hat{p}$ was calculated at boundaries with equation (14).

Figures 2(a) and 2(b) are plots of u and v, respectively, through the vortex center for the previously mentioned cases. The location of the vortex center for case 1 is very close to that shown by Mills (ref. 1). For case 3, the vortex center is shown to be slightly higher but at the same axial location compared with the results of Mills. This is possibly due to slightly different pressure gradients in the two calculations. For case 2, the vortex center is at about the same height as for case 1, but the axial location has been displaced to the left and the profile is more symmetric. Also the slope of the u-profile is lower at the upper boundary. These results can be attributed to greater diffusion at $R = 10$.

In figures 3(a) and 3(b), the pressure coefficient for case 1 through the vortex center is presented in the normal and axial direction, respectively. From the wall ($y = 0$) to $y = 0.5$, there is good agreement between the present results and those of Mills. (See fig. 3(a).) From $y = 0.5$ to the moving boundary ($y = 1.0$), there is poor agreement. Consequently, the agreement between pressure coefficients of the present work and those of Mills through the vortex center ($y = 0.75$) in the axial direction is likewise poor. The reason for this disagreement is not known.

Figures 4(a) and 4(b) are velocity vector diagrams for case 1 and case 2, respectively. The vectors are of equal length since a characteristic length was used as the reference. This was done to amplify the velocities at the cavity bottom. For case 2 (fig. 4(b)), the possible formation of vortices is indicated in the bottom left and right corners. This result is shown in reference 1. When either of the results of figure 4 are superimposed on the results of Mills, a very good comparison is obtained.

A note may be made of the pressure gradients through the cavity. In figure 3, the pressures are generally in poor agreement with published results. However, considering the good agreement obtained for the velocities in figures 2 and 4, it is assumed that the pressure gradients computed in the present analysis must be reasonably well predicted.

Other conditions were considered in investigating this problem. Solving for $\hat{p}$ on the boundaries by the third method discussed previously (e.g., $p(1,j) = p(2,j)$) resulted in values for u, v, and p which were not in good agreement with results obtained by computing $\hat{p}$ at the boundaries by equations (12) and (13) or by equation (14). A convergence criterion on u and v of 10^{-4} rather than 10^{-3} gave much better agreement with results of reference 1. Convergence could not be obtained if accuracy on $\hat{p}$ was raised from 10^{-3} to 10^{-4}.

For any of the applications, the values of u and v are not iterated to a required convergence at each time step. Convergence is only tested for the values at the current and previous time steps. This type of time marching would only produce convergence at steady state, and the transient results are not accurate.

Since most of the documented results on this flow problem are presented in terms of stream-function—vorticity variables, an overall comparison of the present results computed in primitive variables is difficult. However, where at least a cursory comparison is possible, slightly lower levels for u and v are computed by the method discussed in this paper, and a poor comparison for the pressures is indicated. This implies that the results obtained by the simplified approach presented herein are not so accurate as the results obtained by a more rigorous analysis.

CONCLUDING REMARKS

An alternating-direction implicit (ADI) finite-difference procedure has been employed to compute the two-dimensional viscous incompressible flow generated within a rectangular cavity by a moving surface at the cavity open end. The pressure through the cavity was computed by the Spalding SIMPLE procedure.

Although the present method does not predict axial and normal velocities as high as indicated by the more exact methods, the values of the velocities through the vortex center are reasonably predicted and the overall velocity vector diagrams appear satisfactory. The pressure levels are generally in poor agreement with other predictions. However, the pressure gradients must be reasonably well predicted because of the accurate results obtained for the velocities.

REFERENCES

1. Mills, Ronald D.: Numerical Solutions of the Viscous Flow Equations for a Class of Closed Flows. J. Roy. Aeronaut. Soc., vol. 69, no. 658, Oct. 1965, pp. 714-718; Correction, vol. 69, no. 660, Dec. 1965, p. 880.

2. Caretto, L. S.; Gosman, A. D.; Patankar, S. V.; and Spalding, D. B.: Two Calculation Procedures for Steady, Three-Dimensional Flows With Recirculation. Proceedings of the Third International Conference on Numerical Methods in Fluid Mechanics, Volume II. Volume 19 of Lecture Notes in Physics, Henri Cabannes and Roger Temam, eds., Springer-Verlag, July 1972, pp. 60-68.

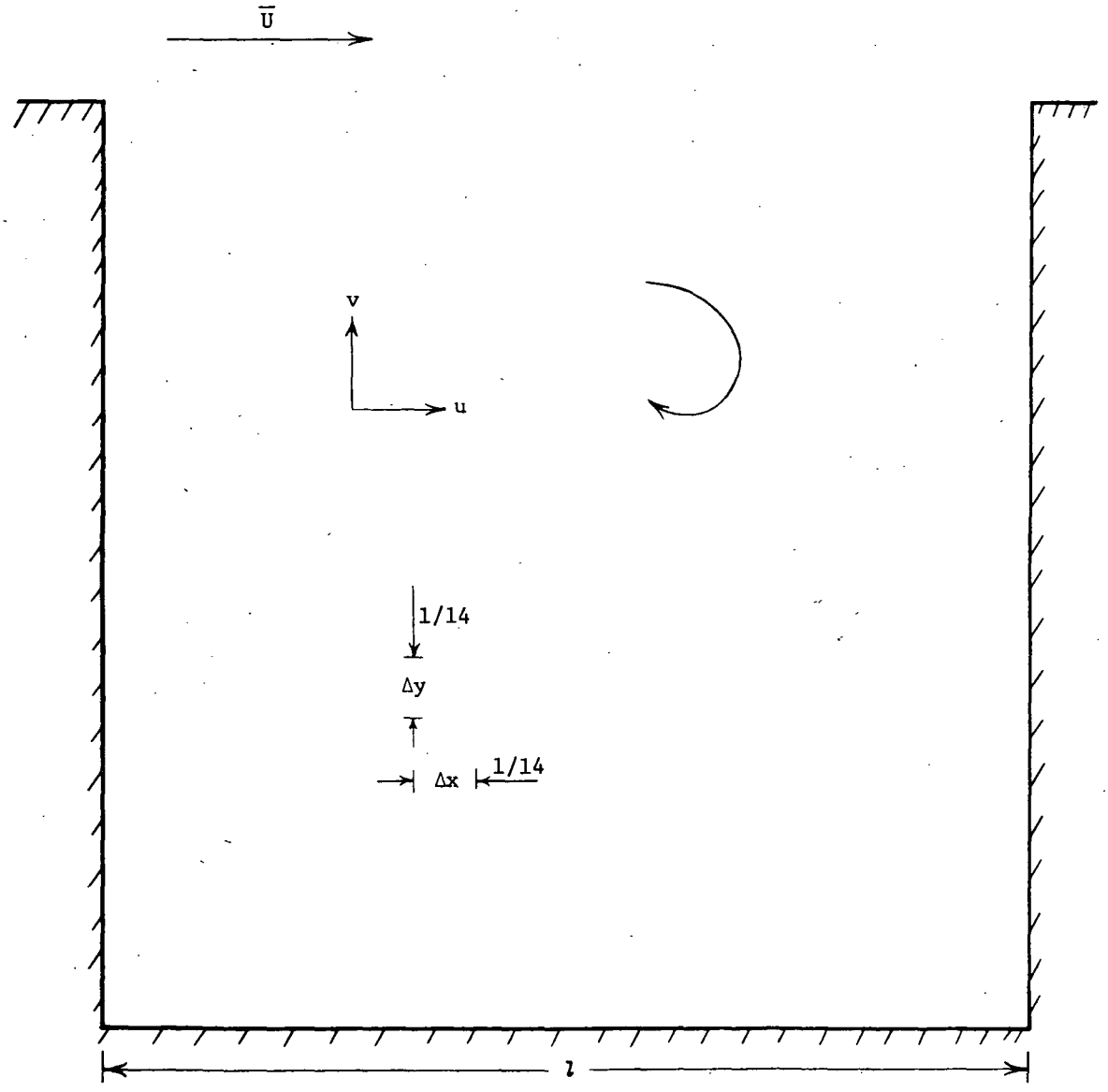

Figure 1.- Sketch of square cavity.

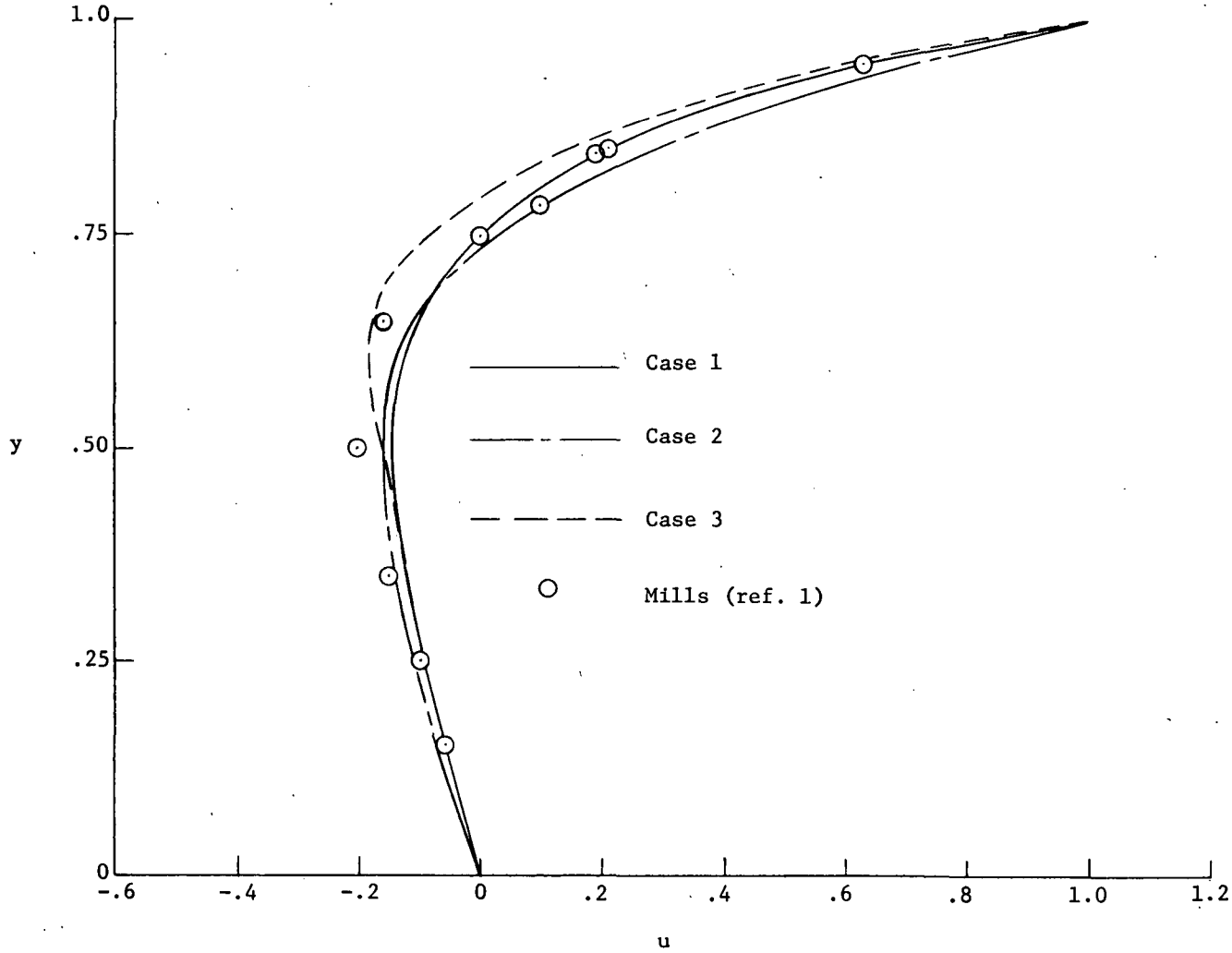

(a) u-profile. Vortex center at $y = 0.75$.

Figure 2.- Velocity profiles through vortex center.

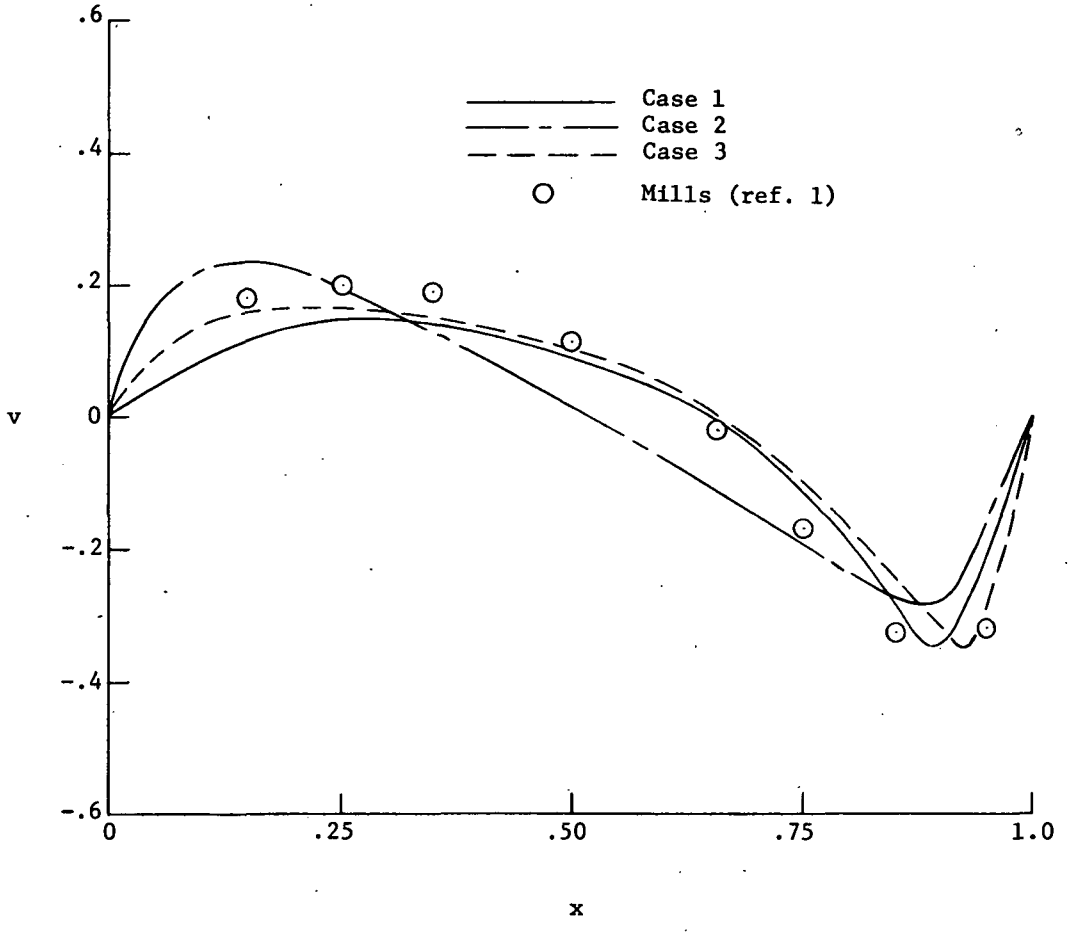

(b) v-profile. Vortex center at x = 0.65.

Figure 2.- Concluded.

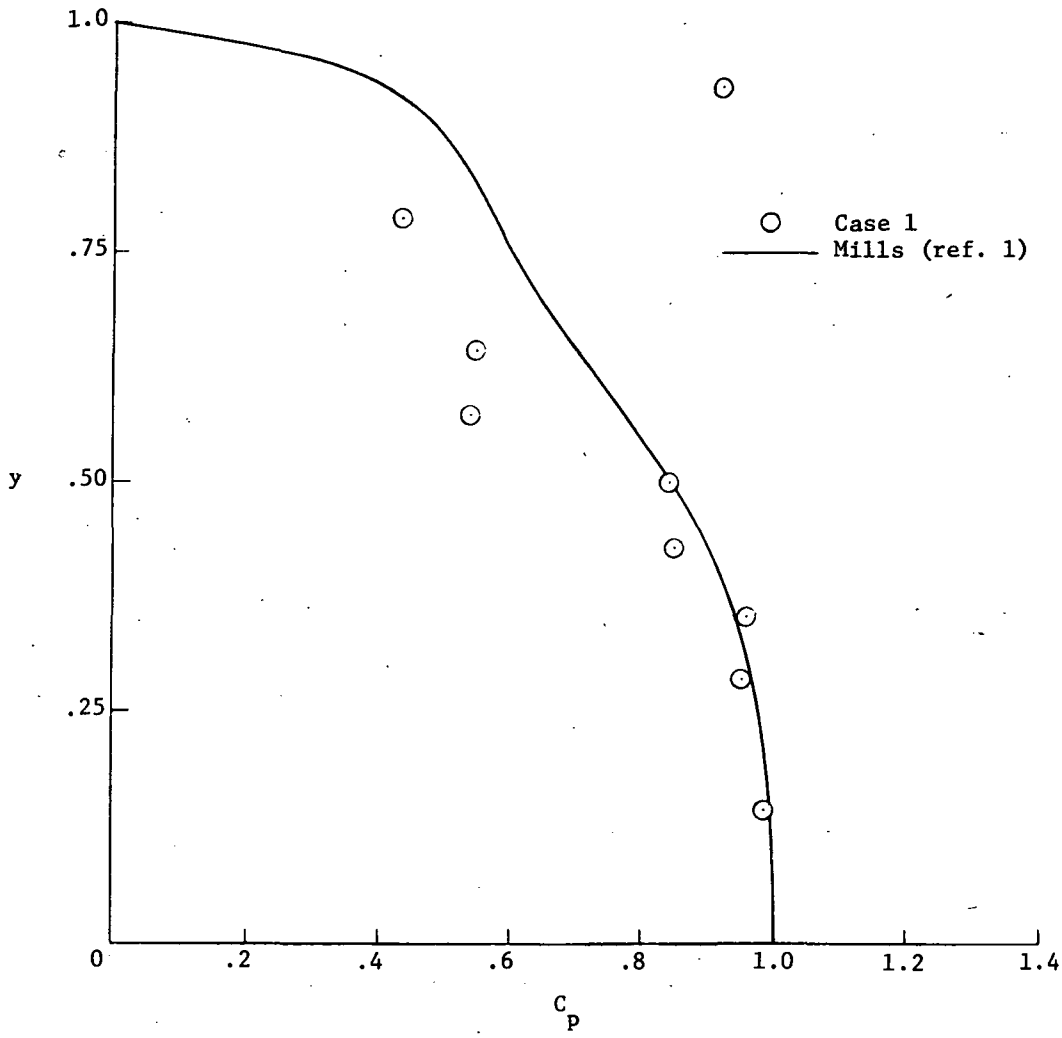

(a) Profile in y-direction.

Figure 3.- Pressure coefficient through vortex center.

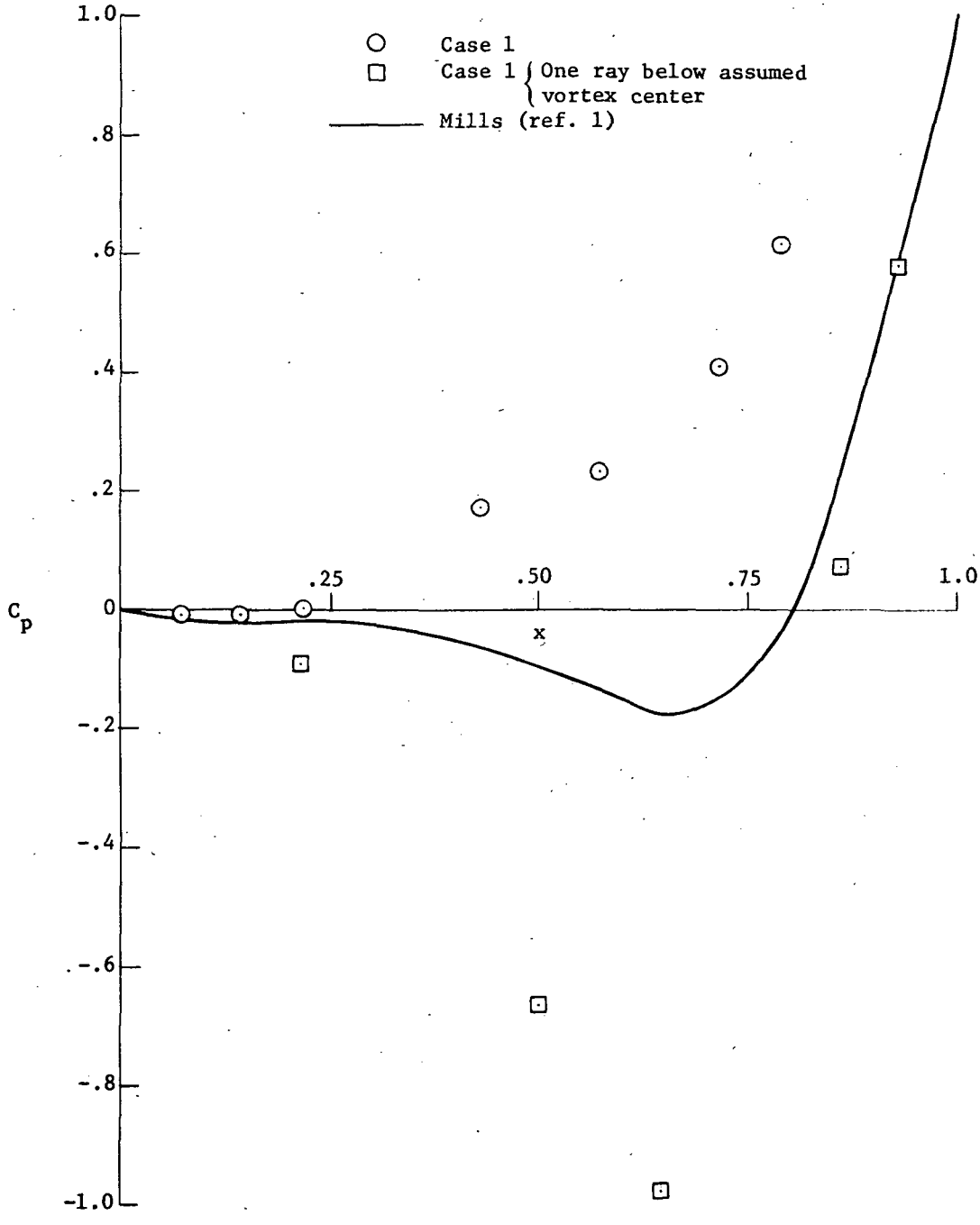

(b) Profile in x-direction.

Figure 3.- Concluded.

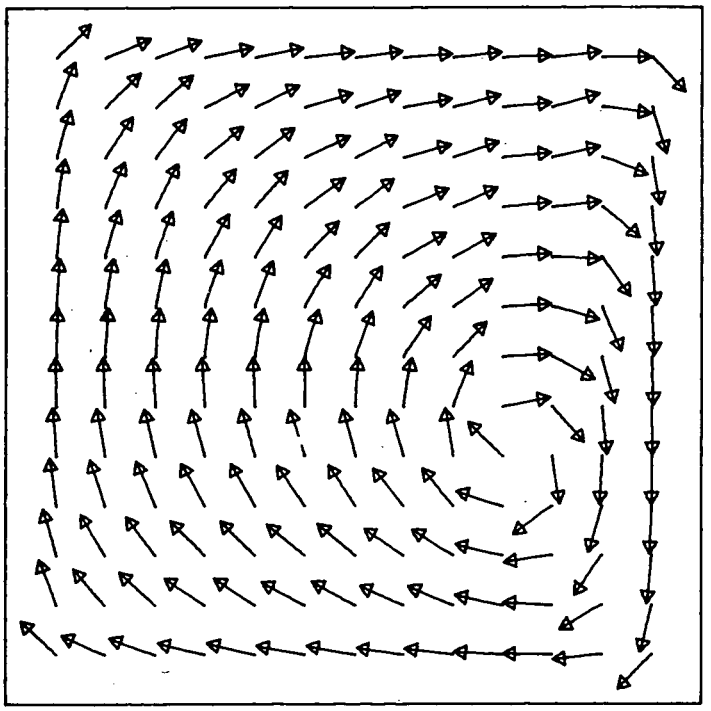

(a) Case 1.

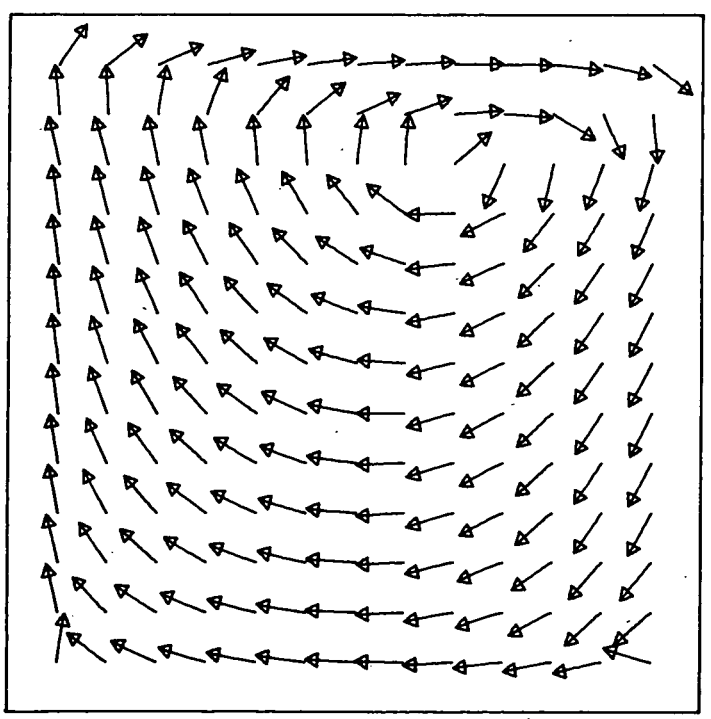

(b) Case 2.

Figure 4.- Velocity vector diagrams.

9. CUBIC SPLINE SOLUTION FOR THE DRIVEN CAVITY

Stanley G. Rubin* and Randolph A. Graves, Jr.
Langley Research Center

SUMMARY

A cubic spline procedure for solution of the vorticity—stream-function system for flow in a driven cavity has been described. The spline results were compared with finite-difference results and were found to be more accurate, even near the boundaries. A nonuniform grid was also used with increased mesh density in regions where diffusion was important. Considerable advantages of the spline procedure with a nonuniform grid were indicated in regions of large gradients.

INTRODUCTION

The present paper describes a cubic spline procedure for the solution of the driven cavity problem. (See paper no. 1 by Rubin and Harris for details of this problem.) A vorticity—stream-function system is considered. A finite-difference discretization is used for the marching or timelike direction. Unlike a finite-element or Galerkin procedure, there are no quadratures to evaluate and the coefficient matrix is tridiagonal. The spline approximation is second-order accurate even with relatively large variations in the mesh. Moreover, for the convective terms (first derivatives) the spline procedure is third-order accurate with a nonuniform mesh and fourth-order accurate with a uniform mesh. A detailed discussion of splines and spline procedures for fluid dynamics can be found in reference 1.

SYMBOLS

a,b end points of interval

h_i,k_j mesh widths; $x_i - x_{i-1}$ and $y_j - y_{j-1}$, respectively

L_i,M_i spline second derivative in y- and x-direction, respectively

ℓ_i,m_i spline first derivative in y- and x-direction, respectively

---

*Visiting professor at Old Dominion University, Norfolk, Va. Now professor of aerospace engineering, Polytechnic Institute of New York, Farmingdale, N.Y.

N	number of nodes in interval [a,b] excluding boundaries
R	Reynolds number
S_Δ	cubic spline function
t	time
Δt	time step
u,v	axial and normal velocity component, respectively
x_i	nodal points
x,y	coordinate in axial and normal direction, respectively
ζ	vorticity
θ	index of finite-difference scheme; 0 for explicit, 1/2 for Crank-Nicolson, 1 for implicit
τ	fictitious time
$\Delta\tau$	fictitious time step
ψ	stream function

Superscripts:

n	index of time step Δt
s	index of fictitious time step $\Delta\tau$

Subscripts:

i,j	index of nodal points in x- and y-direction, respectively
max	maximum

t differentiation with respect to time

x,y differentiation with respect to x or y

SPLINE FORMULATION

Basic Spline Theory

Consider a mesh with nodal points (knots) x_i such that

$$a = x_0 < x_1 < x_2 \ldots < x_N < x_{N+1} = b$$

and with

$$h_i = x_i - x_{i-1} > 0$$

Consider a function $u(x)$ such that at the mesh points x_i,

$$u(x_i) = u_i$$

The cubic spline is a function $S_\Delta(u;x) = S_\Delta(x)$ which is continuous, together with its first and second derivatives, on the interval $[a,b]$, corresponds to a cubic polynomial in each subinterval $x_{i-1} \leqq x \leqq x_i$, and satisfies $S_\Delta(u_i;x_i) = u_i$.

If $S_\Delta(x)$ is cubic on $[x_{i-1},x_i]$, then in general

$$S''_\Delta(x) = M_{i-1}\left(\frac{x_i - x}{h_i}\right) + M_i\left(\frac{x - x_{i-1}}{h_i}\right)$$

where

$$M_i \equiv S''_\Delta(x_i)$$

Therefore,

$$S_\Delta(x) = M_{i-1}\frac{(x_i - x)^3}{6h_i} + M_i\frac{(x - x_{i-1})^3}{6h_i} + \left(u_{i-1} - \frac{M_{i-1}h_i^2}{6}\right)\frac{x_i - x}{h_i} + \left(u_i - \frac{M_i h_i^2}{6}\right)\frac{x - x_{i-1}}{h_i} \qquad (1)$$

The unknown derivatives M_i are related by enforcing the continuity condition on $S'_\Delta(x)$. With $S'(x_i^-) = m_i^-$ on $[x_{i-1},x_i]$ and $S'_\Delta\, x_i^+ = m_i^+$ on $[x_i,x_{i+1}]$,

$$m_i^- = m_i^+ = m_i$$

For $i = 1, \ldots, N$,

$$\frac{h_i}{6} M_{i-1} + \frac{h_i + h_{i+1}}{3} M_i + \frac{h_{i+1}}{6} M_{i+1} = \frac{u_{i+1} - u_i}{h_{i+1}} - \frac{u_i - u_{i-1}}{h_i} \tag{2}$$

$$m_i = \frac{h_i}{3} M_i + \frac{h_i}{6} M_{i-1} + \frac{u_i - u_{i-1}}{h_i} \tag{3}$$

$$m_i = -\frac{h_{i+1}}{3} M_i - \frac{h_{i+1}}{6} M_{i+1} + \frac{u_{i+1} - u_i}{h_{i+1}} \tag{4}$$

Equation (2) lead to a system of N equations for the $N + 2$ unknown M_i.

Splines for Solving Partial Differential Equations

If the values u_i are not prescribed but represent the solution of a quasi-linear second-order partial differential equation, such as

$$u_t = f(u,u_x,u_{xx})$$

then an approximate solution for u_i can be obtained by considering the solution of

$$(u_t)_i = f(u_i,m_i,M_i)$$

where the time derivative is discretized in the usual finite-difference fashion; that is,

$$\frac{u_i^{n+1} - u_i^n}{\Delta t} = (1 - \theta)f^n + \theta f^{n+1}$$

where $\theta = 0$, 1, and $1/2$ for explicit, implicit, and Crank-Nicolson finite-difference schemes, respectively. The physical time t equals $n\,\Delta t$ (Δt is the time increment at each step).

For equations with two space dimensions such that

$$u_t = f(u, u_x, u_y, u_{xx}, u_{yy})$$

a spline-alternating-direction-implicit (SADI) formulation is developed. The two-step procedure, with quasi-linearization or some other iterative process used for nonlinear terms, is of the following form:

Step 1

$$u_{i,j}^{n+1/2} = u_{i,j}^{n} + \frac{\Delta t}{2} f\left(u_{i,j}^{n+1/2}, m_{i,j}^{n+1/2}, M_{i,j}^{n+1/2}, \ell_{i,j}^{n}, L_{i,j}^{n}\right) \tag{5a}$$

Step 2

$$u_{i,j}^{n+1} = u_{i,j}^{n+1/2} + \frac{\Delta t}{2} f\left(u_{i,j}^{n+1/2}, m_{i,j}^{n+1/2}, M_{i,j}^{n+1/2}, \ell_{i,j}^{n+1}, L_{i,j}^{n+1}\right) \tag{5b}$$

where $\ell_{i,j}$ and $L_{i,j}$ are the spline approximations to $(u_y)_{i,j}$ and $(u_{yy})_{i,j}$, respectively.

INCOMPRESSIBLE FLOW IN A CAVITY

Equations

For the driven cavity the governing equations, in terms of vorticity and stream function, are

$$\left.\begin{aligned} \psi_{xx} + \psi_{yy} &= \zeta \\ \zeta_t + u\zeta_x + v\zeta_y &= \frac{1}{R}(\zeta_{xx} + \zeta_{yy}) \end{aligned}\right\} \tag{6}$$

where ψ is the stream function, ζ is the vorticity, and $u = \psi_y$ and $v = -\psi_x$ are the velocities in the x- and y-directions, respectively. For all calculations the initial conditions are $\psi(x,y) = 0$ and $\zeta(x,y) = 0$.

Solutions are obtained by the iterative SADI procedure. The SADI system representing equations (6) is given in two steps for both stream function and vorticity.

Stream function.- For step 1,

$$\psi_{i,j}^{n+1,s+1/2} = \psi_{i,j}^{n+1,s} + \frac{\Delta\tau}{2}\left[\left(L_{i,j}^{\psi}\right)^{n+1,s+1/2} + \left(M_{i,j}^{\psi}\right)^{n+1,s} - \zeta_{i,j}^{n+1}\right] \tag{7a}$$

For step 2,

$$\psi_{i,j}^{n+1,s+1} = \psi_{i,j}^{n+1,s+1/2} + \frac{\Delta\tau}{2}\left[\left(L_{i,j}^{\psi}\right)^{n+1,s+1/2} + \left(M_{i,j}^{\psi}\right)^{n+1,s+1} - \zeta_{i,j}^{n+1}\right] \tag{7b}$$

where $\Delta\tau$ is a fictitious time step and $\tau = s\,\Delta\tau$. Solutions for equations (6) are obtained as the steady-state limit ($\tau \to \infty$) of equations (7). The notation $L_{i,j}^{A}$ and $M_{i,j}^{A}$ denote the spline approximations to $\partial^2 A/\partial y^2$ and $\partial^2 A/\partial x^2$, respectively. (The superscript ψ implies that $A = \psi$.) First derivatives $\psi_y = u$ and $\psi_x = -v$ are represented by $\ell_{i,j}^{\psi}$ and $m_{i,j}^{\psi}$, respectively.

Vorticity.- For step 1,

$$\zeta_{i,j}^{n+1/2} = \zeta_{i,j}^{n} + \frac{\Delta t}{2}\left[-\ell_{i,j}^{\overline{\psi}}\left(m_{i,j}^{\zeta}\right)^{n} + m_{i,j}^{\overline{\psi}}\left(\ell_{i,j}^{\zeta}\right)^{n+1/2} + R^{-1}\left(L_{i,j}^{\zeta}\right)^{n+1/2} + R^{-1}\left(M_{i,j}^{\zeta}\right)^{n}\right] \tag{8a}$$

For step 2,

$$\zeta_{i,j}^{n+1} = \zeta_{i,j}^{n+1/2} + \frac{\Delta t}{2}\left[-\ell_{i,j}^{\overline{\psi}}\left(m_{i,j}^{\zeta}\right)^{n+1} + m_{i,j}^{\overline{\psi}}\left(\ell_{i,j}^{\zeta}\right)^{n+1/2} + R^{-1}\left(L_{i,j}^{\zeta}\right)^{n+1/2} + R^{-1}\left(M_{i,j}^{\zeta}\right)^{n+1}\right] \tag{8b}$$

The bar over superscript ψ in the spline derivatives denotes an average of values at time steps n and $n + 1$. The ζ superscript denotes ζ spline derivatives.

Numerical Solution Procedure

The iterative procedure is as follows:

(1) With $\psi_{i,j}^{n}$ and $\zeta_{i,j}^{n}$ given either as initial conditions or at time $n\,\Delta t$, all the ψ spline derivatives are determined from equations (1) to (4). On the vertical surfaces, $M_{i,j}^{\psi} = \zeta_{i,j}$; on the horizontal boundaries, $L_{i,j}^{\psi} = \zeta_{i,j}$.

(2) The vorticity $\zeta_{i,j}^{n+1}$ is obtained with the SADI technique outlined by equations (5). At the boundaries, $\zeta_{i,j}$ is found from an expression similar to equation (3) or (4). At the upper moving wall (w),

$$\ell_{i,w}^{\psi} = 1 = \frac{k_{i,w} L_{i,w}^{\psi}}{3} + \frac{k_{i,w} L_{i,w-1}^{\psi}}{6} + \frac{\psi_{i,w} - \psi_{i,w-1}}{k_{i,w}}$$

where $k_j = y_j - y_{j-1}$. With $\psi_{i,w} = 0$ and $L_{i,w}^{\psi} = \zeta_{i,w}$,

$$\zeta_{i,w} = \frac{3}{k_{i,w}} - \frac{L_{i,w-1}^{\psi}}{2} + \frac{3\psi_{i,w-1}}{k_{i,w}^2}$$

Similar relations can be derived for the three stationary walls. Boundary values for $M_{i,j}^{\zeta}$ and $L_{i,j}^{\zeta}$ are obtained from equations (8) evaluated at the surface. For the moving wall, equations (3) and (4) are used to eliminate $m_{i,j}^{\zeta}$. In addition, $\zeta_{i,w}^{n+1/2}$ is evaluated with the three-point formula; that is,

$$\zeta_{i,w}^{n+1/2} = \frac{3\zeta_{i,w}^{n+1} + 6\zeta_{i,w}^{n} - \zeta_{i,w}^{n-1}}{8} + O\left[(\Delta t)^2\right]$$

(3) The vorticity $\zeta_{i,j}^{n+1}$ is used in equations (7) and the SADI procedure is applied over the fictitious time τ until a converged solution, to any specified tolerance, is obtained.

(4) If only the steady-state solution is required, the calculation proceeds to the next time step $n + 2$ by returning to step (2) with n replacing $n + 1$. The spline derivatives for ψ have already been determined in step (3).

If an accurate transient solution is required, the calculation proceeds to step (2) with $\psi_{i,j}$ and all spline derivatives of ψ replaced by averages over the n and $n + 1$ time steps. Then $\zeta_{i,j}^{n+1}$ is recalculated. This process continues until convergence is reached.

Results

Calculations are presented for a square cavity with $R = 100$. Comparisons are given with finite-difference calculations in both divergence and nondivergence form as

obtained from the results of Morris (paper no. 5) and Smith and Kidd (paper no. 6) in this volume and of Bozeman and Dalton (ref. 2).

The results are presented in tables I to IV and in figure 1. In all instances, the values of ψ_{max} and the vorticity ζ_{wall} at the midpoint of the moving wall are depicted. For these quantities, comparisons between the spline and finite-difference solutions are possible even when the grid alinements differ. In addition, the distributions of ψ and ζ for the spline solutions and, in several cases, for the finite-difference solutions are presented. Figure 1 depicts the horizontal velocity component $u_{i,j}$ or $\ell^{\psi}_{i,j}$ along a vertical line passing through the vortex center.

The values of ψ_{max} and ζ_{wall} are shown on table I for a variety of grids. Also included is a limiting solution obtained by Richardson extrapolation from the two or three calculated values of each procedure. It is evident that the divergence finite-difference solution is more accurate than the nondivergence result; however, the spline solution, which is obtained in nondivergence form, appears to be even more accurate than the divergence finite-difference result. For example, the value of ψ_{max} obtained from the spline calculation with a uniform grid of 15 points in each direction is about 1 percent higher than the extrapolated value; the 17-point divergence finite-difference result is about 4 percent lower than its extrapolated value. The nondivergence 15-point finite-difference result is low by about 12 percent. These results seem to reflect the higher order accuracy of convection terms in the spline procedure. In the vortex core region the flow is inviscid dominated. However, near the moving wall where diffusion is important, the vorticity results appear to show a similar trend; the spline values are always somewhat more accurate than the divergence finite-difference solutions.

Another interesting result is shown on table I(c). The velocity at the first grid point away from the upper left boundary is depicted. With 15 points the spline result has a sign opposite that obtained with the nondivergence finite-difference method. With a finer grid the finite-difference solution changes sign, so that once again the spline procedure prevails. Unfortunately, the more accurate divergence finite-difference solutions were obtained with a slightly different grid, so that a direct comparison is not possible. However, a change in sign with mesh reduction is observed for the velocity in the corner region. An interpolation procedure is used to estimate the value at the desired location. These results are also given on table I(c). The extrapolated limit closely approximates the solution obtained with splines. The velocity profiles through the vortex center are shown in figure 1. The solutions for ψ and ζ are given in table II.

A spline solution was also obtained with a 19-point nonuniform mesh. In the central region of the cavity, $h_i = 1/14$, as with the 15-point mesh; however, near the boundaries there is some grid realinment to increase the mesh density in the surface boundary layers. The increased accuracy near the boundaries, where diffusion is most important,

leads to a solution that is almost as accurate throughout the entire flow domain as the 29-point results. The improved accuracy of this 19-point solution is seen on table I where ψ_{max} and ζ_{wall} are indicated. These results imply the considerable advantages of the spline procedure with a nonuniform grid in regions of large gradients. With the spline procedure the accuracy of the second-order diffusion terms is enhanced in domains where diffusion effects are significant. In inviscid regions the fourth-order accurate convection terms are dominant and mesh reduction is not as important. The improved resolution of the corner vortices is seen in the ψ and ζ distributions of table III; the comparisons with the 65-point divergence finite-difference solutions (table IV) are reasonably good.

CONCLUDING REMARKS

A comparison between results of the spline-alternating-direction-implicit (SADI) and finite-difference procedures indicated that the spline solution for flow in a driven cavity was more accurate, even near the boundaries. A nonuniform grid was also used with increased mesh density in the boundary layers where diffustion was most important. The spline solution with a 19-point nonuniform grid was almost as accurate throughout the entire flow domain as the spline solution with a 29-point uniform grid. Thus, considerable advantages of the spline procedure with a nonuniform grid are indicated in regions of large gradients.

REFERENCES

1. Rubin, Stanley G.; and Graves, Randolph A., Jr.: A Cubic Spline Approximation for Problems in Fluid Mechanics. NASA TR R-436, 1975.

2. Bozeman, James D.; and Dalton, Charles: Numerical Study of Viscous Flow in a Cavity. J. Comput. Phys., vol. 12, no. 3, July 1973, pp. 348-363.

TABLE I.- RESULTS FOR SQUARE CAVITY WITH R = 100

(a) Vorticity at center of moving wall

Calculation method	Points	Vorticity at center of moving wall
Spline	15 × 15	7.1376
Spline	29 × 29	6.6876
Extrapolated spline	------	6.5376
Spline (unequal spacing)	19 × 19	6.2970
Finite difference	15 × 15	8.9160
Finite difference	57 × 57	6.6960
Extrapolated finite difference	------	6.5480
Finite difference[a]	17 × 17	7.3755
Finite difference[a]	33 × 33	6.7653
Finite difference[a]	65 × 65	6.6091
Extrapolated finite difference[a]	------	6.5567

[a]Divergence form.

(b) Maximum stream function

Calculation method	Points	Maximum stream function
Spline	15 × 15	-0.10529
Spline	29 × 29	-.10432
Extrapolated spline	------	-.10399
Spline (unequal spacing)	19 × 19	-.10472
Finite difference	15 × 15	-.08742
Finite difference	57 × 57	-.10128
Extrapolated finite difference	------	-.10220
Finite difference[a]	17 × 17	-.09867
Finite difference[a]	33 × 33	-.10213
Finite difference[a]	65 × 65	-.10318
Extrapolated finite difference[a]	------	-.10355
Reference 2	51 × 51	-.10316

[a]Divergence form.

(c) Corner point velocity u

Calculation method	Points	Velocity u at corner (a)
Spline	15 × 15	-0.13230
Spline	29 × 29	-.10036
Extrapolated spline	------	-.08971
Finite difference	15 × 15	.05730
Finite difference	57 × 57	-.06615
Extrapolated finite difference	------	-.07438
Interpolated finite difference[b]	17 × 17	.02079
Interpolated finite difference[b]	33 × 33	-.05189
Interpolated finite difference[b]	65 × 65	-.07560
Extrapolated finite difference[b]	------	-.08399

[a]Locations: 0.07143 down from moving surface; 0.07143 in from left surface.

[b]Divergence form.

TABLE II. - VORTICITY AND STREAM FUNCTION CALCULATED WITH SADI PROCEDURE WITH EQUALLY SPACED 15 × 15 GRID

(a) Stream function

y \ x	0	0.0714	0.1428	0.2143	0.2857	0.3571	0.4286	0.5000	0.5714	0.6428	0.7143	0.7857	0.8571	0.9286	1.0
1.0000	0	0	0	0	0	0	0	0	0	0	0	0	0	0	0
.9286	0	-1.647×10^{-2}	-3.110×10^{-2}	-3.939×10^{-2}	-4.507×10^{-2}	-4.928×10^{-2}	-5.249×10^{-2}	-5.485×10^{-2}	-5.632×10^{-2}	-5.676×10^{-2}	-5.588×10^{-2}	-5.322×10^{-2}	-4.701×10^{-2}	-2.821×10^{-2}	0
.8571	0	-9.847×10^{-3}	-2.815×10^{-2}	-4.447×10^{-2}	-5.761×10^{-2}	-6.827×10^{-2}	-7.683×10^{-2}	-8.333×10^{-2}	-8.751×10^{-2}	-8.882×10^{-2}	-8.634×10^{-2}	-7.839×10^{-2}	-6.054×10^{-2}	-2.715×10^{-2}	0
.7857	0	-7.413×10^{-3}	-2.368×10^{-2}	-4.196×10^{-2}	-5.895×10^{-2}	-7.377×10^{-2}	-8.615×10^{-2}	-9.572×10^{-2}	-1.018×10^{-1}	-1.033×10^{-1}	-9.865×10^{-2}	-8.515×10^{-2}	-5.905×10^{-2}	-2.246×10^{-2}	0
.7143	0	-6.355×10^{-3}	-2.110×10^{-2}	-3.904×10^{-2}	-5.703×10^{-2}	-7.349×10^{-2}	-8.753×10^{-2}	-9.831×10^{-2}	-1.047×10^{-1}	-1.053×10^{-1}	-9.795×10^{-2}	-8.016×10^{-2}	-5.091×10^{-2}	-1.729×10^{-2}	0
.6428	0	-5.649×10^{-3}	-1.902×10^{-2}	-3.579×10^{-2}	-5.317×10^{-2}	-6.942×10^{-2}	-8.333×10^{-2}	-9.372×10^{-2}	-9.917×10^{-2}	-9.796×10^{-2}	-8.813×10^{-2}	-6.828×10^{-2}	-4.021×10^{-2}	-1.254×10^{-2}	0
.5714	0	-4.956×10^{-3}	-1.675×10^{-2}	-3.172×10^{-2}	-4.741×10^{-2}	-6.217×10^{-2}	-7.466×10^{-2}	-8.352×10^{-2}	-8.721×10^{-2}	-8.410×10^{-2}	-7.285×10^{-2}	-5.351×10^{-2}	-2.951×10^{-2}	-8.584×10^{-3}	0
.5000	0	-4.163×10^{-3}	-1.410×10^{-2}	-2.678×10^{-2}	-4.010×10^{-2}	-5.256×10^{-2}	-6.283×10^{-2}	-6.955×10^{-2}	-7.133×10^{-2}	-6.690×10^{-2}	-5.573×10^{-2}	-3.895×10^{-2}	-2.030×10^{-2}	-5.569×10^{-3}	0
.4286	0	-3.284×10^{-3}	-1.117×10^{-2}	-2.128×10^{-2}	-3.189×10^{-2}	-4.168×10^{-2}	-4.946×10^{-2}	-5.403×10^{-2}	-5.427×10^{-2}	-4.944×10^{-2}	-3.965×10^{-2}	-2.650×10^{-2}	-1.314×10^{-2}	-3.424×10^{-3}	0
.3571	0	-2.383×10^{-3}	-8.189×10^{-3}	-1.569×10^{-2}	-2.356×10^{-2}	-3.071×10^{-2}	-3.615×10^{-2}	-3.894×10^{-2}	-3.830×10^{-2}	-3.392×10^{-2}	-2.627×10^{-2}	-1.685×10^{-2}	-7.988×10^{-3}	-1.975×10^{-3}	0
.2857	0	-1.542×10^{-3}	-5.405×10^{-3}	-1.048×10^{-2}	-1.583×10^{-2}	-2.063×10^{-2}	-2.414×10^{-2}	-2.568×10^{-2}	-2.478×10^{-2}	-2.139×10^{-2}	-1.603×10^{-2}	-9.890×10^{-3}	-4.465×10^{-3}	-1.034×10^{-3}	0
.2143	0	-8.371×10^{-4}	-3.053×10^{-3}	-6.066×10^{-3}	-9.276×10^{-3}	-1.214×10^{-2}	-1.417×10^{-2}	-1.495×10^{-2}	-1.420×10^{-2}	-1.198×10^{-2}	-8.701×10^{-3}	-5.135×10^{-3}	-2.169×10^{-3}	-4.473×10^{-4}	0
.1428	0	-3.277×10^{-4}	-1.312×10^{-3}	-2.731×10^{-3}	-4.276×10^{-3}	-5.661×10^{-3}	-6.629×10^{-3}	-6.965×10^{-3}	-6.544×10^{-3}	-5.408×10^{-3}	-3.795×10^{-3}	-2.109×10^{-3}	-7.909×10^{-4}	-1.180×10^{-4}	0
.0714	0	-5.630×10^{-5}	-2.974×10^{-4}	-6.803×10^{-4}	-1.108×10^{-3}	-1.495×10^{-3}	-1.767×10^{-3}	-1.860×10^{-3}	-1.736×10^{-3}	-1.407×10^{-3}	-9.465×10^{-4}	-4.790×10^{-4}	-1.361×10^{-4}	3.981×10^{-6}	0
0	0	0	0	0	0	0	0	0	0	0	0	0	0	0	0

(b) Vorticity

y \ x	0	0.0714	0.1428	0.2143	0.2857	0.3571	0.4286	0.5000	0.5714	0.6428	0.7143	0.7857	0.8571	0.9286	1.0
1.0000	----------	3.292×10	2.128×10	1.588×10	1.249×10	1.015×10	8.374	7.137	6.390	6.192	6.673	8.026	1.114×10	2.419×10	----------
.9286	-1.124×10	1.892	5.839	6.381	6.285	5.999	5.678	5.392	5.187	5.125	5.267	5.894	8.143	9.865	-2.030×10
.8571	-5.087	-2.293	9.294×10^{-2}	1.402	2.155	2.675	3.078	3.424	3.750	4.085	4.477	5.216	6.305	1.823	-1.666×10
.7857	-3.529	-1.826	-6.207×10^{-1}	2.357×10^{-1}	8.790×10^{-1}	1.425	1.942	2.460	2.995	3.555	4.168	4.811	4.109	-1.749	-1.231×10
.7143	-2.939	-1.658	-6.205×10^{-1}	1.204×10^{-1}	6.871×10^{-1}	1.191	1.696	2.225	2.782	3.351	3.854	3.834	1.856	-3.065	-8.683
.6428	-2.586	-1.464	-5.610×10^{-1}	1.012×10^{-1}	6.184×10^{-1}	1.091	1.574	2.076	2.573	2.994	3.123	2.404	1.338×10^{-1}	-3.194	-5.858
.5714	-2.264	-1.277	-4.969×10^{-1}	6.595×10^{-2}	5.082×10^{-1}	9.192×10^{-1}	1.339	1.756	2.115	2.290	2.032	9.989×10^{-1}	-8.585×10^{-1}	-2.742	-3.772
.5000	-1.899	-1.079	-4.436×10^{-1}	6.369×10^{-3}	3.554×10^{-1}	6.758×10^{-1}	9.909×10^{-1}	1.274	1.452	1.397	9.413×10^{-1}	-3.486×10^{-3}	-1.210	-2.091	-2.316
.4286	-1.491	-8.744×10^{-1}	-3.989×10^{-1}	-6.750×10^{-2}	1.834×10^{-1}	4.046×10^{-1}	6.043×10^{-1}	7.498×10^{-1}	7.756×10^{-1}	5.969×10^{-1}	1.517×10^{-1}	-5.101×10^{-1}	-1.154	-1.462	-1.351
.3571	-1.072	-6.710×10^{-1}	-3.584×10^{-1}	-1.418×10^{-1}	1.737×10^{-2}	1.497×10^{-1}	2.544×10^{-1}	3.021×10^{-1}	2.494×10^{-1}	5.931×10^{-2}	-2.649×10^{-1}	-6.425×10^{-1}	-9.199×10^{-1}	-9.520×10^{-1}	-7.345×10^{-1}
.2857	-6.799×10^{-1}	-4.811×10^{-1}	-3.185×10^{-1}	-2.055×10^{-1}	-1.259×10^{-1}	-6.339×10^{-2}	-2.085×10^{-2}	-1.917×10^{-2}	-8.235×10^{-2}	-2.192×10^{-1}	-4.059×10^{-1}	-5.799×10^{-1}	-6.581×10^{-1}	-5.786×10^{-1}	-3.525×10^{-1}
.2143	-3.531×10^{-1}	-3.170×10^{-1}	-2.772×10^{-1}	-2.521×10^{-1}	-2.406×10^{-1}	-2.324×10^{-1}	-2.269×10^{-1}	-2.355×10^{-1}	-2.713×10^{-1}	-3.357×10^{-1}	-4.101×10^{-1}	-4.583×10^{-1}	-4.399×10^{-1}	-3.263×10^{-1}	-1.242×10^{-1}
.1428	-1.224×10^{-1}	-1.880×10^{-1}	-2.330×10^{-1}	-2.783×10^{-1}	-3.282×10^{-1}	-3.698×10^{-1}	-3.940×10^{-1}	-4.019×10^{-1}	-4.004×10^{-1}	-3.943×10^{-1}	-3.798×10^{-1}	-3.463×10^{-1}	-2.802×10^{-1}	-1.679×10^{-1}	-5.912×10^{-3}
.0714	-1.086×10^{-2}	-9.361×10^{-2}	-1.777×10^{-1}	-2.815×10^{-1}	-3.948×10^{-1}	-4.939×10^{-1}	-5.579×10^{-1}	-5.744×10^{-1}	-5.415×10^{-1}	-4.667×10^{-1}	-3.652×10^{-2}	-2.556×10^{-1}	-1.551×10^{-1}	-6.777×10^{-2}	2.058×10^{-2}
0	0	-8.545×10^{-3}	-1.003×10^{-1}	-2.633×10^{-1}	-4.500×10^{-1}	-6.209×10^{-1}	-7.424×10^{-1}	-7.846×10^{-1}	-7.290×10^{-1}	-5.801×10^{-1}	-3.731×10^{-1}	-1.669×10^{-1}	-2.446×10^{-2}	1.798×10^{-2}	0

TABLE III.- VORTICITY AND STREAM FUNCTION CALCULATED WITH SADI PROCEDURE WITH UNEQUALLY SPACED 19 × 19 GRID

(a) Stream function

y \ x	0	0.0201	0.0482	0.0877	0.1428	0.2143	0.2857	0.3571	0.4286	0.5000	0.5714	0.6428	0.7143	0.7857	0.8571	0.9123	0.9517	0.9799	1.0
0	0	0	0	0	0	0	0	0	0	0	0	0	0	0	0	0	0	0	0
.9799	0	-5.558×10^{-3}	-1.167×10^{-2}	-1.461×10^{-2}	-1.627×10^{-2}	-1.729×10^{-2}	-1.790×10^{-2}	-1.832×10^{-2}	-1.862×10^{-2}	-1.883×10^{-2}	-1.892×10^{-2}	-1.890×10^{-2}	-1.874×10^{-2}	-1.838×10^{-2}	-1.764×10^{-2}	-1.636×10^{-2}	-1.368×10^{-2}	-6.871×10^{-3}	0
.9517	0	-3.149×10^{-3}	-1.204×10^{-2}	-2.126×10^{-2}	-2.814×10^{-2}	-3.298×10^{-2}	-3.602×10^{-2}	-3.818×10^{-2}	-3.977×10^{-2}	-4.087×10^{-2}	-4.146×10^{-2}	-4.148×10^{-2}	-4.076×10^{-2}	-3.905×10^{-2}	-3.551×10^{-2}	-2.924×10^{-2}	-1.824×10^{-2}	-5.278×10^{-3}	0
.9123	0	-1.762×10^{-3}	-8.216×10^{-3}	-1.926×10^{-2}	-3.118×10^{-2}	-4.286×10^{-2}	-5.057×10^{-2}	-5.634×10^{-2}	-6.073×10^{-2}	-6.390×10^{-2}	-6.576×10^{-2}	-6.608×10^{-2}	-6.442×10^{-2}	-6.003×10^{-2}	-5.068×10^{-2}	-3.534×10^{-2}	-1.688×10^{-2}	-3.852×10^{-3}	0
.8571	0	-1.028×10^{-3}	-5.254×10^{-3}	-1.433×10^{-2}	-2.857×10^{-2}	-4.498×10^{-2}	-5.830×10^{-2}	-6.906×10^{-2}	-7.763×10^{-2}	-8.403×10^{-2}	-8.799×10^{-2}	-8.891×10^{-2}	-8.585×10^{-2}	-7.715×10^{-2}	-5.896×10^{-2}	-3.465×10^{-2}	-1.399×10^{-2}	-2.888×10^{-3}	0
.7857	0	-6.970×10^{-4}	-3.727×10^{-3}	-1.091×10^{-2}	-2.411×10^{-2}	-4.245×10^{-2}	-5.954×10^{-2}	-7.443×10^{-2}	-8.680×10^{-2}	-9.624×10^{-2}	-1.021×10^{-1}	-1.031×10^{-1}	-9.784×10^{-2}	-8.363×10^{-2}	-5.726×10^{-2}	-2.942×10^{-2}	-1.075×10^{-2}	-2.084×10^{-3}	0
.7143	0	-5.796×10^{-4}	-3.126×10^{-3}	-9.343×10^{-3}	-2.138×10^{-2}	-3.943×10^{-2}	-5.747×10^{-2}	-7.393×10^{-2}	-8.791×10^{-2}	-9.852×10^{-2}	-1.046×10^{-1}	-1.047×10^{-1}	-9.675×10^{-2}	-7.837×10^{-2}	-4.902×10^{-2}	-2.310×10^{-2}	-7.949×10^{-3}	-1.485×10^{-3}	0
.6428	0	-5.115×10^{-4}	-2.762×10^{-3}	-8.297×10^{-3}	-1.920×10^{-2}	-3.604×10^{-2}	-5.342×10^{-2}	-6.962×10^{-2}	-8.341×10^{-2}	-9.358×10^{-2}	-9.869×10^{-2}	-9.699×10^{-2}	-8.663×10^{-2}	-6.642×10^{-2}	-3.852×10^{-2}	-1.702×10^{-2}	-5.606×10^{-3}	-1.017×10^{-3}	0
.5714	0	-4.473×10^{-4}	-2.415×10^{-3}	-7.259×10^{-3}	-1.686×10^{-2}	-3.184×10^{-2}	-4.750×10^{-2}	-6.216×10^{-2}	-7.448×10^{-2}	-8.308×10^{-2}	-8.642×10^{-2}	-8.291×10^{-2}	-7.129×10^{-2}	-5.185×10^{-2}	-2.821×10^{-2}	-1.183×10^{-2}	-3.763×10^{-3}	-6.667×10^{-4}	0
.5000	0	-3.743×10^{-4}	-2.021×10^{-3}	-6.082×10^{-3}	-1.415×10^{-2}	-2.680×10^{-2}	-4.005×10^{-2}	-5.239×10^{-2}	-6.247×10^{-2}	-6.894×10^{-2}	-7.042×10^{-2}	-6.570×10^{-2}	-5.436×10^{-2}	-3.767×10^{-2}	-1.941×10^{-2}	-7.802×10^{-3}	-2.406×10^{-3}	-4.170×10^{-4}	0
.4286	0	-2.929×10^{-4}	-1.586×10^{-3}	-4.788×10^{-3}	-1.118×10^{-2}	-2.124×10^{-2}	-3.177×10^{-2}	-4.143×10^{-2}	-4.903×10^{-2}	-5.339×10^{-2}	-5.341×10^{-2}	-4.842×10^{-2}	-3.861×10^{-2}	-2.562×10^{-2}	-1.259×10^{-2}	-4.874×10^{-3}	-1.461×10^{-3}	-2.477×10^{-4}	0
.3571	0	-2.096×10^{-4}	-1.142×10^{-3}	-3.473×10^{-3}	-8.174×10^{-3}	-1.563×10^{-2}	-2.431×10^{-2}	-3.045×10^{-2}	-3.575×10^{-2}	-3.838×10^{-2}	-3.781×10^{-2}	-3.316×10^{-2}	-2.556×10^{-2}	-1.631×10^{-2}	-7.677×10^{-3}	-2.861×10^{-3}	-8.311×10^{-4}	-1.373×10^{-4}	0
.2857	0	-1.323×10^{-4}	-7.299×10^{-4}	-2.252×10^{-3}	-5.384×10^{-3}	-1.042×10^{-2}	-1.571×10^{-2}	-2.042×10^{-2}	-2.383×10^{-2}	-2.527×10^{-2}	-2.431×10^{-2}	-2.090×10^{-2}	-1.561×10^{-2}	-9.591×10^{-2}	-4.307×10^{-3}	-1.530×10^{-3}	-4.246×10^{-4}	-6.721×10^{-5}	0
.2143	0	-6.803×10^{-5}	-3.865×10^{-4}	-1.231×10^{-3}	-3.035×10^{-3}	-6.021×10^{-3}	-9.189×10^{-3}	-1.200×10^{-2}	-1.397×10^{-2}	-1.469×10^{-2}	-1.392×10^{-2}	-1.170×10^{-2}	-8.478×10^{-3}	-4.992×10^{-3}	-2.100×10^{-3}	-6.858×10^{-4}	-1.721×10^{-4}	-2.428×10^{-5}	0
.1428	0	-2.264×10^{-5}	-1.414×10^{-4}	-4.914×10^{-4}	-1.301×10^{-3}	-2.708×10^{-3}	-4.233×10^{-3}	-5.591×10^{-3}	-6.532×10^{-3}	-6.846×10^{-3}	-6.417×10^{-3}	-5.389×10^{-3}	-3.703×10^{-3}	-2.055×10^{-3}	-7.668×10^{-4}	-2.004×10^{-4}	-3.252×10^{-5}	-1.245×10^{-6}	0
.0877	0	-3.407×10^{-6}	-3.354×10^{-5}	-1.496×10^{-4}	-4.553×10^{-4}	-1.017×10^{-3}	-1.638×10^{-3}	-2.197×10^{-3}	-2.585×10^{-3}	-2.713×10^{-3}	-2.530×10^{-3}	-2.054×10^{-3}	-1.393×10^{-3}	-7.208×10^{-4}	-2.204×10^{-4}	-2.741×10^{-5}	9.607×10^{-6}	4.551×10^{-6}	0
.0482	0	1.168×10^{-6}	-2.216×10^{-6}	-3.194×10^{-5}	-1.252×10^{-4}	-3.053×10^{-4}	-5.068×10^{-4}	-6.892×10^{-4}	-8.173×10^{-4}	-8.606×10^{-4}	-8.007×10^{-4}	-6.431×10^{-4}	-4.240×10^{-4}	-2.037×10^{-4}	-4.564×10^{-5}	7.514×10^{-6}	1.034×10^{-5}	3.087×10^{-6}	0
.0201	0	6.493×10^{-7}	1.172×10^{-6}	-3.106×10^{-6}	-1.956×10^{-5}	-5.240×10^{-5}	-8.938×10^{-5}	-1.230×10^{-4}	-1.468×10^{-4}	-1.552×10^{-4}	-1.442×10^{-4}	-1.149×10^{-4}	-7.398×10^{-5}	-3.305×10^{-5}	-4.484×10^{-6}	3.991×10^{-6}	3.045×10^{-6}	7.754×10^{-7}	0
0	0	0	0	0	0	0	0	0	0	0	0	0	0	0	0	0	0	0	0

(b) Vorticity

y \ x	0	0.0201	0.0482	0.0877	0.1428	0.2143	0.2857	0.3571	0.4286	0.5000	0.5714	0.6428	0.7143	0.7857	0.8571	0.9123	0.9517	0.9799	1.0
1.0000	----------	1.076×10^{2}	5.022×10^{2}	2.991×10	2.006×10	1.435×10	1.109×10	8.870	7.310	6.297	5.848	6.045	7.056	9.086	1.323×10	2.017×10	3.591×10	9.549×10	----------
.9799	-4.751 × 10	1.332×10	2.832×10	2.242×10	1.711×10	1.311×10	1.057×10	8.762	7.418	6.464	5.904	5.808	6.276	7.582	1.030×10	1.580×10	2.748×10	2.295×10	-5.973 × 10
.9517	-1.985 × 10	-9.382	4.485	1.061×10	1.101×10	9.884	8.694	7.675	6.831	6.166	5.701	5.491	5.619	6.318	8.225	1.255×10	1.256×10	-9.458	-3.542 × 10
.9123	-9.916	-6.472	-2.682	1.370	4.007	5.093	5.342	5.314	5.195	5.062	4.963	4.944	5.073	5.566	7.220	8.397	6.179×10^{-1}	-1.259 × 10	-2.235 × 10
.8571	-5.466	-4.459	-2.964	-1.364	1.835×10^{-1}	1.418	2.188	2.725	3.142	3.502	3.839	4.177	4.559	5.206	6.061	3.252	4.297	-1.116 × 10	-1.590 × 10
.7857	-3.616	-3.128	-2.457	-1.567	-6.139×10^{-1}	2.502×10^{-1}	8.973×10^{-1}	1.453	1.982	2.514	3.063	3.628	4.217	4.748	3.799	-4.883×10^{-1}	-5.409	-8.867	-1.104 × 10
.7143	-2.996	-2.617	-2.088	-1.410	-6.214×10^{-1}	1.307×10^{-1}	7.021×10^{-1}	1.211	1.722	2.259	2.821	3.383	3.839	3.693	1.552	-2.094	-4.979	-6.681	-7.688
.6428	-2.643	-2.301	-1.838	-1.245	-5.588×10^{-1}	1.082×10^{-1}	6.275×10^{-1}	1.102	1.586	2.088	2.579	2.977	3.047	2.233	-7.392×10^{-2}	-2.542	-4.037	-4.783	-5.166
.5714	-2.314	-2.008	-1.598	-1.084	-4.957×10^{-1}	6.985×10^{-2}	5.119×10^{-1}	9.214×10^{-1}	1.338	1.748	2.092	2.237	1.933	8.638×10^{-1}	-9.533×10^{-1}	-2.356	-3.016	-3.252	-3.330
.5000	-1.935	-1.681	-1.342	-9.188×10^{-1}	-4.425×10^{-1}	7.976×10^{-3}	3.554×10^{-1}	6.723×10^{-1}	9.812×10^{-1}	1.254	1.415	1.337	8.617×10^{-1}	-7.653×10^{-2}	-1.226	-1.892	-2.100	-2.103	-2.050
.4286	-1.512	-1.322	-1.069	-7.523×10^{-1}	-3.977×10^{-1}	-6.692×10^{-2}	1.818×10^{-1}	3.989×10^{-1}	5.923×10^{-1}	7.285×10^{-1}	7.428×10^{-1}	5.539×10^{-1}	1.086×10^{-1}	-5.322×10^{-1}	-1.134	-1.377	-1.377	-1.291	-1.198
.3571	-1.077	-9.577×10^{-1}	-7.954×10^{-1}	-5.896×10^{-1}	-3.568×10^{-1}	-1.412×10^{-1}	1.608×10^{-2}	1.452×10^{-2}	2.452×10^{-1}	2.873×10^{-1}	2.296×10^{-1}	3.853×10^{-2}	-2.780×10^{-1}	-6.375×10^{-1}	-8.921×10^{-1}	-9.277×10^{-1}	-8.498×10^{-1}	-7.446×10^{-1}	-6.499×10^{-1}
.2857	-6.731×10^{-1}	-6.191×10^{-1}	-5.417×10^{-1}	-4.379×10^{-1}	-3.163×10^{-1}	-2.041×10^{-1}	-1.258×10^{-1}	-6.514×10^{-2}	-2.511×10^{-2}	-2.578×10^{-2}	-8.971×10^{-2}	-2.238×10^{-1}	-4.032×10^{-1}	-5.663×10^{-1}	-6.345×10^{-1}	-5.843×10^{-1}	-4.875×10^{-1}	-3.889×10^{-1}	-3.066×10^{-1}
.2143	-3.383×10^{-1}	-3.364×10^{-1}	-3.268×10^{-1}	-3.049×10^{-1}	-2.744×10^{-1}	-2.496×10^{-1}	-2.386×10^{-1}	-2.311×10^{-1}	-2.265×10^{-1}	-2.355×10^{-1}	-2.705×10^{-1}	-3.322×10^{-1}	-4.019×10^{-1}	-4.450×10^{-1}	-4.233×10^{-1}	-3.448×10^{-1}	-2.521×10^{-1}	-1.672×10^{-1}	-9.843×10^{-2}
.1428	-1.033×10^{-1}	-1.338×10^{7}	-1.663×10^{-1}	-1.969×10^{-1}	-2.296×10^{-1}	-2.751×10^{-1}	-3.248×10^{-1}	-3.661×10^{-1}	-3.899×10^{-1}	-3.974×10^{-1}	-3.951×10^{-1}	-3.875×10^{-1}	-3.711×10^{-1}	-3.359×10^{-1}	-2.695×10^{-1}	-1.889×10^{-1}	-1.116×10^{-1}	-4.379×10^{-2}	1.096×10^{-2}
.0877	-6.433×10^{-2}	-4.279×10^{-2}	-8.363×10^{-2}	-1.286×10^{-1}	-1.889×10^{-1}	-2.795×10^{-1}	-3.769×10^{-1}	-4.607×10^{-1}	-5.129×10^{-1}	-5.250×10^{-1}	-4.977×10^{-1}	-4.385×10^{-1}	-3.580×10^{-1}	-2.676×10^{-1}	-1.761×10^{-1}	-1.049×10^{-1}	-4.951×10^{-2}	-3.511×10^{-3}	3.392×10^{-2}
.0482	1.256×10^{-2}	-1.213×10^{-2}	-4.120×10^{-2}	-8.067×10^{-2}	-1.515×10^{-1}	-2.737×10^{-1}	-4.090×10^{-1}	-5.290×10^{-1}	-6.088×10^{-1}	-6.311×10^{-1}	-5.895×10^{-1}	-4.915×10^{-1}	-3.585×10^{-1}	-2.212×10^{-1}	-1.095×10^{-1}	-5.029×10^{-2}	-1.843×10^{-2}	3.581×10^{-3}	2.035×10^{-2}
.0201	5.165×10^{-3}	-1.364×10^{-3}	-1.183×10^{-2}	-4.005×10^{-2}	-1.171×10^{-1}	-2.649×10^{-1}	-4.311×10^{-1}	-5.811×10^{-1}	-6.855×10^{-1}	-7.194×10^{-1}	-6.692×10^{-1}	-5.406×10^{-1}	-3.630×10^{-1}	-1.842×10^{-1}	-5.403×10^{-2}	-6.096×10^{-3}	3.196×10^{-3}	4.346×10^{-3}	4.668×10^{-3}
0	0	5.152×10^{-3}	1.249×10^{-2}	-5.197×10^{-3}	-8.790×10^{-2}	-2.567×10^{-1}	-4.472×10^{-1}	-6.209×10^{-1}	-7.452×10^{-1}	-7.894×10^{-1}	-7.334×10^{-1}	-5.808×10^{-1}	-3.673×10^{-1}	-1.544×10^{-1}	-8.233×10^{-3}	3.065×10^{-2}	2.009×10^{-2}	4.663×10^{-3}	0

TABLE IV.- VORTICITY AND STREAM FUNCTION CALCULATED WITH DIVERGENCE FINITE-DIFFERENCE FORM WITH EQUALLY SPACED 65 × 65 GRID

(a) Stream function

y \ x	0	0.0625	0.1250	0.1815	0.2500	0.3125	0.3570	0.4375	0.5000	0.5625	0.6250	0.6875	0.7500	0.8125	0.8750	0.9375	1.0
1.0000	0	0	0	0	0	0	0	0	0	0	0	0	0	0	0	0	0
.9375	0	-1.449×10^{-2}	-2.717×10^{-2}	-3.465×10^{-2}	-3.958×10^{-2}	-4.316×10^{-2}	-4.590×10^{-2}	-4.802×10^{-2}	-4.957×10^{-2}	-5.055×10^{-2}	-5.085×10^{-2}	-5.035×10^{-2}	-4.876×10^{-2}	-4.559×10^{-2}	-3.932×10^{-2}	-2.429×10^{-2}	0
.8750	0	-9.562×10^{-3}	-2.509×10^{-2}	-3.878×10^{-2}	-4.990×10^{-2}	-5.897×10^{-2}	-6.641×10^{-2}	-7.244×10^{-2}	-7.709×10^{-2}	-8.020×10^{-2}	-8.148×10^{-2}	-8.044×10^{-2}	-7.629×10^{-2}	-6.765×10^{-2}	-5.138×10^{-2}	-2.322×10^{-2}	0
.8125	0	-6.834×10^{-3}	-2.097×10^{-2}	-3.633×10^{-2}	-5.062×10^{-2}	-6.330×10^{-2}	-7.426×10^{-2}	-8.344×10^{-2}	-9.065×10^{-2}	-9.551×10^{-2}	-9.745×10^{-2}	-9.559×10^{-2}	-8.867×10^{-2}	-7.471×10^{-2}	-5.108×10^{-2}	-1.924×10^{-2}	0
.7500	0	-5.554×10^{-3}	-1.825×10^{-2}	-3.353×10^{-2}	-4.891×10^{-2}	-6.329×10^{-2}	-7.614×10^{-2}	-8.708×10^{-2}	-9.567×10^{-2}	-1.013×10^{-1}	-1.030×10^{-1}	-9.984×10^{-2}	-9.013×10^{-2}	-7.215×10^{-2}	-4.521×10^{-2}	-1.514×10^{-2}	0
.6875	0	-4.848×10^{-3}	-1.636×10^{-2}	-3.089×10^{-2}	-4.617×10^{-2}	-6.088×10^{-2}	-7.426×10^{-2}	-8.571×10^{-2}	-9.453×10^{-2}	-9.989×10^{-2}	-1.008×10^{-1}	-9.588×10^{-2}	-8.385×10^{-2}	-6.375×10^{-2}	-3.710×10^{-2}	-1.142×10^{-2}	0
.6250	0	-4.312×10^{-3}	-1.468×10^{-2}	-2.807×10^{-2}	-4.244×10^{-2}	-5.649×10^{-2}	-6.937×10^{-2}	-8.029×10^{-2}	-8.844×10^{-2}	-9.285×10^{-2}	-9.240×10^{-2}	-8.595×10^{-2}	-7.258×10^{-2}	-5.249×10^{-2}	-2.869×10^{-2}	-8.273×10^{-3}	0
.5625	0	-3.780×10^{-3}	-1.292×10^{-2}	-2.483×10^{-2}	-3.773×10^{-2}	-5.043×10^{-2}	-6.204×10^{-2}	-7.171×10^{-2}	-7.856×10^{-2}	-8.160×10^{-2}	-7.982×10^{-2}	-7.236×10^{-2}	-5.894×10^{-2}	-4.070×10^{-2}	-2.110×10^{-2}	-5.771×10^{-3}	0
.5000	0	-3.203×10^{-3}	-1.097×10^{-2}	-2.116×10^{-2}	-3.224×10^{-2}	-4.314×10^{-2}	-5.300×10^{-2}	-6.099×10^{-2}	-6.626×10^{-2}	-6.791×10^{-2}	-6.513×10^{-2}	-5.746×10^{-2}	-4.520×10^{-2}	-2.994×10^{-2}	-1.484×10^{-2}	-3.883×10^{-3}	0
.4375	0	-2.587×10^{-3}	-8.906×10^{-3}	-1.723×10^{-2}	-2.630×10^{-2}	-3.519×10^{-2}	-4.312×10^{-2}	-4.932×10^{-2}	-5.303×10^{-2}	-5.353×10^{-2}	-5.029×10^{-2}	-4.320×10^{-2}	-3.290×10^{-2}	-2.100×10^{-2}	-1.002×10^{-2}	-2.517×10^{-3}	0
.3750	0	-1.965×10^{-3}	-6.822×10^{-3}	-1.327×10^{-2}	-2.032×10^{-2}	-2.720×10^{-2}	-3.323×10^{-2}	-3.776×10^{-2}	-4.017×10^{-2}	-3.993×10^{-2}	-3.676×10^{-2}	-3.079×10^{-2}	-2.276×10^{-2}	-1.406×10^{-2}	-6.473×10^{-3}	-1.562×10^{-3}	0
.3125	0	-1.376×10^{-3}	-4.853×10^{-3}	-9.537×10^{-3}	-1.469×10^{-2}	-1.969×10^{-2}	-2.402×10^{-2}	-2.714×10^{-2}	-2.859×10^{-2}	-2.802×10^{-2}	-2.532×10^{-2}	-2.072×10^{-2}	-1.491×10^{-2}	-8.924×10^{-3}	-3.957×10^{-3}	-9.094×10^{-4}	0
.2500	0	-8.596×10^{-4}	-3.117×10^{-3}	-6.233×10^{-3}	-9.699×10^{-3}	-1.307×10^{-2}	-1.595×10^{-2}	-1.797×10^{-2}	-1.879×10^{-2}	-1.819×10^{-2}	-1.617×10^{-2}	-1.298×10^{-2}	-9.074×10^{-3}	-5.248×10^{-3}	-2.219×10^{-3}	-4.722×10^{-4}	0
.1875	0	-4.467×10^{-4}	-1.712×10^{-3}	-3.531×10^{-3}	-5.594×10^{-3}	-7.614×10^{-3}	-9.333×10^{-3}	-1.051×10^{-2}	-1.094×10^{-2}	-1.051×10^{-2}	-9.208×10^{-3}	-7.226×10^{-3}	-4.912×10^{-3}	-2.716×10^{-3}	-1.063×10^{-3}	-1.913×10^{-4}	0
.1250	0	-1.615×10^{-4}	-7.092×10^{-4}	-1.553×10^{-3}	-2.535×10^{-3}	-3.509×10^{-3}	-4.341×10^{-3}	-4.909×10^{-3}	-5.109×10^{-3}	-4.878×10^{-3}	-4.222×10^{-3}	-3.241×10^{-3}	-2.121×10^{-3}	-1.093×10^{-3}	-3.642×10^{-4}	-3.438×10^{-5}	0
.0625	0	-1.956×10^{-5}	-1.491×10^{-4}	-3.737×10^{-4}	-6.433×10^{-4}	-9.139×10^{-4}	-1.148×10^{-3}	-1.309×10^{-3}	-1.368×10^{-3}	-1.303×10^{-3}	-1.115×10^{-3}	-8.335×10^{-4}	-5.158×10^{-4}	-2.326×10^{-4}	-4.674×10^{-5}	-1.459×10^{-5}	0
0	0	0	0	0	0	0	0	0	0	0	0	0	0	0	0	0	0

(b) Vorticity

y \ x	0	0.0625	0.1250	0.1815	0.2500	0.3125	0.3750	0.4375	0.5000	0.5625	0.6250	0.6875	0.7500	0.8125	0.8750	0.9375	1.0
1.0000	----------	4.086×10	2.280×10	1.639×10	1.286×10	1.048×10	8.753	7.479	6.609	6.115	6.182	6.788	8.140	1.059×10	1.537×10	2.985	----------
.9375	-1.598×10	3.667	7.571	8.004	7.694	7.216	6.725	6.274	5.891	5.548	5.439	5.455	5.754	6.591	8.676	9.828	-2.996
.8750	-6.836	-1.847	7.319×10^{-1}	1.986	2.692	3.134	3.440	3.676	3.882	4.083	4.303	4.574	4.971	5.664	6.317	7.905×10^{-1}	-1.827×10
.8125	-4.256	-2.136	-6.314×10^{-1}	3.006×10^{-1}	9.452×10^{-1}	1.452	1.893	2.309	2.719	3.139	3.577	4.043	4.548	4.953	3.889	-2.755	-1.289×10
.7500	-3.303	-1.934	-8.273×10^{-1}	-5.295×10^{-2}	5.156×10^{-1}	9.865×10^{-1}	1.424	1.861	2.313	2.785	3.271	3.748	4.109	3.887	1.649	-3.868	-9.290
.6875	-2.847	-1.725	-7.959×10^{-1}	-1.121×10^{-1}	4.055×10^{-1}	8.458×10^{-1}	1.267	1.699	2.147	2.602	3.035	3.369	3.383	2.521	-3.220×10^{-2}	-3.873	-6.579
.6250	-2.527	-1.533	-7.225×10^{-1}	-1.207×10^{-1}	3.396×10^{-1}	7.380×10^{-1}	1.127	1.527	1.934	2.320	2.626	2.727	2.369	1.167	-1.037	-3.369	-4.531
.5625	-2.216	-1.343	-6.446×10^{-1}	-1.313×10^{-1}	2.602×10^{-1}	6.000×10^{-1}	9.321×10^{-1}	1.269	1.594	1.866	2.004	1.877	1.296	1.201×10^{-1}	-1.448	-2.683	-3.026
.5000	-1.875	-1.146	-5.698×10^{-1}	-1.518×10^{-1}	1.633×10^{-1}	4.336×10^{-1}	6.923×10^{-1}	9.431×10^{-1}	1.163	1.304	1.291	1.024	4.174×10^{-1}	-4.999×10^{-1}	-1.453	-2.003	-1.955
.4375	-1.507	-9.437×10^{-1}	-4.989×10^{-1}	-1.788×10^{-1}	5.882×10^{-2}	2.577×10^{-1}	4.401×10^{-1}	6.031×10^{-1}	7.225×10^{-1}	7.562×10^{-1}	6.500×10^{-1}	3.529×10^{-1}	-1.433×10^{-1}	-7.464×10^{-1}	-1.246	-1.420	-1.218
.3750	-1.132	-7.439×10^{-1}	-4.312×10^{-1}	-2.062×10^{-1}	-4.185×10^{-2}	9.139×10^{-2}	2.069×10^{-1}	2.984×10^{-1}	3.446×10^{-1}	3.159×10^{-1}	1.827×10^{-1}	-6.782×10^{-2}	-4.082×10^{-1}	-7.511×10^{-1}	-9.687×10^{-1}	-9.615×10^{-1}	-7.214×10^{-1}
.3125	-7.776×10^{-1}	-5.552×10^{-1}	-3.659×10^{-1}	-2.286×10^{-1}	-1.304×10^{-1}	-5.332×10^{-2}	1.013×10^{-2}	5.351×10^{-2}	6.066×10^{-2}	1.333×10^{-2}	-1.000×10^{-1}	-2.736×10^{-1}	-4.741×10^{-1}	-6.404×10^{-1}	-7.036×10^{-1}	-6.208×10^{-1}	-3.930×10^{-1}
.2500	-4.678×10^{-1}	-3.869×10^{-1}	-3.038×10^{-1}	-2.429×10^{-1}	-2.026×10^{-1}	-1.729×10^{-1}	-1.486×10^{-1}	-1.338×10^{-1}	-1.393×10^{-1}	-1.763×10^{-1}	-2.481×10^{-1}	-3.449×10^{-1}	-4.411×10^{-1}	-4.998×10^{-1}	-4.857×10^{-1}	-3.786×10^{-1}	-1.787×10
.1875	-2.228×10^{-1}	-2.472×10^{-1}	-2.457×10^{-1}	-2.475×10^{-1}	-2.578×10^{-1}	-2.701×10^{-1}	-2.782×10^{-1}	-2.821×10^{-1}	-2.876×10^{-1}	-3.018×10^{-1}	-3.270×10^{-1}	-3.577×10^{-1}	-3.795×10^{-1}	-3.736×10^{-1}	-3.224×10^{-1}	-2.148×10^{-1}	-4.481×10^{-2}
.1250	-5.867×10^{-2}	-1.414×10^{-2}	-1.913×10^{-1}	-2.411×10^{-1}	-2.966×10^{-1}	-3.501×10^{-1}	-3.914×10^{-1}	-4.148×10^{-1}	-4.202×10^{-1}	-4.112×10^{-1}	-3.917×10^{-1}	-3.636×10^{-1}	-3.255×10^{-1}	-2.738×10^{-1}	-2.041×10^{-1}	-1.098×10^{-1}	2.319×10^{-2}
.0625	1.102×10^{-2}	-6.582×10^{-2}	-1.337×10^{-1}	-2.202×10^{-1}	-3.205×10^{-1}	-4.195×10^{-1}	-5.017×10^{-1}	-5.540×10^{-1}	-5.683×10^{-1}	-5.421×10^{-1}	-4.792×10^{-1}	-3.897×10^{-1}	-2.878×10^{-1}	-1.895×10^{-1}	-1.070×10^{-1}	-4.139×10^{-2}	2.746×10^{-2}
0	0	1.082×10^{-2}	-5.194×10^{-2}	-1.782×10^{-1}	-3.326×10^{-1}	-4.887×10^{-1}	-6.253×10^{-1}	-7.221×10^{-1}	-7.594×10^{-1}	-7.233×10^{-1}	-6.125×10^{-1}	-4.444×10^{-1}	-2.548×10^{-1}	-8.932×10^{-1}	1.093×10^{-2}	2.689×10^{-2}	0

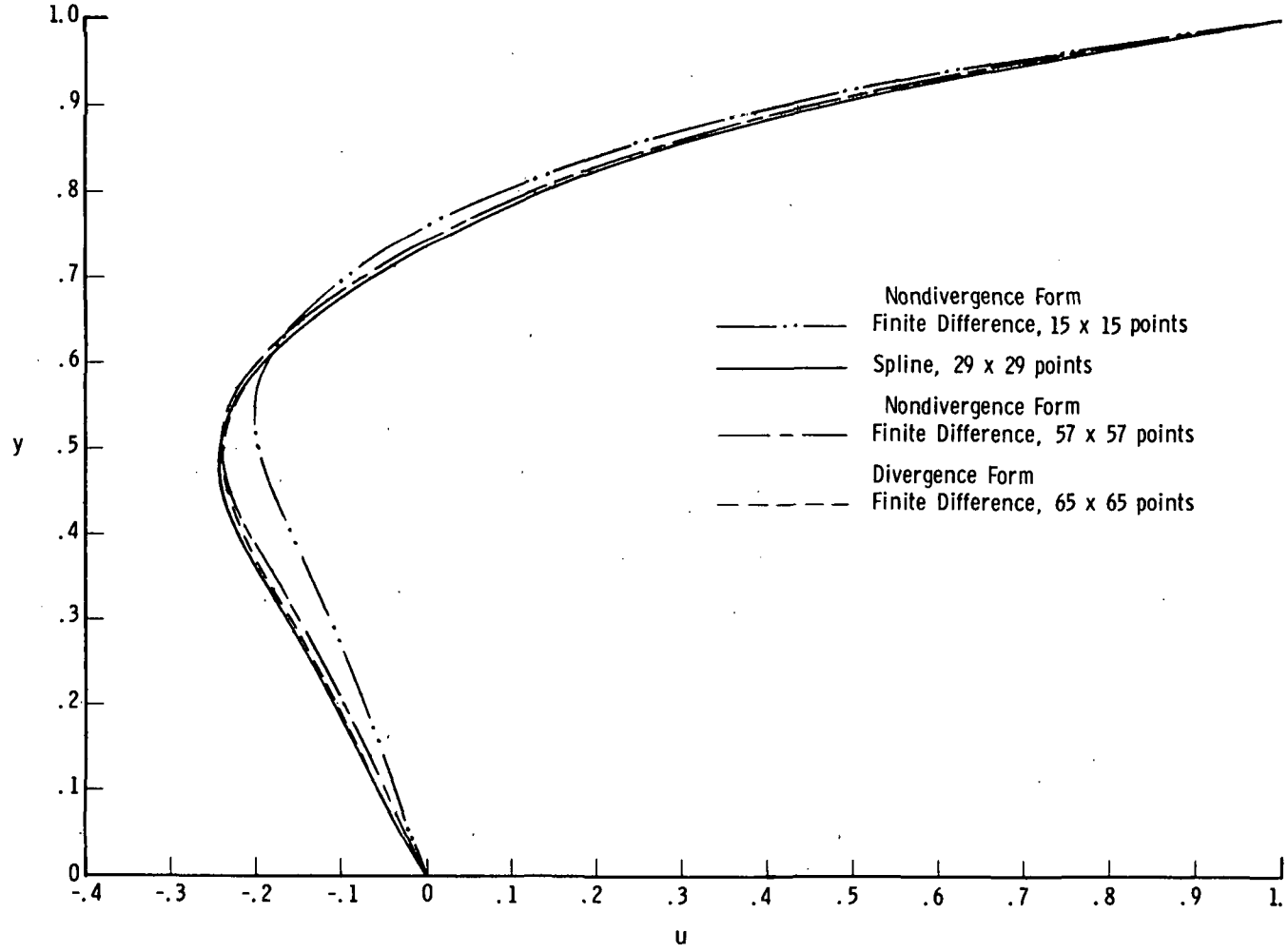

Figure 1.- Comparison of calculated u through point of maximum ψ for R = 100.

"The aeronautical and space activities of the United States shall be conducted so as to contribute . . . to the expansion of human knowledge of phenomena in the atmosphere and space. The Administration shall provide for the widest practicable and appropriate dissemination of information concerning its activities and the results thereof."

—NATIONAL AERONAUTICS AND SPACE ACT OF 1958

NASA SCIENTIFIC AND TECHNICAL PUBLICATIONS

TECHNICAL REPORTS: Scientific and technical information considered important, complete, and a lasting contribution to existing knowledge.

TECHNICAL NOTES: Information less broad in scope but nevertheless of importance as a contribution to existing knowledge.

TECHNICAL MEMORANDUMS: Information receiving limited distribution because of preliminary data, security classification, or other reasons. Also includes conference proceedings with either limited or unlimited distribution.

CONTRACTOR REPORTS: Scientific and technical information generated under a NASA contract or grant and considered an important contribution to existing knowledge.

TECHNICAL TRANSLATIONS: Information published in a foreign language considered to merit NASA distribution in English.

SPECIAL PUBLICATIONS: Information derived from or of value to NASA activities. Publications include final reports of major projects, monographs, data compilations, handbooks, sourcebooks, and special bibliographies.

TECHNOLOGY UTILIZATION PUBLICATIONS: Information on technology used by NASA that may be of particular interest in commercial and other non-aerospace applications. Publications include Tech Briefs, Technology Utilization Reports and Technology Surveys.

Details on the availability of these publications may be obtained from:

SCIENTIFIC AND TECHNICAL INFORMATION OFFICE

NATIONAL AERONAUTICS AND SPACE ADMINISTRATION

Washington, D.C. 20546